Disruption of Cell-Cell Adhesion Codes Underlies the Unique X-linked Inheritance Pattern of Protocadherin 19 Girls Clustering Epilepsy

Daniel Tyler Pederick

B.Sc. (Biomedical Science), Honours (Biochemistry)

A thesis submitted in fulfilment of the requirements for the degree of Doctor of Philosophy

Department of Molecular and Cellular Biology

School of Biological Science

The University of Adelaide, Australia

February 2017

Contents

Abstract

Epilepsy is a disease of the central nervous system (CNS) caused by increased neuronal activity resulting in seizures and often loss of consciousness. Epilepsy can result from both traumas to the brain or a genetic predisposition. Recent advances in DNA sequencing technology has identified many forms of epilepsy caused by mutations in single genes. Although such monogenic epilepsies are rare, investigating their underlying molecular mechanisms provides important insights into pathways and processes that cause seizures and assists in the application of pharmacotherapy and surgical strategies.

The second most common form of monogenic epilepsy is *Protocadherin 19* Girls Clustering Epilepsy (*PCDH19*-GCE) caused by mutation of the X-linked gene *PCDH19*. This disorder is characterised by clusters of febrile seizures beginning in early childhood that is often accompanied by variable intellectual disability and autism spectrum disorder. The most striking feature of *PCDH19*-GCE is its unique X-linked inheritance pattern; heterozygous females with *PCDH19* mutations are affected whereas hemizygous males are not. It is hypothesised that the mixture of PCDH19-WT and PCDH19-mutant neurons (generated by random X-inactivation in female brains) causes abnormal neuronal connections leading to disease. However, there is no experimental evidence supporting this hypothesis and the cellular and molecular mechanisms underpinning this unique inheritance pattern are unknown.

To better understand how mutation of *PCDH19* leads to the unique X-linked inheritance pattern this thesis uses a *Pcdh19* null mouse, cell culture assays and unique CRISPR-Cas9 engineered mouse models. It is shown that heterozygous and homozygous deletion of *Pcdh19* in mice does not cause any gross brain morphological abnormalities and that *Pcdh19*

null neurons are present within the correct layers in the cortex despite their slight increase in migration potential *in vitro.*

Using cultured K562 cells it is shown that PCDH19 and other non-clustered (NC) PCDH members contribute to combinatorial adhesion codes that dictate specific cell-cell interactions. Similarly, mosaic expression of *Pcdh19* in heterozygous mice leads to abnormal cell sorting in the developing cortex such that cells separate into PCDH19 positive and negative patches, correlating with altered brain network activity consistent with changes that can underlie seizures in adult mice. Deletion of *Pcdh19* in heterozygous embryos using CRISPR-Cas9 technology eliminates this incompatibility of adhesion codes and prevents abnormal cell sorting from occurring. In addition, variable cortical folding malformations in *PCDH19*-GCE epilepsy patients were identified. Collectively these results highlight the role of PCDH19 in determining specific adhesion codes during brain development and how disruption of these codes is associated with the unique X-linked inheritance pattern of *PCDH19*-GCE. Importantly, a framework is provided for investigating how this abnormal neuronal segregation phenotype leads to seizures and cognitive deficits.

PhD Thesis Declaration

I certify that this work contains no material which has been accepted for the award of any other degree or diploma in my name in any university or other tertiary institution and, to the best of my knowledge and belief, contains no material previously published or written by another person, except where due reference has been made in the text. In addition, I certify that no part of this work will, in the future, be used in a submission in my name for any other degree or diploma in any university or other tertiary institution without the prior approval of the University of Adelaide and where applicable, any partner institution responsible for the joint award of this degree.

I give consent to this copy of my thesis when deposited in the University Library, being made available for loan and photocopying, subject to the provisions of the Copyright Act 1968.

The author acknowledges that copyright of published works contained within this thesis resides with the copyright holder(s) of those works.

I also give permission for the digital version of my thesis to be made available on the web, via the University's digital research repository, the Library Search and also through web search engines, unless permission has been granted by the University to restrict access for a period of time.

I acknowledge the support I have received for my research through the provision of an Australian Government Research Training Program Scholarship.

Daniel Pederick

Acknowledgements

I would firstly like to thank all my colleagues, friends and family for their support, kindness and tolerance that has made my PhD adventure so enjoyable and rewarding.

I owe many of my achievements (and hopefully future success) to Prof. Paul Thomas who has undoubtedly changed the way I approach my research. I appreciate that your door is rarely ever closed, allowing me to discuss new experiments I have planned, even sometimes letting me do them. This to me is priceless as it has helped me gain some key skills needed to become an independent scientist. I am equally as grateful for all your support of my future endeavours; hopefully we can form successful collaborations in the future.

Dr. James Hughes, you have been an excellent co-supervisor and friend over the years. I thank you for your always insightful scientific and non-scientific discussions and also your technical guidance in the lab. Without your assistance I doubt I would've been able to work independently within the lab.

Prof. Jozef Gecz, thank you for your role as co-supervisor. Your "external" point of view is always greatly valued and appreciated, as are the heated table tennis matches over the years at past Epilepsy Retreats. Thanks also to members of your group who have assisted me throughout my research.

I also appreciate all the help from all past/current lab members and collaborators specifically Dale McAninch, Bryan Haines, Sandie Piltz and Kay Richards

I would also like to thank the all of the professional staff within the School of Biological Sciences, especially Alan McLennan who has always been willing to help above and beyond what his job requires.

Staff at university provided services such as Adelaide Microscopy and Laboratory Animal Services; I thank you for your time and efforts, especially Agatha Labrinidis and Tiffany Boehm.

Thank you to all members of the Biochemistry/Molecular and Cellular Biology Disciplines for providing such an excellent research environment and always being prepared to help.

I must also acknowledge my parents Greg and Mary and all of my relatives. Without your support and belief it would not have been possible. Thank you also for allowing me to follow my interest in science.

Finally, I thank my partner Gabby for her love and support over the past four years. If you were not so understanding I doubt I would have been able to complete my PhD and maintain my sanity. I look forward to more of your unwavering support in the future.

Publications

Pederick, D.T., Homan, C.C., Jaehne, E.J., Piltz, S.G., Haines, B.P., Baune, B.T., Jolly, L.A., Hughes, J.N., Gecz, J., and Thomas, P.Q. (2016). Pcdh19 Loss-of-Function Increases Neuronal Migration In Vitro but is Dispensable for Brain Development in Mice. Sci. Rep. *6*, 26765.

*Submitted manuscript

Pederick, D.T., Richards, K.L., Piltz, S.G., Mandelstam, S.A., Dale, R.C., Scehffer, I.E., Gecz, J., Petrou, S., Hughes, J.N., Thomas, P.Q. (2017) Abnormal cell sorting is associated with the unique X-linked inheritance of *PCDH19* epilepsy. Submitted to: *Science* on 27.1.2017

Conference Oral Presentations

Mosaic Expression of *Pcdh19* Causes Segregation of PCDH19-wild type and PCDH19-null Neurons in the Developing Mouse Cortex Leading to an Epileptic Phenotype

Daniel T. Pederick, Kay L. Richards, Sandra G. Piltz, Simone A. Mandelstam, Ian Dodd, Ingrid E. Scheffer, Jozef Gecz, Steven Petrou, James N. Hughes and Paul Q. Thomas

Australian Society for Medical Research, South Australian Scientific Meeting (June 2016)

Mosaic Expression of *Pcdh19* Causes Segregation of PCDH19-wild type and PCDH19-null Neurons in the Developing Mouse Cortex Leading to an Epileptic Phenotype

Daniel T. Pederick, Kay L. Richards, Sandra G. Piltz, Simone A. Mandelstam, Ian Dodd, Ingrid E. Scheffer, Jozef Gecz, Steven Petrou, James N. Hughes and Paul Q. Thomas

Adelaide Protein Group Student Awards (June 2016)

Mosaic Expression of *Pcdh19* Causes Segregation of PCDH19-wild type and PCDH19-null Neurons in the Developing Mouse Cortex Leading to an Epileptic Phenotype

Daniel T. Pederick, Kay L. Richards, Sandra G. Piltz, Simone A. Mandelstam, Ian Dodd, Ingrid E. Scheffer, Jozef Gecz, Steven Petrou, James N. Hughes and Paul Q. Thomas

Gordon Research Seminar-Neurodevelopment (July 2016)

Mosaic Expression of *Pcdh19* Causes Segregation of PCDH19-wild type and PCDH19-null Neurons in the Developing Mouse Cortex Leading to an Epileptic Phenotype

Daniel T. Pederick, Kay L. Richards, Sandra G. Piltz, Simone A. Mandelstam, Ian Dodd, Ingrid E. Scheffer, Jozef Gecz, Steven Petrou, James N. Hughes and Paul Q. Thomas

Gordon Research Conference-Neurodevelopment (August 2016)

Playing TAG with PCDH19: Investigating the Cellular and Molecular Mechanism of *PCDH19* Human Epilepsy

Daniel T. Pederick, Kay L. Richards, Sandra G. Piltz, Simone A. Mandelstam, Ian Dodd, Ingrid E. Scheffer, Jozef Gecz, Steven Petrou, James N. Hughes and Paul Q. Thomas

ComBio 2016 (October 2016)

Mosaic loss of *Pcdh19 in* mice leads to abnormal cell sorting and epileptiform brain activity

Daniel T. Pederick, Kay L. Richards, Sandra G. Piltz, Simone A. Mandelstam, Ian Dodd, Ingrid E. Scheffer, Jozef Gecz, Steven Petrou, James N. Hughes and Paul Q. Thomas

2016 ANZSCDB Adelaide Meeting

Mosaic loss of *Pcdh19 in* mice leads to abnormal cell sorting and epileptiform brain activity

Daniel T. Pederick, Kay L. Richards, Sandra G. Piltz, Simone A. Mandelstam, Ian Dodd, Ingrid E. Scheffer, Jozef Gecz, Steven Petrou, James N. Hughes and Paul Q. Thomas

School of Biological Sciences Research Day, The University of Adelaide

Awards

Best student poster - Robinson Research Institute Symposium (2014)

Robinson Research Institute Prize (Best presentation in the field of Reproduction, Pregnancy or Child Health) - Australian Society of Medical Research South Australian Scientific Meeting (2016)

Most outstanding oral presentation - Adelaide Protein Group Student Awards (2016)

Robinson Research Institute Travel Grant (2016)

David Walsh Student Prize (Best oral presentation in the fields of cell or developmental biology by a student) – ComBio (2016)

Outstanding Student Oral Presentation Prize – 6th ANZSCDB Adelaide Meeting (2016)

Department of Molecular Cellular Biology Student Publication Prize - School of Biological Sciences Research Day, The University of Adelaide (2016)

CHAPTER 1

Introduction

1.1 Epilepsy

Epilepsy is a neurological disease caused by a combination of genetic and environmental factors and with 3-4% of the population developing the disorder at some stage in their life this presents a serious burden to society. It is primarily defined by recurrent seizures and while anti-epileptic drugs are an effective treatment for many patients, up to 30% of epilepsy cases are drug refractory. Epileptic seizures can be the result of a genetic predisposition or a structural abnormality in the brain e.g. a tumour or trauma. Seizure types can vary and are important in classifying and managing an individual's epilepsy. Partial seizures are limited to only one region of the brain and can be termed "simple" if there is no loss of consciousness and "complex" if consciousness is lost. Generalised seizures involve the whole brain and consciousness is normally impaired. There are six major types of generalized seizures; tonic-clonic, absence, myoclonic, tonic, clonic and atonic. The characteristics of each seizure type vary depending on how they affect the neuronal networks in the brain. Understanding the normal neuronal networks in the brain and how epilepsy alters their function is essential to investigate the cause of epilepsy and for effective therapeutic intervention.

Identifying the causes of different epileptic disorders is essential to provide key information that guides therapeutic treatment. Improvements in understanding the causes of epilepsy have largely been due to advances in DNA sequencing technology. In 1975 Hauser and Kurland estimated that the majority of epilepsy cases could be classified as "idiopathic" (unknown cause) (Hauser and Kurland, 1975). Today, the term idiopathic has been left behind and such cases are now thought to be monogenic syndromes (caused by mutation of a single gene) or more genetically complex disorders which may involve modified susceptibility loci (Figure 1-1) (Thomas and Berkovic, 2014).

Although single gene epilepsies are rare, investigating and understanding their molecular causes provides important information regarding the molecular pathways and cellular

processes that are involved in causing or propagating seizures and in guidance for pharmacotherapy and surgical intervention.

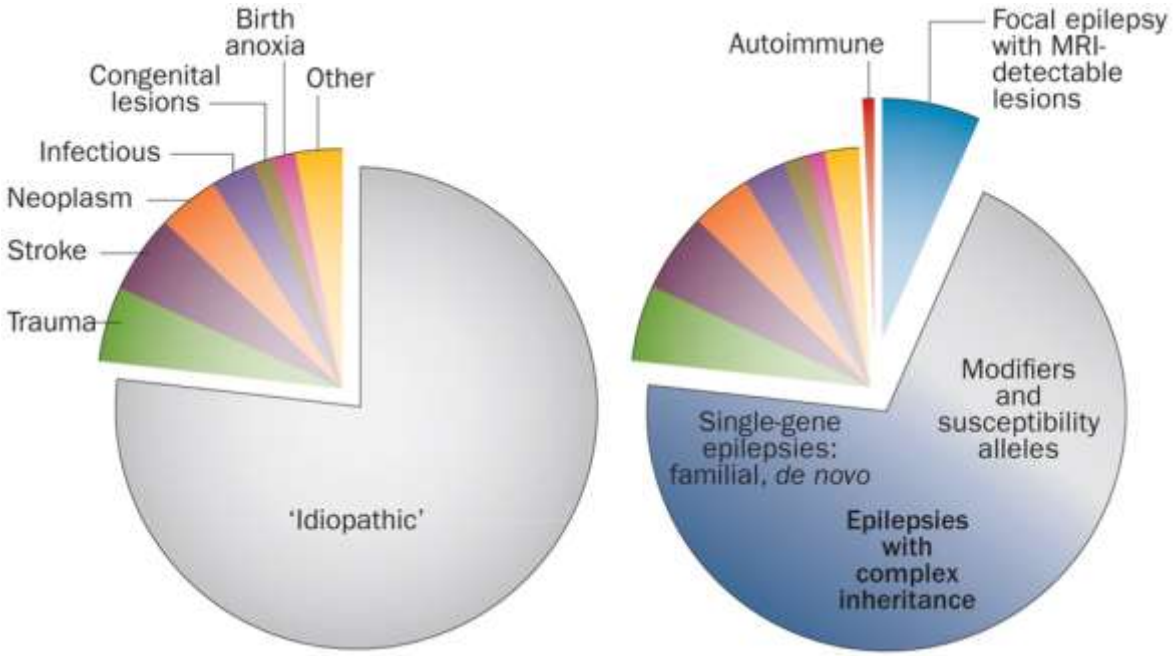

1975 (Hauser and Kurland) 2014 paradigm

Figure 1-1. The majority of epilepsy cases are thought to be caused by a genetic predisposition. Hauser and Kurland (1975) described most epilepsy cases as "idiopathic". In recent years, with the advances in DNA sequencing technology, it is thought that cases previously described as idiopathic largely have a genetic basis. Adapted from Thomas and Berkovic (2014).

1.2 *Protocadherin 19* Girls Clustering Epilepsy

PROTOCADHERIN 19 Girls Clustering Epilepsy (*PCDH19*-GCE; also known as Epilepsy and Mental Retardation limited to Females (EFMR)) is a female-specific condition caused by mutation in the X-linked gene *PCDH19* (Dibbens et al., 2008; Ryan et al., 1997). The disorder is primarily defined by clusters of febrile seizures beginning in early childhood with variable intellectual disability and autism spectrum disorder (ASD) (Marini et al., 2010; Ryan et al., 1997; Scheffer et al., 2008). *PCDH19*-GCE is now recognised as the second most common monogenic epilepsy disorder behind Dravet syndrome (Duszyc et al., 2014; Marini et al., 2010). Symptoms in affected females vary from mild to severe, ranging from benign focal epilepsy with normal cognitive function to severe seizures and intellectual disability that resemble Dravet syndrome (Depienne and LeGuern, 2012; Scheffer et al., 2008). Febrile seizures are the initial indicator in approximately half of all cases with seizure types mostly involving generalized tonic, clonic or tonic-clonic and or focal seizures (Marini et al., 2010).

PCDH19-GCE exhibits a unique X-linked mode of inheritance (Ryan et al., 1997). X-linked diseases are usually characterized by affected males and unaffected carrier females (i.e. a recessive mode of inheritance). In contrast, *PCDH19*-GCE only affects heterozygous females, with transmitting hemizygous males showing normal cognitive function and no seizures (Figure 2-1) (Depienne and LeGuern, 2012; Fabisiak and Erickson, 1990; Juberg and Hellman, 1971; Ryan et al., 1997; Scheffer et al., 2008).

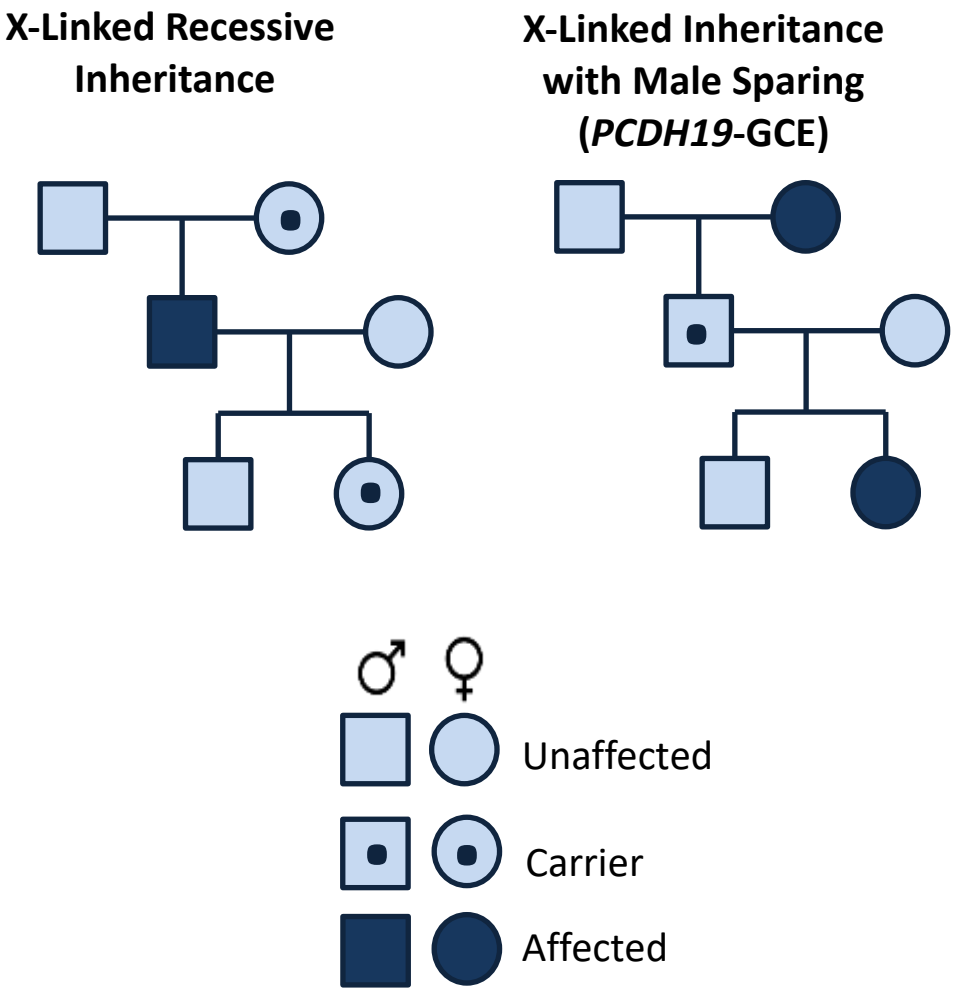

Figure 2-1. *PCDH19*-GCE displays a unique X-linked inheritance pattern. Most X-linked disorders exhibit recessive inheritance in which hemizygous males are affected while heterozygous female carriers are not (left). In contrast, *PCDH19*-GCE affects heterozygous females, while hemizygous males are spared (right).

Recent analysis of *PCDH19*-GCE individuals by multiple research groups has identified over 100 mutations in the *PCDH19* gene with both inherited and *de novo* mutations reported. These include nonsense mutations, nucleotide insertions and deletions, mutations altering the splice sites, missense mutations, intragenic and whole gene deletions (Figure 3-1) (Depienne and LeGuern, 2012). The majority of pathological disease mutations are nonsense and missense mutations positioned in exon 1, affecting highly conserved amino acids in the extracellular domain of PCDH19. *PCDH19* mRNAs with premature stop codons have been shown to undergo nonsense mediated decay and together with identification of whole gene deletions this suggests that loss of function is the likely outcome from the mutations which has been confirmed through a series of bead aggregation assays (Cooper et al., 2016; Dibbens et al., 2008). Furthermore, there does not appear to be any correlation between the severity of the phenotype and the type of mutation i.e. the same mutation results in variable degrees of disease severity in different individuals (Depienne et al., 2011; Higurashi et al., 2013; Scheffer et al., 2008). This is further highlighted by different phenotypes presented in a pair of monozygotic twins with *PCDH19*-GCE (Higurashi et al., 2013).

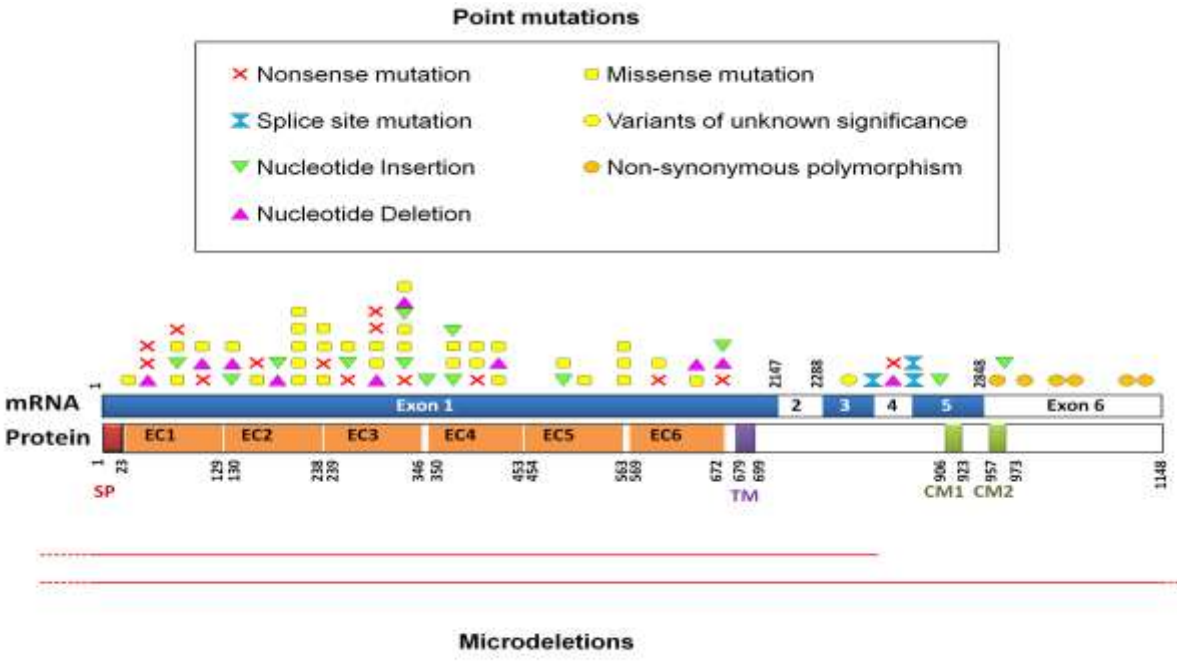

Figure 3-1. Schematic diagram highlighting the types and location of mutations leading to *PCDH19*-GCE. Over 100 unique disease mutations have now been identified, the most common being missense mutations positioned in exon 1. Adapted from Depienne and LeGuern (2012).

1.3 *Pcdh19* expression in the mammalian brain

Pcdh19 was first discovered in 2001 when its mRNA expression was reported in multiple tissues (Wolverton and Lalande, 2001). *Pcdh19* expression is tightly controlled both spatially and temporally within the central nervous system during mammalian development (Figure 4-1) (Dibbens et al., 2008; Gaitan and Bouchard, 2006). *In situ* hybridisation of WT *Pcdh19* in mice indicates widespread expression in both the embryonic and postnatal CNS including the cortex, hippocampus, retina, nasal epithelium and spinal cord (Dibbens et al., 2008; Gaitan and Bouchard, 2006). *Pcdh19* is highly expressed in the sub-ventricular zone, intermediate zone, sub-plate, hippocampus, specific layers (II, IV, V and VI) of the cerebral cortex and the subiculum. Expression in these specific regions suggests important functional roles in neuronal development as well as potential roles in the formation of neuronal networks and synaptogenesis.

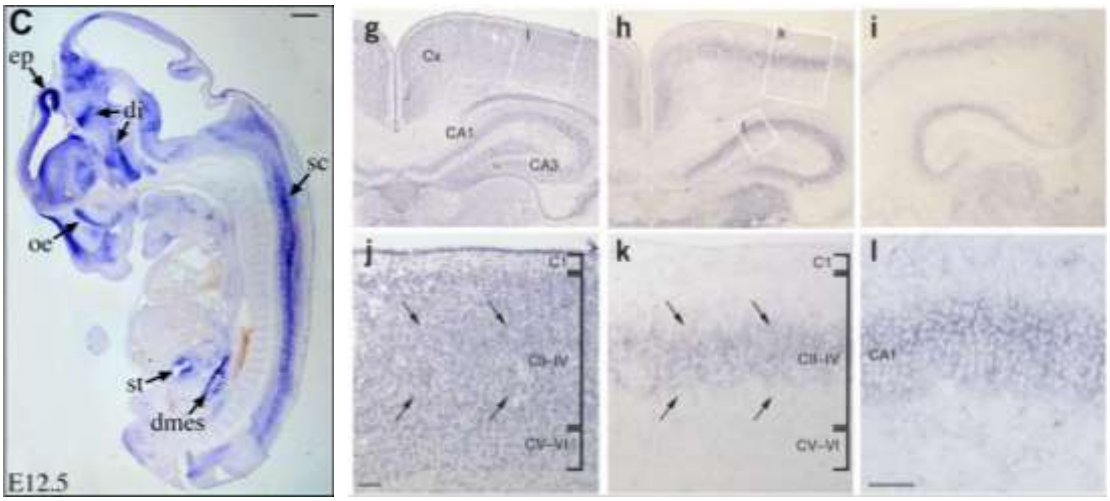

Figure 4-1. *Pcdh19* expression is widespread in the developing and postnatal mouse CNS. c) High *Pcdh19* mRNA levels were observed in multiple brain regions of sagittal 12.5 dpc embryo sections. di, diencephalons; dmes, dorsal mesentery; ep, epiphysis; oe, olfactory epithelium; sc, spinal cord. Scale bar 500 μm. Adapted from Gaitan and Bouchard (2006). g,h) Adjacent coronal section through the mid-hippocampal region stained with haematoxylin and eosin and processed for *Pcdh*19 *in situ* respectively. i) a more posterior brain section to h, showing *Pcdh*19 expression. j-l) Higher-magnification images of the boxed regions in g and h. Arrowheads in j and k showing *Pcdh*19 expression within cortical layers II-IV. Cx-cortex. Scale bars in a,b,f-I 200μM, in c-e, j-I 50μM. Adapted from Dibbens et al. (2008)

1.4 The Cadherin Superfamily

To comprehend how mutation of *PCDH19* leads to human disease it is important to understand its normal function. PCDH19 is a member of the protocadherin family, a subgroup of the cadherin superfamily.

Cadherins are calcium-dependent cell-cell adhesion molecules that play major roles in development, tissue morphogenesis, maintaining structural integrity of solid tissues and regulating turnover and reorganization of tissue structures (Gumbiner, 1996, 2005; Hatta and Takeichi, 1986; Hatta et al., 1988; Leckband and Prakasam, 2006; Patel et al., 2003; Takeichi, 1995; Takeichi et al., 1981). They are single-pass transmembrane proteins defined by multiple cadherin repeat sequences in their extracellular domain which mediate homotypic cell-cell adhesion. The links between these repeats are made more rigid and strengthened by the specific binding of Ca^{2+} ions (Boggon et al., 2002; Nagar et al., 1996). The intracellular domains of the different cadherins are variable, allowing different functional roles for each cadherin.

Cadherins are divided into three major subfamilies, the classical cadherins, desmosomal cadherins and the protocadherins (Figure 5-1). Classical cadherins were the first group to be discovered and can be split into two subfamilies; Type 1 and Type 2. They have common features such as five extracellular cadherin repeats and conserved cytoplasmic domains that interact with cytoskeletal proteins, most importantly α- and β-catenin. Absence of α- or β-catenin leads to defective cell-cell adhesion and failure of cadherin-catenin complexes to associate with the actin

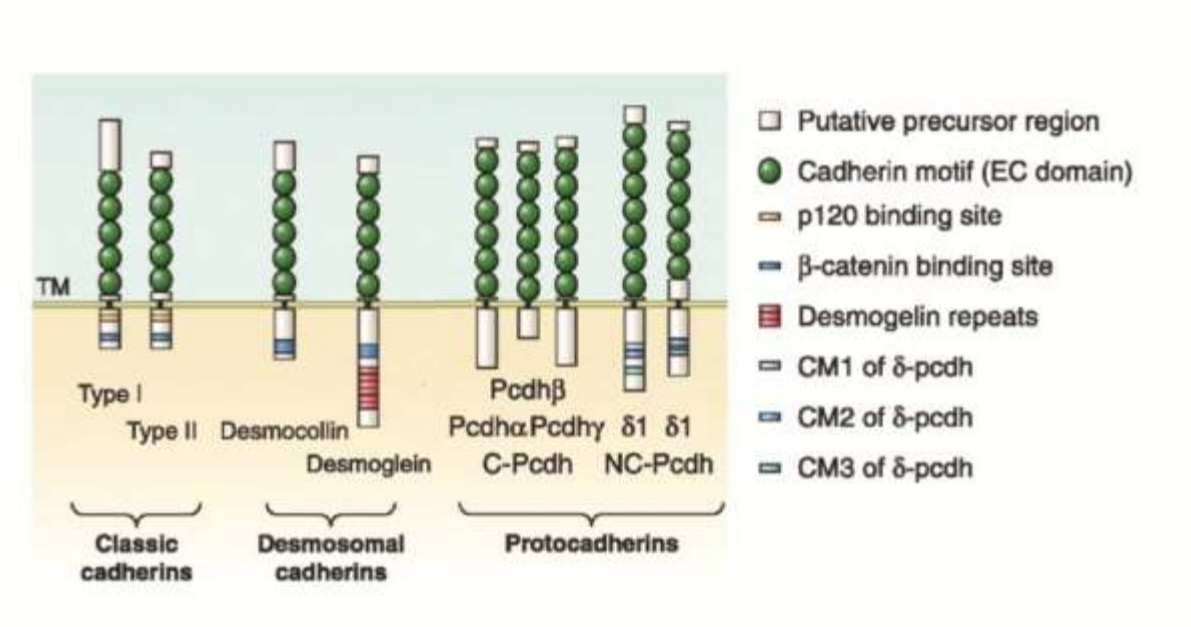

Figure 5-1. Cadherins are divided into three main subgroups. Variation occurs in the number of extracellular cadherin repeats present as well as the interaction domains in the cytoplasmic regions. Adapted from Hirano and Takeichi (2012).

cytoskeleton (Hatta and Takeichi, 1986; Pettitt, 2005). Type 1 classical cadherins contain an extracellular tryptophan residue (W2) and a corresponding hydrophobic pocket in the cadherin repeat sequence, while type 2 classical cadherins contain two conserved tryptophan residues (W2 and W4) and two hydrophobic pockets. The conserved tryptophan residues and hydrophobic pockets are critical for both homodimerization and cell-cell adhesion (Boggon et al., 2002). Desmosomal cadherins are highly similar to type 1 classical cadherins but contain 4 extracellular repeats and have a different cytoplasmic domain allowing connection to intermediate filaments. It is suggested that desmosomal cadherins are required for strong cell-cell adhesion but is unclear whether this is primarily due to homophilic or heterophilic interactions (Delva et al., 2009).

Protocadherins are structurally similar to classical cadherins however the conserved tryptophan residues are replaced with two cysteine residues that are thought to perform a similar function (Morishita et al., 2006). Currently more than 70 protocadherin genes have been identified, making up the largest subgroup of the cadherin family. Protocadherins are divided into two groups based on their genomic arrangement: clustered and non-clustered (Figure 6-1). Clustered protocadherins are grouped within the genome, encoding 58 transcripts from only three gene clusters located on the same chromosome. Non-clustered protocadherins are scattered throughout the genome and can be divided into two groups PCDHδ and "other" protocadherins. Clustered protocadherins have six extracellular cadherin repeats while members of the non-clustered family have between four and seven cadherin repeats (Kim et al., 2011; Morishita and Yagi, 2007; Redies et al., 2005). There are nine PCDHδ members, all of which contain two highly conserved regions (CM1 and CM2)

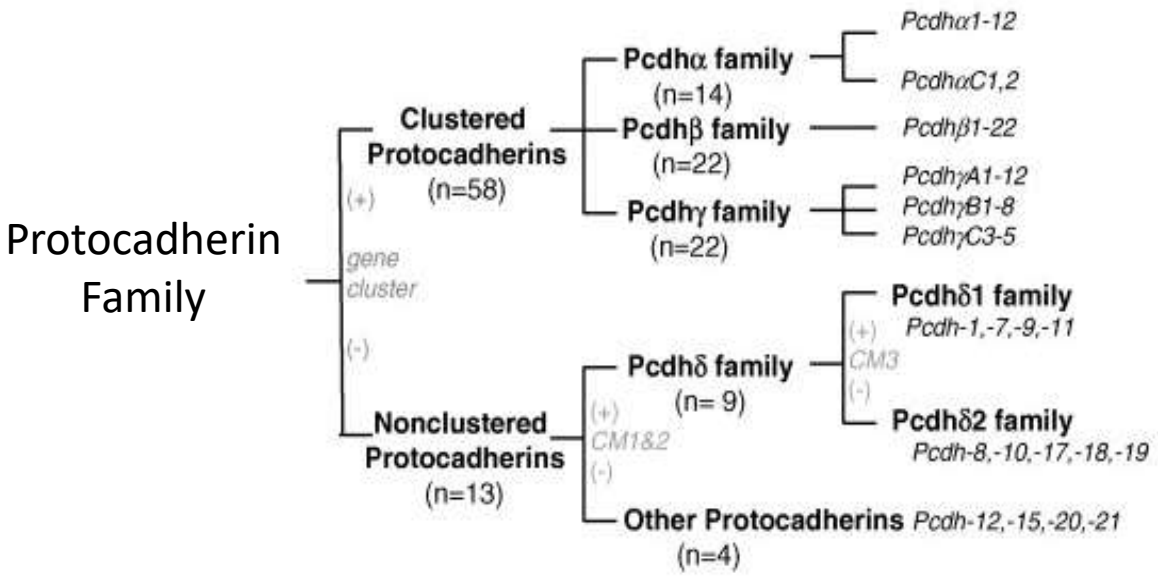

Figure 6-1. Clustered PCDHs consist of the α, β and γ subfamilies. Non-clustered PCDHs are divided into two groups, PCDHδ family and other PCDHs. PCDHδ members are further categorized by the presence/absence of a third highly conserved extracellular domain. Adapted from Morishita and Yagi (2007).

in their cytoplasmic domains (Morishita and Yagi, 2007). The PCDHδ family can be further divided into two subgroups depending on; overall homology, number of EC repeats present and conservation of specific amino acids within the cytoplasmic domain (Figure 6-1). The PCDHδ1 subgroup consists of Pcdh-1, 7, 9 and 11, and the PCDHδ2 subgroup contains PCDH-8, 10, 17, 18 and 19 (Morishita and Yagi, 2007). While the extracellular domain of protocadherins is essential for homotypic cell-cell interactions (Morishita and Yagi, 2007; Patel et al., 2003; Redies et al., 2005; Yagi and Takeichi, 2000) the cytoplasmic domains of protocadherins are structurally diverse and may have the ability to form novel interactions.

Overall PCDHs have homotypic adhesion function which is regulated through the extracellular domains, in contrast to the intracellular domains which are variable amongst family members and are hypothesised to have unique functions.

1.5 Adhesive Functions of Protocadherins in the Mammalian Brain

Protocadherins have been reported to be implicated in many different processes within the CNS including neuronal migration, organisation of different neuronal populations, synaptogenesis, ectoderm differentiation, neuronal self-avoidance, cytoskeletal changes and cell differentiation (Frank and Kemler, 2002; Hoshina et al., 2013a; Junghans et al., 2005; Lefebvre et al., 2012; Morishita and Yagi, 2007; Redies et al., 2005).

In recent years the adhesive function of clustered PCDHs has been proposed to be crucial for neuron identification of self from non-self within the mammalian brain, similar to the function of DSCAM genes in Drosophila (Soba et al., 2007). Deletion of clustered *Pcdhγ* genes disrupts the self-avoidance of neuronal processes in retinal starburst amacrine cells and Purkinje cells (Figure 7-1A, left) (Lefebvre et al., 2012). Furthermore replacement of the deleted *Pcdhγ* cluster with a single *Pcdhγ* isoform restores self-avoidance suggesting that homophilic adhesion interactions between neurites from the same neuron generate a repulsive signal leading to self-avoidance (Figure 7-1A, right) (Lefebvre et al., 2012). It has been proposed that interactions between different neurons are allowed to occur as dendrites will rarely encounter a matched set of clustered PCDHs, unless they originate from the same soma (Lefebvre et al., 2012). Therefore, it is crucial that each neuron in the brain expresses a unique combination of clustered PCDHs which is supported by the random expression pattern of clustered PCDHs which is dependent on *cis* regulatory elements that determine which members of the clusters are to be expressed (Ribich et al., 2006; Yokota et al., 2011). For example, Purkinje cells express ~2 of the 5' 12 *Pcdhα* isoforms, ~4 of the 5' 19 *Pcdhγ* members and ~4 of the 22 *Pcdhβ* isoforms while the 3' members of the α and γ clusters are expressed constitutively in all Purkinje cells (Yagi, 2012). This random pattern of expression in

A

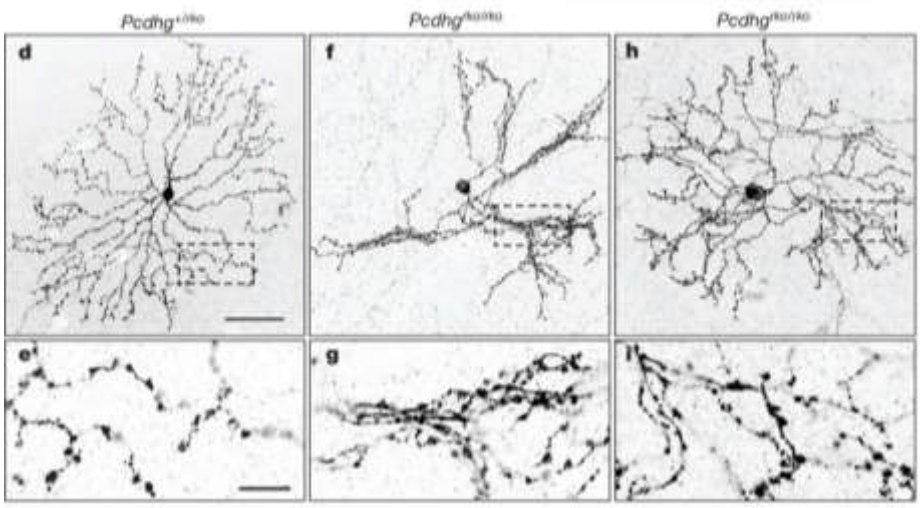
Pcdhg+/ko
Pcdhgko/ko
Pcdhgko/ko
d
f
h
e
g
i

B

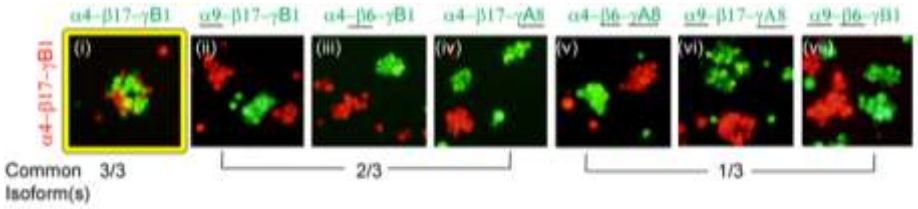
α4–β17–γB1
α9–β17–γB1
α4–β6–γB1
α4–β17–γA8
α4–β6–γA8
α9–β17–γA8
α9–β6–γB1
α4–β17–γB1
(i)
(ii)
(iii)
(iv)
(v)
(vi)
(vii)
Common Isoform(s) 3/3
2/3
1/3

C

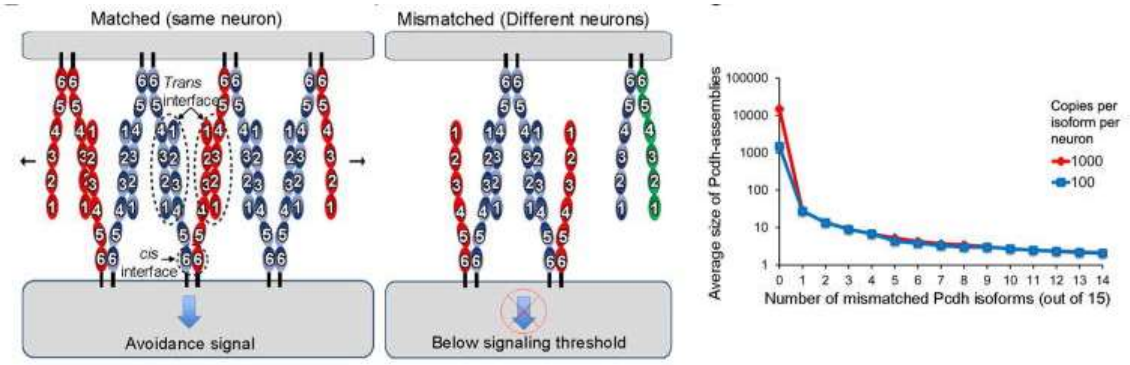
Matched (same neuron)
Mismatched (Different neurons)
Trans interface
cis interface
Avoidance signal
Below signaling threshold
Average size of Pcdh-assemblies
100000
10000
1000
100
10
1
0 1 2 3 4 5 6 7 8 9 10 11 12 13 14
Number of mismatched Pcdh isoforms (out of 15)
Copies per isoform per neuron
1000
100

Figure 7-1. Clustered PCDHs have a functional role in neuronal self-avoidance which is thought to arise by dictating specific interactions between cells. A) Deletion of all *Pcdh*γ members in starburst amacrine cells leads to increased amount of "self" interactions. This can be rescued by the expression of a single PCDHγ protein in PCDHγ null star amacrine cells. Adapted from Lefebvre et al. (2012) B) K562 cells expressing the same clustered PCDH combinations display extensive mixing. In contrast, mixing cells expressing different clustered PCDH combinations results in segregation of green and red cells. Adapted from Thu et al. (2014). C) A model for PCDH mediated cell-cell recognition based on lattice-like structures. A single mismatch of PCDH isoforms between cells terminates chain extension. It is proposed that interaction of clustered PCDHs leads to an avoidance event through an intracellular signalling. A repulsion signal is only achieved through the formation of extensive PCDH lattice molecules. Mathematical modelling predicts that the size of the PCDH lattice-like complex is dramatically reduced with just one PCDH mismatch between cells. Adapted from Rubinstein et al. (2015).

Purkinje cells suggests that almost every neuron in the brain will contain a different profile of clustered PCDH expression (Yagi, 2012).

The molecular logic of how clustered PCDHs determine self-avoidance has been investigated through a series of cell aggregation and structural modelling experiments (Goodman et al., 2016; Nicoludis et al., 2015, 2016; Rubinstein et al., 2015; Schreiner and Weiner, 2010; Thu et al., 2014). Using K562 cells (which express no classical cadherins or PCDHs) it was shown that homophilic interactions between different combinations of clustered PCDHs are dependent on all isoforms expressed, such that a single mismatched isoform disrupts adhesion of cells (Figure 7-1B) (Rubinstein et al., 2015; Schreiner and Weiner, 2010; Thu et al., 2014). Structural studies by multiple groups revealed that EC1-EC4 domains are critical for homophilic *trans* binding of PCDHs between adjacent cells and that the EC6 domain is essential for heterophilic *cis* interactions of different PCDHs within the same cell (Goodman et al., 2016; Nicoludis et al., 2015, 2016; Rubinstein et al., 2015). Rubinstein et al (2015) proposed a model whereby clustered PCDHs form *cis* heterodimers that engage in a head-to-tail homophilic *trans* interaction across two cells that form a zipper-like structure. When two neurites from the same cell interact large zipper-like PCDH complexes will form and lead to repulsive downstream signalling, but if two neurites from different cells interact the zipper-like structure will terminate due to the mismatch in PCDHs providing a size dependent mechanism for self-avoidance (Figure 7-1C) (Rubinstein et al., 2015). It is thought that only large lattice structures will generate sufficient avoidance signalling to cause neurite repulsion, in contrast to smaller mismatched lattice structures where the avoidance signalling will be below the repulsion threshold.

The homophilic function of *Pcdhγ* isoforms has also been shown to regulate synapse formation between distant neurons and deletion of the *Pcdhγ* cluster in cortical and

hippocampal neurons leads to simplified dendritic arbors (Garrett et al., 2012; Kostadinov and Sanes, 2015; Suo et al., 2012). Furthermore, the homotypic adhesive function of *Pcdhγ* molecules promotes dendritic arborisation at local sites between neurons and between neurons and astrocytes (Molumby et al., 2016).

The degree of functional overlap between clustered and non-clustered PCDHs is unclear and in particular whether PCDH19 and other non-clustered PCDHs act combinatorially has not been addressed. Combinatorial activity of non-clustered PCDHs may be possible given that the expression of non-clustered PCDHs spatially overlap in the developing and postnatal rat CNS and individual neurons in the mouse somatosensory cortex have been shown to express multiple non-clustered PCDH molecules (Figure 8-1) (Kim et al., 2007, 2010; Krishna-K et al., 2011). Furthermore *in vitro* bead assays showed that PCDH19 interacts with N-cadherin (N-CAD) to form a novel adhesion complex that cannot form *trans* interactions with PCDH19 or N-CAD alone (Emond et al., 2011). This is reminiscent of the combinatorial activity of the clustered PCDHs and supports the potential for PCDH19 to interact with adhesion molecules including non-clustered PCDHs to form combinatorial adhesion specificity.

Additionally, the non-stochastic nature of non-clustered PCDH expression suggests that combinatorial adhesive codes dictated by this group of molecules will play roles in guiding neurons to coalesce/form connections with other appropriate neurons, rather than providing unique identity to each neuron.

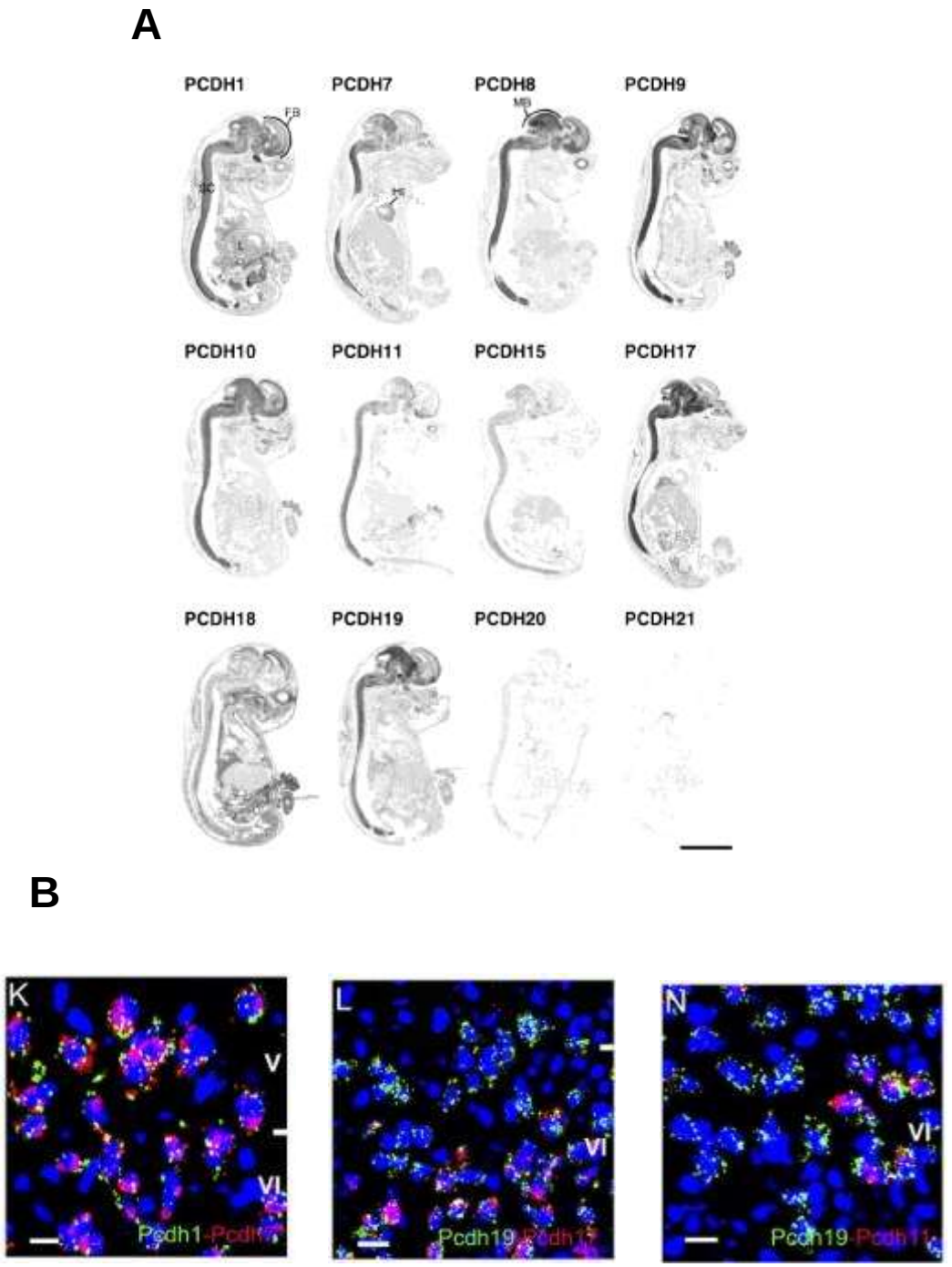

Figure 8-1. Non-clustered PCDHs display overlapping expression in the developing and postnatal rodent cortex. A) In situ hybridisation of rat embryos displays overlapping expression of many non-clustered PCDHs in the CNS. Adapted from (Kim et al., 2007). B) Double fluorescent in situ hybridisation of the mouse somatosensory cortex shows that multiple non-clustered PCDHs are expressed within the same neuron. Adapted from Krishna-K et al. (2011).

1.6 Neural Function of PCDH19

To date the endogenous function of PCDH19 has not been investigated in a mammalian brain, primarily being limited to studies performed *in vitro* and using the model organism *Danio rerio* (zebrafish).

Cell culture assays have been utilised to show PCDH19 can cause calcium dependent cell aggregation (Tai et al., 2010). Additionally, cells expressing PCDH19 were labelled and mixed with cells expressing PCDH10 and both populations formed aggregates predominantly containing either PCDH19 or PCDH10 cells, confirming the homotypic adhesion function of PCDH19 (Tai et al., 2010). The function of endogenous PCDH19 has been investigated in zebrafish using knock down and knock out approaches (Cooper et al., 2015; Emond et al., 2009). Unfortunately, these studies provided conflicting results making it difficult to interpret the role of PCDH19 in the CNS. Morpholino injections targeting *pcdh19* resulted in a significant knockdown of *pcdh19* gene expression (Emond et al., 2009). Morphant embryos exhibited a misfolded midbrain-hindbrain region compared to wild type embryos at 28 hours post fertilisation. At the 10 somite stage *pcdh19* morphants exhibited malformations of the anterior neural rod, displayed impaired convergent cell movements in the lateral plate and a significantly wider neural plate. Knockdown of *pcdh19* also resulted in cell motility defects in the anterior neural plate including a decrease in the directional specificity and a reduced level of coupled migration with neighbouring cells. A second study deleted *pcdh19* in zebrafish using TALEN genome editing technology (Cooper et al., 2015). In contrast to the above mentioned study, Pcdh19 null zebrafish were viable and fertile and did not display any defects in neural plate morphology. However, disruption of columnar organisation in the optic tectum was observed leading to defects of visually guided behaviours. These data suggest a role for Pcdh19 in organisation of the developing nervous system. However, the conflicting phenotypes resulting from knock down versus knock out

experiments makes it difficult to interpret the endogenous role of Pcdh19 in the mammalian brain and to gain insight into how mutation leads to disease.

The adhesive roles of multiple non-clustered PCDHs in the mammalian brain have been investigated using genetically modified mice (Hayashi et al., 2014; Hoshina et al., 2013b; Uemura et al., 2007; Yamagata et al., 1999; Yasuda et al., 2007). *Pcdh17* null mice have been shown to have defects in both the regulation of presynaptic assembly in corticobasal ganglia circuits and abnormalities in axon projections from the amygdala to the hypothalamus (Hayashi et al., 2014; Hoshina et al., 2013a). Similarly, *Pcdh10* deficient mice have defects in axonal pathways through the ventral telencephalon (Uemura et al., 2007). Studies of *Pcdh7* and *Pcdh8* in mice have revealed their roles in retinal ganglion cell dendrite arborisation and disruption of axonogenesis and the regulation of dendritic spine density and synaptogenesis, respectively (Leung et al., 2013; Piper et al., 2008). The cytoplasmic domains of PCDH17, PCDH10 and PCDH8 are also likely to play a role in axon guidance as they have been shown to interact with the WAVE regulatory complex which controls actin cytoskeletal dynamics (Chen et al., 2014). PCDH19 has also been reported to interact with WAVE complex proteins and therefore could also be implicated in the process of axon guidance (Chen et al., 2014).

As non-clustered PCDHs are highly conserved amongst members these studies provide us with insights into possible functions of PCDH19 in the mammalian brain.

1.7 What causes the unusual inheritance of *PCDH19*-GCE?

The most striking characteristic of *PCDH19*-GCE is its unique pattern of X-linked inheritance. This feature is poorly understood as current model organism studies have been limited to zebrafish where *pcdh19* is positioned on chromosome 14. To date multiple theories have been proposed to explain the unique pattern of inheritance but there is a lack of supporting evidence.

Given that males with *PCDH19* mutations (hemizygous) do not develop seizures and have normal cognitive function, it is suggested that the complete loss of PCDH19 is not pathogenic. On the other hand, females with one wild type and one mutated allele of *PCDH19* (heterozygous) are affected. Therefore it was initially proposed that *PCDH19* mutations were dominant negative, but the identification of whole gene deletions and cases of nonsense mediated decay provided strong evidence opposing this hypothesis (Dibbens et al., 2008). It was also suggested that males may be able to compensate for the loss of PCDH19 through the Y-linked PCDH11Y. However, this has also been ruled out due to the discovery of several mosaic males with early somatic mutations in PCDH19, that phenocopy affected girls with heterozygous mutations (Depienne et al., 2009; Terracciano et al., 2016). The current withstanding hypothesis proposes that the coexistence of WT and mutant PCDH19 neurons arising through random X-inactivation underlie the unique pattern of inheritance (Figure 9-1) (Depienne et al., 2009; Dibbens et al., 2008). It is suggested that this mosaicism leads to abnormal neuronal connections between PCDH19 WT and PCDH19 mutant cells affecting neural network formation. However, it remains to be determined how mosaicism could lead to *PCDH19*-GCE at the molecular, cellular and network level. Furthermore, this is unable to explain how the complete absence of PCDH19 does not result in epilepsy.

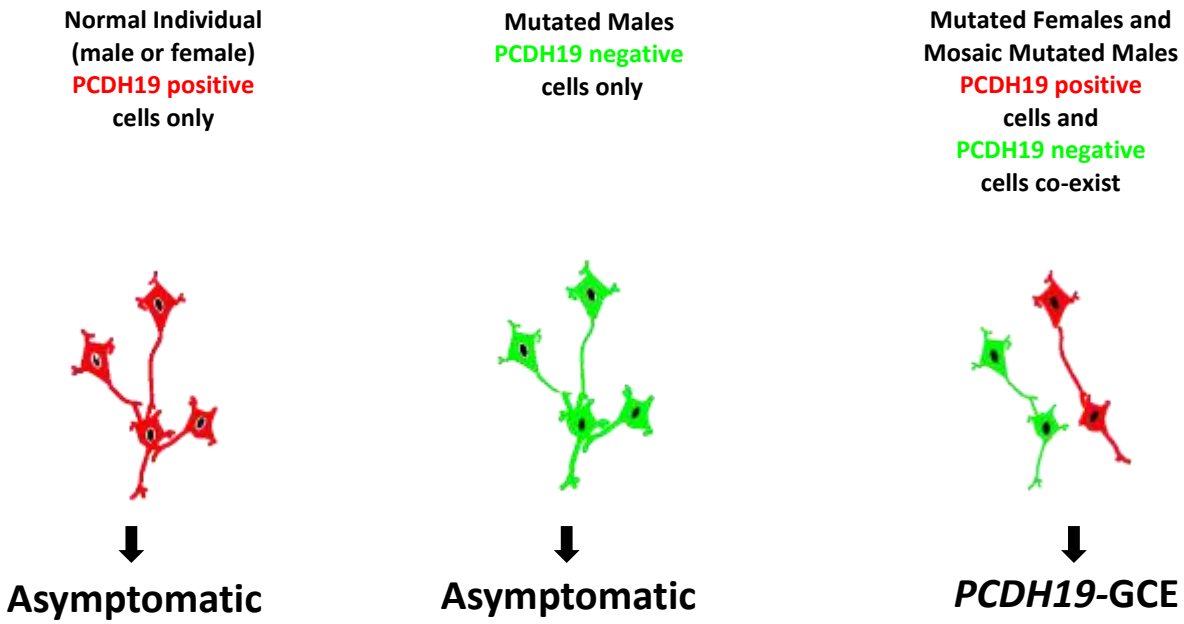

Figure 9-1. *PCDH19*-GCE is proposed to be caused by abnormal connections between PCDH19 positive and PCDH19 negative neurons. A) Normal individuals will have one population of PCDH19 containing cells and will be able to form proper neural networks. B) Similarly, hemizygous males will have population of PCDH19 negative cells and will form normal neuronal connections like normal individuals. C) Heterozygous females have two populations of cells, PCDH19 positive and PCDH19 negative, which cannot interact with each other to form appropriate neural networks, leading to disease. Adapted from Depienne et al. (2009).

1.8 *Pcdh19* Null Mouse

Genetically manipulated mice are commonly used to understand how genetic mutations contribute to disease phenotypes. By knocking in or knocking out genes implicated in disease the functional role proteins play in disease and the phenotype can be studied, leading to better understanding of the disease and potential new treatments for humans.

As *Pcdh*19 is also X-linked in mice a suitable approach to investigate to the cellular and molecular basis of *PCDH19*-GCE would be to generate a mouse model in which *Pcdh19* is mutated to mimic a human *PCDH19*-GCE mutation. However, this approach assumes that the pathogenic mechanism underpinning *PCDH19*-GCE is conserved in mouse and human.

Epilepsy has an obvious seizure phenotype providing an accessible target to study as a complex trait in experimental animal models. Several examples of laboratory mice exist that model epilepsy, including *Cntnap2* deficient mice, which model temporal lobe epilepsy (Buckmaster and Lew, 2011; Peñagarikano et al., 2011). Spontaneous mouse models of epilepsy also exist in the form of DBA mice which experience severe tonic-clonic seizures in response to audiogenic stimuli (Hall, 1947) and the EL mouse strain which has limbic and tonic-clonic convulsions that are induced by routine animal handling (Rise et al., 1991; Suzuki and Yurie, 1977).

With this in mind we acquired a potential disease mouse model for *PCDH19*-GCE. Lexicon Pharmaceuticals engineered a mouse where exon 1,2 and 3 of the *Pcdh19* gene are replaced with a β-galactosidase/neomycin fusion cassette as selection markers. Exon 1, 2 and 3 encode the entire extracellular and transmembrane region so by deleting these regions it should result in loss of PCDH19 function. Since it is thought that *PCDH19*-GCE mutations are loss-of-function it was hypothesised that the *Pcdh19* mutant mouse could be used to model *PCDH19*-GCE and gain insight into the cellular and molecular cause of the disease.

1.9 Project Rationale

PCDH19 is a homotypic cell-cell adhesion molecule, which when mutated causes epilepsy and cognitive impairment in humans. *PCDH19*-GCE has a unique X-linked inheritance pattern whereby heterozygous females are affected and hemizygous males are not. It has been proposed that abnormal neuronal interactions occur between PCDH19 WT and PCDH19 mutant cells in the brain of heterozygous females leading to disease. However, the molecular and cellular mechanism causing disease is unknown. Furthermore, it is not understood how the complete absence of PCDH19 in hemizygous males does not lead to pathology. These are the key questions that will be investigated in the research of this thesis, with the aims of:

1. Characterising the endogenous function of PCDH19 in the mammalian brain.

2. Investigating the cellular mechanism that underlies the unique inheritance pattern of *PCDH19*-GCE.

CHAPTER 2

Pcdh19 Loss-of-Function Increases Neuronal Migration *In Vitro* but is Dispensable for Brain Development in Mice

Daniel T. Pederick, Claire C. Homan, Emily J. Jaenhe, Sandra G. Piltz, Bryan P. Haines, Bernhard T. Baune, Lachlan A. Jolly, James N. Hughes, Jozef Gecz and Paul Q. Thomas

Published in: *Scientific Reports* 2016. *6*, 26765.

2.1 Summary

Using cultured cell assays PCDH19 has been shown to have weak homotypic cell-cell adhesion activity, interact with N-cadherin to form novel adhesion complexes and interact with various members of the WAVE complex (Emond et al., 2011; Tai et al., 2010). To understand the endogenous role of PCDH19 in the CNS the majority of studies have used zebrafish as a model organism. Two independent studies using morpholino knockdown of *pcdh19* or TALEN mediated null zebrafish gave severe and mild phenotypes, respectively (Cooper et al., 2015; Emond et al., 2009). These conflicting data make it difficult to interpret the endogenous function of PCDH19 in the CNS. Furthermore, the endogenous role of PCDH19 in the mammalian brain has yet to be investigated and therefore was addressed in the paper presented in this chapter entitled "*Pcdh19* Loss-of-Function Increases Neuronal Migration *In Vitro* but is Dispensable for Brain Development in Mice".

In this paper we validated the first *Pcdh19* null allele in mice confirming the expression of PCDH19 protein in the hippocampus, cortex and cerebellum. We also showed that the *β-Galactosidase/Neomycin* reporter allele, marking *Pcdh19* null cells, was expressed in the same brain regions. We confirmed the expression of PCDH19 in the synapses of hippocampal neurons and ruled out the presence of gross morphological defects in the brains of *Pcdh19* heterozygous and homozygous null mice. We also showed that *Pcdh19* null cells were not ectopically located in the developing and postnatal brains of *Pcdh19* heterozygous and homozygous null mice. Furthermore, we showed a subtle increase in neuronal migration potential of *Pcdh19* null cells *in vitro* although this did not translate to overt positional changes of neurons in the developing and adult mouse brain. While further detailed analysis of this mouse model may reveal subtle defects in *Pcdh19* null mouse brains, overall we show that despite widespread expression of *Pcdh19* in the CNS, deletion of *Pcdh19* does not grossly affect brain develop

Statement of Authorship

Title of Paper	Pcdh19 Loss-of-Function Increases Neuronal Migration In Vitro but is Dispensable for Brain Development in Mice
Publication Status	☑ Published ☐ Accepted for Publication ☐ Submitted for Publication ☐ Unpublished and Unsubmitted work written in manuscript style
Publication Details	Pederick, D.T., Homan, C.C., Jaehne, E.J., Piltz, S.G., Haines, B.P., Baune, B.T., Jolly, L.A., Hughes, J.N., Gecz, J., and Thomas, P.Q. (2016). Pcdh19 Loss-of-Function Increases Neuronal Migration In Vitro but is Dispensable for Brain Development in Mice. Sci. Rep. 6, 26765.

Principal Author

Name of Principal Author (Candidate)	Daniel Pederick
Contribution to the Paper	Conceived, designed and performed experiments, generated reagents, analysed data and wrote manuscript.
Overall percentage (%)	90%
Certification:	This paper reports on original research I conducted during the period of my Higher Degree by Research candidature and is not subject to any obligations or contractual agreements with a third party that would constrain its inclusion in this thesis. I am the primary author of this paper.
Signature	Date 17.10.16

Co-Author Contributions

By signing the Statement of Authorship, each author certifies that:

i. the candidate's stated contribution to the publication is accurate (as detailed above);
ii. permission is granted for the candidate in include the publication in the thesis; and
iii. the sum of all co-author contributions is equal to 100% less the candidate's stated contribution.

Name of Co-Author	Claire Homan
Contribution to the Paper	Performed neuronal migration assay experiments.
Signature	Date 17.10.16

Name of Co-Author	Emily Jaehne
Contribution to the Paper	Conceived and designed experiments.
Signature	Date 17.10.16

Name of Co-Author	Sandra Piltz
Contribution to the Paper	Assisted with animal care and husbandry.
Signature	Date 17/10/16

Name of Co-Author	Bryan Haines
Contribution to the Paper	Conceived and designed experiments.
Signature	Date 19.10.16

Name of Co-Author	Bernhard Baune
Contribution to the Paper	Conceived and designed experiments.
Signature	Date 17.10.16

Name of Co-Author	Lachlan Jolly
Contribution to the Paper	Supervised, conceived and designed experiments, analysed data.
Signature	Date 9.2.17

Name of Co-Author	James Hughes		
Contribution to the Paper	Supervised, conceived and designed experiments, analysed data and wrote manuscript.		
Signature		Date	17.10.16

Name of Co-Author	Jozef Gecz		
Contribution to the Paper	Supervised, conceived and designed experiments, analysed data and wrote manuscript.		
Signature		Date	20.10.16

Name of Co-Author	Paul Thomas		
Contribution to the Paper	Supervised, conceived and designed experiments, analysed data and wrote manuscript.		
Signature		Date	17/10/16

www.nature.com/scientificreports

SCIENTIFIC REPORTS

OPEN

Pcdh19 Loss-of-Function Increases Neuronal Migration *In Vitro* but is Dispensable for Brain Development in Mice

Received: 25 February 2016
Accepted: 28 April 2016
Published: 31 May 2016

Daniel T. Pederick[1,2], Claire C. Homan[1,2], Emily J. Jaehne[3], Sandra G. Piltz[1,2], Bryan P. Haines[1,2], Bernhard T. Baune[3], Lachlan A. Jolly[2,3], James N. Hughes[1,2], Jozef Gecz[1,2,3] & Paul Q. Thomas[1,2]

Protocadherin 19 (*Pcdh19*) is an X-linked gene belonging to the protocadherin superfamily, whose members are predominantly expressed in the central nervous system and have been implicated in cell-cell adhesion, axon guidance and dendrite self-avoidance. Heterozygous loss-of-function mutations in humans result in the childhood epilepsy disorder *PCDH19* Girls Clustering Epilepsy (*PCDH19* GCE) indicating that *PCDH19* is required for brain development. However, understanding *PCDH19* function *in vivo* has proven challenging and has not been studied in mammalian models. Here, we validate a murine *Pcdh19* null allele in which a *β-Geo* reporter cassette is expressed under the control of the endogenous promoter. Analysis of *β-Geo* reporter activity revealed widespread but restricted expression of *PCDH19* in embryonic, postnatal and adult brains. No gross morphological defects were identified in *Pcdh19*$^{+/\beta\text{-Geo}}$ and *Pcdh19*$^{Y/\beta\text{-Geo}}$ brains and the location of *Pcdh19* null cells was normal. However, *in vitro* migration assays revealed that the motility of *Pcdh19* null neurons was significantly elevated, potentially contributing to pathogenesis in patients with *PCDH19* mutations. Overall our initial characterization of *Pcdh19*$^{+/\beta\text{-Geo}}$, *Pcdh19*$^{\beta\text{-Geo}/\beta\text{-Geo}}$ and *Pcdh19*$^{Y/\beta\text{-Geo}}$ mice reveals that despite widespread expression of *Pcdh19* in the CNS, and its role in human epilepsy, its function in mice is not essential for brain development.

Protocadherins comprise a large family of single pass transmembrane glycoproteins that have important roles in cell-cell adhesion, dendrite self-avoidance and axon guidance. In mammals, ~70 protocadherin genes have been identified, the majority of which are located in three genomic "clusters" termed α, β and γ. The remainder, termed "non-clustered protocadherins" are scattered throughout the genome and are classified as δ1, δ2 and "other". Non-clustered protocadherins are widely expressed in the central nervous system and have been implicated in homotypic cell adhesion, neuronal migration and synaptic plasticity[1–4].

Pcdh19 is an X-chromosome linked member of the δ2 protocadherin subfamily and is highly expressed in the developing mouse cortex and hippocampus[5]. *PCDH19* is highly conserved across human, mouse, zebrafish and chicken and has weak homotypic cell adhesion properties. It has been shown to interact with N-cadherin and members of the WAVE complex (Nap1 and Cyfip2) suggesting a role in actin cytoskeletal dynamics[6,7]. Genetic disruption of the closely related *Pcdh10* or *Pcdh17* genes (members of the δ2 subfamily) in mice have revealed roles in axon extension, regulation of presynaptic assembly and growth of striatal axons and thalamocortical projections[8–10]. These studies raise the possibility *Pcdh19* functions similarly during mouse brain development; however this remains unexplored due to the lack of a validated *Pcdh19* null mouse.

The majority of studies investigating the endogenous role of *Pcdh19* have been performed in zebrafish[11–15]. These studies have utilized either morpholino knockdown or mutation of *Pcdh19* with each approach producing different phenotypes. Morpholino knockdown results in a severe phenotype where cell motility in the neural plate is compromised resulting in a severe disruption to early brain morphogenesis[13]. In contrast, *pcdh19* null zebrafish generated by TALEN-induced frame-shift mutation are viable and fertile, and exhibit disruption of

[1]School of Biological Sciences, The University of Adelaide, Adelaide, South Australia 5005, Australia. [2]Robinson Research Institute, University of Adelaide, Adelaide, South Australia 5005, Australia. [3]School of Medicine, The University of Adelaide, Adelaide, South Australia 5005, Australia. Correspondence and requests for materials should be addressed to P.Q.T. (email: paul.thomas@adelaide.edu.au)

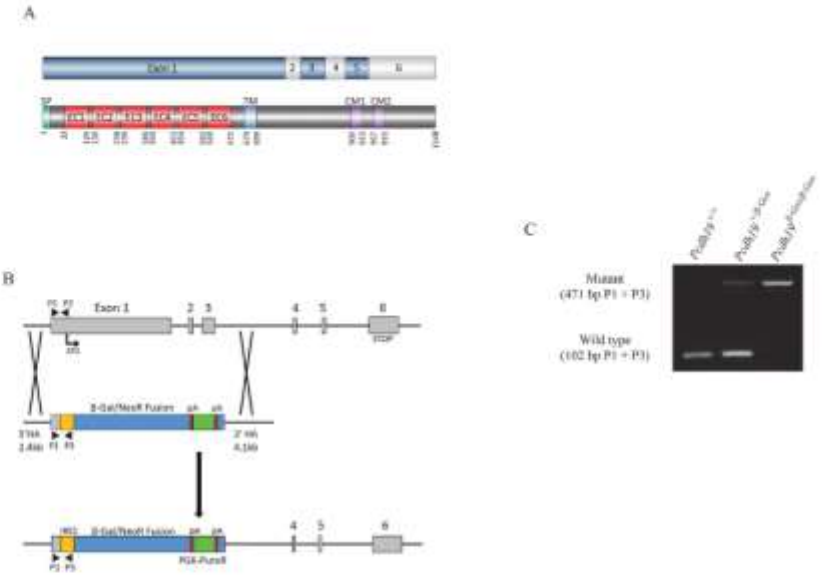

Figure 1. Generation of *Pcdh19* Null Mice. (**A**) *Pcdh19* contains 6 exons. Exon 1 encodes more than half of the protein including the entire extracellular domain and transmembrane domain. (**B**) *Pcdh19* null mice were generated by Taconic through targeted homologous recombination. Exon 1, 2 and 3 were removed and replaced with a *β-Galactosidase-Neomycin* fusion cassette. (**C**) PCR was used to confirm the presence of the β-Galactosidase/Neomycin fusion cassette with primers P1, P2 and P3 (black arrowheads in **B**). The *β-Galactosidase-Neomycin* fusion cassette was only present in $Pcdh19^{+/\beta\text{-}Geo}$ and $Pcdh19^{Y/\beta\text{-}Geo}$ mice.

columnar architecture in the optic tectum resulting in impaired visually guided behaviours[22]. While these data support a role for *pcdh19* in cell-cell recognition during zebrafish brain development, the discordance between the mutant and morphant phenotypes, which is commonly observed in zebrafish[14], makes interpretation of these data difficult.

In humans, heterozygous *PCDH19* mutations cause *PCDH19* GCE[5,15] which is now recognized as the second most common cause of monogenic epilepsy[16]. Mutations of *PCDH19* that cause *PCDH19* GCE are mainly missense, however as some cases have complete gene deletions, all pathogenic mutations are almost certainly loss-of-function. The phenotype of *PCDH19* GCE is variable – affected girls present with symptoms ranging from benign focal epilepsy with normal cognitive function to severe seizures and intellectual disability that resemble Dravet syndrome[16,17]. The inheritance pattern of *PCDH19* GCE is highly unusual for an X-linked gene, and is described as X-linked dominant with male sparing i.e. heterozygous females are affected whereas hemizygous males are not. Due to random X-chromosome inactivation affected females are composed of a mosaic population of normal and *PCDH19* mutant cells. Intriguingly, rare cases of affected males have also been described, which arise from somatic mutation and also display mosaicism[5,18]. It has been proposed that the mosaicism of normal *PCDH19* and mutant expressing cells leads to 'scrambling' of the neuronal circuitry in the brain of affected individuals. However, experimental support for this 'cellular interference' model remains limited.

Here we investigate the *in vivo* expression and function of *Pcdh19* using mutant mice where the *Pcdh19* gene is disrupted by a *β-galactosidase-neomycin* (*β-Geo*) reporter cassette. At this allele, *β-Geo* was expressed under the control of the endogenous *Pcdh19* promoter, whilst *Pcdh19* expression itself was ablated (i.e. a knock-out allele). Using *β-Geo* expression and X-Gal staining we show that *Pcdh19* expression is widely expressed in the developing CNS through to adulthood. Although brain morphology in $Pcdh19^{Y/\beta\text{-}Geo}$, $Pcdh19^{\beta\text{-}Geo/\beta\text{-}Geo}$ and $Pcdh19^{+/\beta\text{-}Geo}$ mutants appears grossly normal, *in vitro* analysis indicates that *Pcdh19* null neurons have a slight but significant increase in motility. These data suggest more subtle roles for *Pcdh19* beyond establishment of gross brain architecture.

Results

Generation and validation of a *Pcdh19* null mouse model. The *Pcdh19* gene contains six exons, with exon 1 encoding the majority of the protein including the entire extracellular and transmembrane domains (Fig. 1A). To investigate the physiological role of *Pcdh19* and the molecular pathology of *PCDH19* GCE, we acquired a *Pcdh19* null mouse model in which exons 1–3 were replaced with a *β-geo* cassette (Fig. 1B). Removal of the first 3 exons leads to deletion of both the extracellular and transmembrane domains of *PCDH19*. The genetic disruption of *Pcdh19* gene was validated by PCR of genomic DNA (Fig. 1C) and ablation of *Pcdh19* expression confirmed by qPCR of 2 week old hippocampal cDNA (Supplementary Fig. 1).

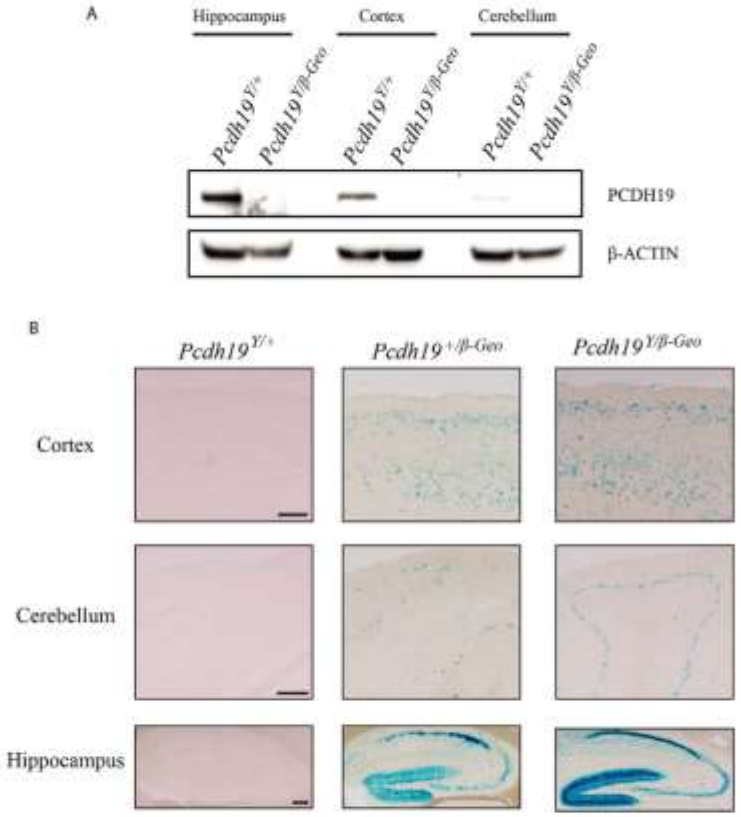

Figure 2. Validation of *Pcdh19* Null mice. (**A**) Protein extracts from hippocampus, cortex and cerebellum brain regions were immunoblotted with *PCDH19* antibody. *PCDH19* was detected in wild type extracts but was absent from $Pcdh19^{Y/\beta\text{-}Geo}$ extracts. (**B**) Frozen sections from the same regions as A) were stained for 3-Galactosidase activity using X-Gal. Staining was present in both $Pcdh19^{+/\beta\text{-}Geo}$ and $Pcdh19^{Y/\beta\text{-}Geo}$ brain sections but absent from wild type brain sections. Scale bar represents 250 μm.

Previous *in situ* hybridisation analysis has demonstrated *Pcdh19* expression in the hippocampus and cortex of postnatal mouse brains[5]. However, expression of endogenous *PCDH19* protein has not been shown. To investigate this issue, we performed western blot analysis using a commercially available *PCDH19* antibody. Consistent with mRNA expression data, robust expression was observed in the hippocampus and cortex (Fig. 2A).

Integration of the *β-geo* cassette into the *Pcdh19* locus potentially provides a reporter allele for null cells that would normally express *Pcdh19*. To confirm the activity of the *β-geo* cassette, X-Gal staining was performed on brain tissue from $Pcdh19^{Y/\beta\text{-}Geo}$, $Pcdh19^{+/\beta\text{-}Geo}$ and $Pcdh19^{+/Y}$ mice. $Pcdh19^{Y/\beta\text{-}Geo}$ brains exhibit positive staining in multiple brain regions including the hippocampus, cortex and cerebellum (Fig. 2B) which is consistent with western blot analysis (Fig. 2A) and previously published RNA expression data[5]. $Pcdh19^{+/\beta\text{-}Geo}$ brains showed staining in the same brain regions but exhibited a mosaic staining pattern (Fig. 2B). $Pcdh19^{+/Y}$ brains showed no staining. This confirms the *β-Geo* cassette is active and that *Pcdh19* undergoes random X-inactivation across multiple tissues similar to results in humans[19].

Chemical fractionation of adult hippocampal samples revealed that *PCDH19* was present within the synaptosome, providing evidence for a role in synaptic function (Fig. 3A). Importantly, no signal was detected in $Pcdh19^{Y/\beta\text{-}Geo}$ samples, further confirming *PCDH19* loss-of-function in this KO mouse model. Furthermore overexpression of FLAG tagged human *PCDH19* (*PCDH19*-FLAG) in primary hippocampal mouse neurons revealed *PCDH19* localisation with SYNAPSIN further supporting *PCDH19* expression in synapses (Fig. 3B).

$Pcdh19^{+/\beta\text{-}Geo}$, $Pcdh19^{\beta\text{-}Geo/\beta\text{-}Geo}$ and $Pcdh19^{Y/\beta\text{-}Geo}$ Mice have No Gross Phenotypic Abnormalities. Breeding of the *Pcdh19* mouse model generated $Pcdh19^{+/\beta\text{-}Geo}$, $Pcdh19^{\beta\text{-}Geo/\beta\text{-}Geo}$ and $Pcdh19^{Y/\beta\text{-}Geo}$ mice at the expected frequencies (Supplementary Fig. 2). Adult mice with these genotypes had normal body size and did not exhibit any overt health issues (data not shown). To date, spontaneous seizures have not been detected in $Pcdh19^{+/\beta\text{-}Geo}$, $Pcdh19^{\beta\text{-}Geo/\beta\text{-}Geo}$ or $Pcdh19^{Y/\beta\text{-}Geo}$ mice after weaning (ie. from 3 weeks of age).

Morpholino knock-down of *pcdh19* in zebrafish embryos results in profound CNS abnormalities. We therefore examined gross brain morphology in *Pcdh19* null mice. Histological analysis of $Pcdh19^{+/\beta\text{-}Geo}$, $Pcdh19^{\beta\text{-}Geo/\beta\text{-}Geo}$

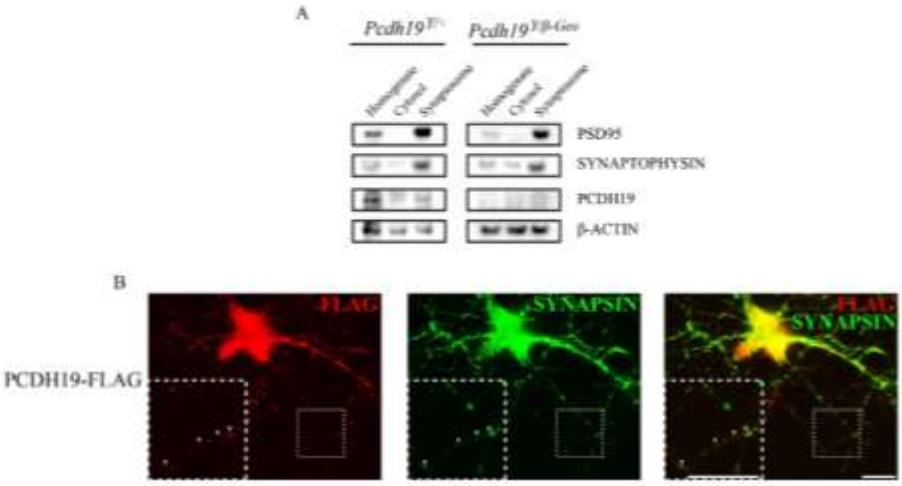

Figure 3. *PCDH19* is expressed in the synapses of hippocampal neurons. (**A**) Synaptosome fractionation of P14 mouse hippocampus was performed and immunoblotted for *PCDH19*. *PCDH19* protein was present in the synaptosome fraction which was also enriched for the synapse proteins PSD95 and SYNAPTOPHYSIN. *PCDH19* was absent from all *Pcdh19*$^{T/\beta\text{-}Geo}$ fractions. (**B**) Primary neurons were harvested from 18.5 dpc hippocampi and nucleofected with *PCDH19*-FLAG ORF. Immunostaning at DIV12 shows *PCDH19* is colocalised with SYNAPSIN positive synapses. Scale bar represents 20μm.

and *Pcdh19*$^{T/\beta\text{-}Geo}$ brains showed no gross morphological abnormalities (Fig. 4A). As *Pcdh19* is highly expressed in the hippocampus and cortex, we performed morphometric analysis of these regions to determine if more subtle defects may be present. Measurements were made of the cortical thickness and CA1 region of the hippocampus with no significant difference observed in *Pcdh19*$^{+/\beta\text{-}Geo}$, *Pcdh19*$^{\beta\text{-}Geo/\beta\text{-}Geo}$ and *Pcdh19*$^{T/\beta\text{-}Geo}$ adult brains compared with *Pcdh19*$^{+/-}$ and *Pcdh19*$^{T/-}$ controls (Fig. 4B). We therefore conclude that mutation of *Pcdh19* in mice does not overtly affect brain structure.

***Pcdh19* Null Cells are Located Normally in the Developing and Adult Brain.** Previous studies in zebrafish have shown that morpholino knockdown of *Pcdh19* results in severe disruption of brain morphogenesis due to an arrest of cell convergence in the anterior neural plate as well as abnormal cell migration during neurulation[11,13], although this was not seen in *pcdh19* null zebrafish[12]. To investigate whether mutation of *Pcdh19* in mice affects neuronal migration during brain development we looked for ectopic localisation of *β-Geo* positive cells in developing (15.5 dpc) brains of *Pcdh19*$^{+/\beta\text{-}Geo}$ and *Pcdh19*$^{T/\beta\text{-}Geo}$ mice using X-gal staining. As the *Pcdh19*-specific antibody used for western blot analysis was not compatible with immunohistochemistry (data not shown), wild type *Pcdh19*-expressing cells were identified by *in situ* hybridisation. At 15.5 dpc, robust *Pcdh19* expression was detected in the developing cortex and hippocampus of *Pcdh19*$^{T/+}$ brains (Fig. 5A). Wild type *Pcdh19*-expressing cells were also present in the cortex and hippocampus of *Pcdh19*$^{+/\beta\text{-}Geo}$ brains, although these were fewer in number consistent with X-inactivation (Fig. 5B). Importantly, analysis of *Pcdh19*$^{T/\beta\text{-}Geo}$ and *Pcdh19*$^{+/\beta\text{-}Geo}$ embryonic brains revealed *β-Geo*-positive cells throughout the cortex and hippocampus in the same regions as wild type *Pcdh19* expressing cells (Fig. 5E,F). To confirm that the different methods used to detect *Pcdh19* expressing and mutant cells did not confound the analysis we performed *in situ* hybridisation of 15.5 dpc brains with a *β-Geo* probe (Supplementary Fig. 3). Cells expressing *β-Geo* were identified in the cortex and hippocampus as expected including the marginal zone, intermediate zone and ventricular/sub-ventricular zones (Fig. 5G). Taken together, these data suggest that mutant cells are not ectopically positioned in *Pcdh19*$^{+/\beta\text{-}Geo}$ and *Pcdh19*$^{T/\beta\text{-}Geo}$ embryonic brains.

Given that *Pcdh19* expression is maintained after birth[4], we next investigated whether *β-Geo* expressing cells were ectopically expressed in *Pcdh19*$^{+/\beta\text{-}Geo}$ and *Pcdh19*$^{T/\beta\text{-}Geo}$ brains at postnatal day 42 (P42). Consistent with our western blot analysis (Fig. 2A), robust expression of *Pcdh19* was detected in the hippocampus and cortex of *Pcdh19* WT brains (Fig. 6A). *Pcdh19* expression was strongest in the CA1 and dentate gyrus of the hippocampus and in layers 2/3 and 5 of the cortex. Mosaic expression was identified in the same regions of *Pcdh19*$^{+/\beta\text{-}Geo}$ brains (Fig. 6B).

β-Geo staining of *Pcdh19*$^{T/\beta\text{-}Geo}$ brains with X-Gal revealed robust expression in the cortex and hippocampus that resembled the pattern of *Pcdh19* expression in *Pcdh19*$^{+/T}$ brains (Fig. 6). Mosaic expression of *β-Geo* was observed in these regions in *Pcdh19*$^{+/\beta\text{-}Geo}$ brains (Fig. 6E). No evidence of ectopic *β-Geo*-positive cells was detected. Thus, it appears that the mutation of *Pcdh19* does not perturb positioning of neurons in postnatal brain development.

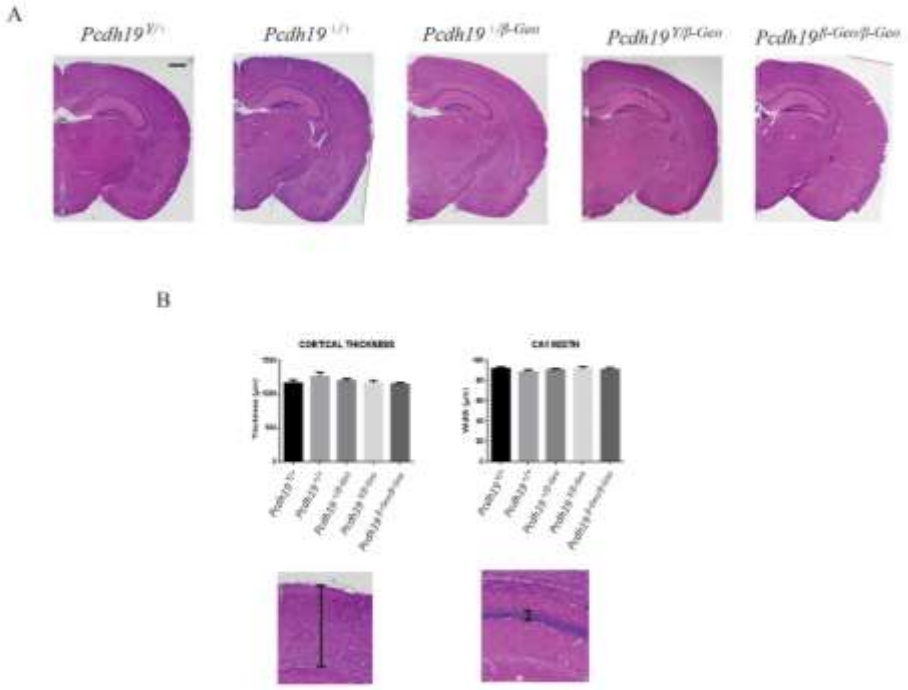

Figure 4. Histological and morphometric analysis of adult *Pcdh19* mutant mouse brains. (**A**) Haematoxylin and Eosin staining was performed on coronal P42 brain sections. Scale bar represents 1 mm. (**B**) Thickness measurement of the lateral parietal association cortex and hippocampus CA1 region in WT and *Pcdh19* mutant brains. Three animals were analysed for each genotype. Error bars = SEM.

The Migration Potential of *Pcdh19* Null Neurons is Increased *In Vitro*. As subtle defects in neuronal migration can be difficult to detect *in vivo*, we next performed *in vitro* migrations assays using neurospheres generated from *Pcdh19* WT and *Pcdh19* null embryos. Neural progenitor cells were isolated from the developing cortex (14.5 dpc) and cultured as non-adherent neurospheres. To model neuronal migration, whole neurospheres were adhered to a poly-L-lysine substrate and the migration of neurons outward from the neurosphere boundary measured[29]. Increased neuronal migration in the *Pcdh19* null neurons was observed, as shown by an increase in the percentage of migrating neurons in the outer migration regions (bins) (Fig. 7A,B). However, this only reached significance in 4/9 of the bins. This data suggests that the mutant cells may have a subtle change in neuronal migration potential that does not translate into overt positional changes of neurons in the developing and adult mouse brain.

Discussion

Mutations of protocadherin genes in humans have been implicated in several neurological diseases and in mice have revealed important functions in neuronal development including axon guidance, neural circuit formation and synaptogenesis. Here we performed validation and gross morphological characterization of *Pcdh19* null mice to determine the function of *Pcdh19 in vivo*.

Previous studies indicate that *Pcdh19* expression is temporally and spatially restricted within the embryonic and neonatal CNS[5,21]. Using *in situ* hybridization and *β-Geo* reporter activity, we have shown that *Pcdh19* expression is maintained in the adult brain. Expression was particularly robust in regions of the brain that are implicated in epilepsy including the hippocampus and in the cortex, where it was restricted to layers 2/3 and 5, although expression in other areas such as the cerebellum and the hypothalamus was also evident. We have attempted to further characterize endogenous *PCDH19* CNS protein expression by immunohistochemistry using several commercially available *PCDH19* antibodies, however none bind specifically to *PCDH19* as evident by the immunostaining patterns that were indistinguishable between *Pcdh19* WT and *Pcdh19* null brain sections (our unpublished data). The *β-Geo* reporter gene in our *Pcdh19* null mouse therefore provides a useful alternative method for identification of cells that normally express *Pcdh19*, especially given that loss of *Pcdh19* function does not overtly affect neuron localization *in vivo* (see below).

Expression *of Pcdh19* in the adult brain also raises the question of its subcellular localization. Using chemical fractionation and primary hippocampal neuron culture, we have shown that *PCDH19* is located within both the synaptosome fraction *in vivo* and synapses *in vitro* suggesting it has synaptic function. Consistent with these results, analysis of chick *PCDH19* in the optic tectum revealed substantial overlap with the synaptic marker

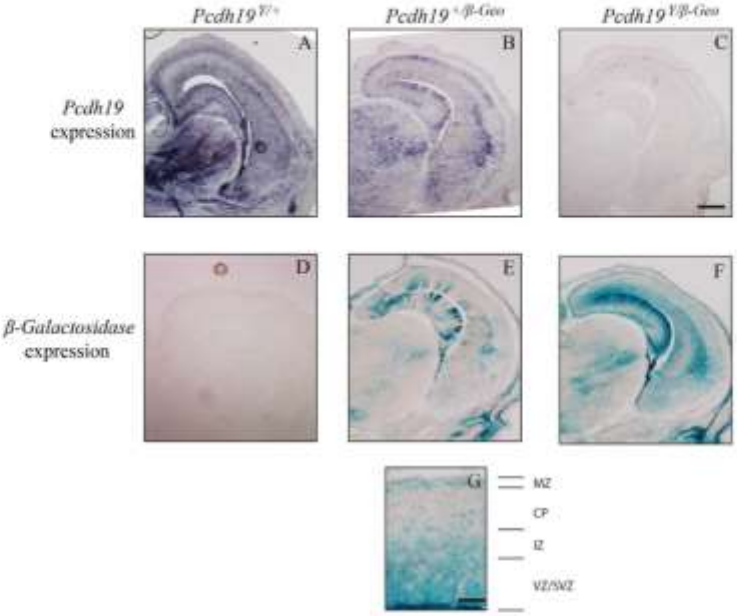

Figure 5. ***Pcdh19*** **null cells are not ectopically located in the developing brain (15.5 dpc).** **(A–C)** *Pcdh19* WT cells were detected by *in situ* hybridisation and were located in the cortex and hippocampus of $Pcdh19^{Y/+}$ **(A)** and $Pcdh19^{-/\beta\text{-}Geo}$ **(B)** developing brains. $Pcdh19^{+/\beta\text{-}Geo}$ brains exhibited less extensive staining consistent with X-inactivation. No specific signal was detected in $Pcdh19^{Y/\beta\text{-}Geo}$ brains **(C)**. **(D–F)** *Pcdh19* null cells were detected by X-Gal staining and were located in the cortex and hippocampus of $Pcdh19^{+/\beta\text{-}Geo}$ **(E)** and $Pcdh19^{Y/\beta\text{-}Geo}$ **(F)** developing brains. $Pcdh19^{+/\beta\text{-}Geo}$ brains showed reduced staining consistent with X-inactivation. No signal was detected in $Pcdh19^{Y/-}$ brains **(D)**. Scale bar represents 500 μm. Three animals were analysed for each genotype and age. **(G)** *Pcdh19* null cells are predominantly located in the ventricular zone (VZ)/subventricular zone (SVZ), the intermediate zone (IZ) and the marginal zone (MZ). Scale bar represents 100 μm.

Syntaxin[7]. Interestingly, *Pcdh17*, the closest related family member to *Pcdh19*, has recently been shown to play a role in synapse formation and synaptic vesicle assembly in murine corticobasal ganglia[9]. These data raise the possibility that *PCDH19* may perform a similar function *in vivo* and supports the hypothesis that abnormal synaptic communication between *PCDH19* WT and *PCDH19* mutant cells contributes to the pathobiology of *PCDH19* GCE[3].

Previous reports have shown that morpholino knockdown or genetic mutation of *pcdh19* in zebrafish resulted in contrasting phenotypes[11–13]. In agreement with mutation of *pcdh19* in zebrafish by Cooper *et al.* we show here that $Pcdh19^{Y/\beta\text{-}Geo}$, $Pcdh19^{\beta\text{-}Geo/\beta\text{-}Geo}$ and $Pcdh19^{+/\beta\text{-}Geo}$ mice are healthy, fertile and do not exhibit gross defects in brain morphology. These striking phenotypic differences in zebrafish may reflect lack of genetic compensation in response to acute morpholino *Pcdh19* knockdown in zebrafish which has been shown to account for similar differences in other studies[22]. In humans, hemizygous males do not exhibit intellectual disability or seizures indicating that brain development occurs relatively normally without *PCDH19*, perhaps due to functional compensation by other *PCDH19* family members[23]. The absence of morphological defects in $Pcdh19^{Y/\beta\text{-}Geo}$ and $Pcdh19^{\beta\text{-}Geo/\beta\text{-}Geo}$ mice is therefore not unexpected and suggests that *Pcdh19* functional redundancy also occurs in mice. In contrast, the majority of *PCDH19* heterozygous human females develop infantile seizures with variable cognitive defects, although there is no evidence of gross morphological defects affected individuals. It has been proposed that this phenotype results from "cellular interference" i.e. segregation of *PCDH19* expressing neurons and *PCDH19* mutant neurons in the developing brain development resulting in abnormal neural circuitry[3,23]. While there is little *in vivo* data to support this model, it is interesting to note that cortical dysplasia and clustering of dysplastic pyramidal neurons has been detected in a single female with *PCDH19* GCE[13]. Although we did not detect any evidence of cortical dysplasia or gross abnormalities in $Pcdh19^{+/\beta\text{-}Geo}$ mice, we cannot exclude the possibility that subtle regionally-restricted defects may be present. Ryan *et al.* also detected dysplastic pyramidal cells ectopically positioned in the deep white layer, suggesting defective neuronal migration. To investigate this phenotype *in* $Pcdh19^{+/\beta\text{-}Geo}$ mice, we determined the location of *Pcdh19* null cells using X-Gal staining in both developing and postnatal $Pcdh19^{+/\beta\text{-}Geo}$ brains. However, no evidence of ectopic *Pcdh19* null cells was detected indicating that *PCDH19* is not critical for neuronal cell migration *in vivo*. In contrast, a modest but significant increase in migration was detected in *Pcdh19* null neurons generated from neurosphere explants. It is therefore possible that loss of *Pcdh19* function compromises the migration potential of some neurons but that this defect is subtle and not associated with overt morphological defects *in vivo*.

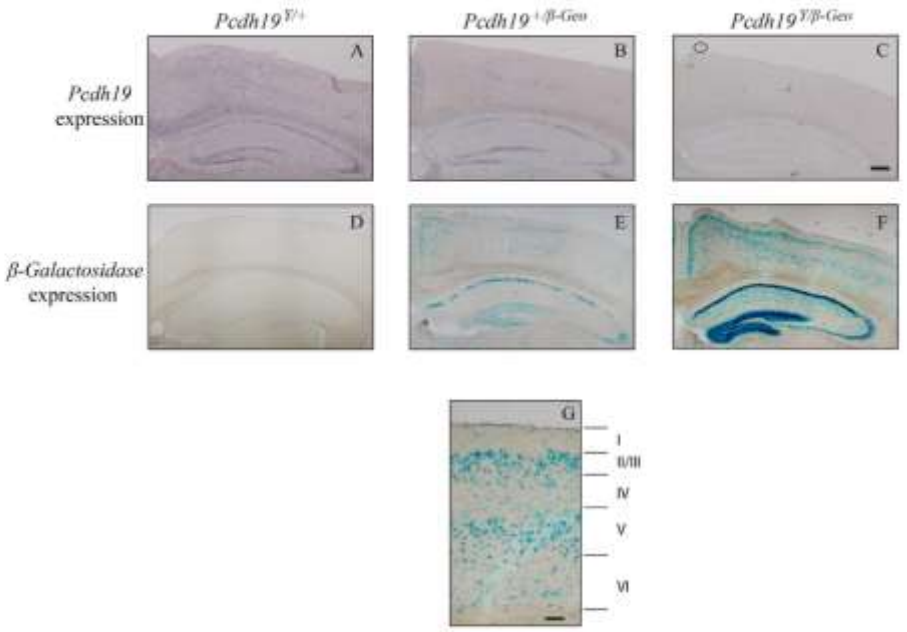

Figure 6. *Pcdh19* null cells are not ectopically located in the adult brain. (A–C) *Pcdh19* WT cells were detected by *in situ* hybridisation and were located in the cortex and hippocampus of $Pcdh19^{Y/+}$ (**A**) and $Pcdh19^{+/\beta\text{-}Geo}$ (**B**) adult (P42) brains. $Pcdh19^{+/\beta\text{-}Geo}$ brains exhibited less staining consistent with X-inactivation. No specific signal was detected in $Pcdh19^{Y/\beta\text{-}Geo}$ brains (**C**). **(D–F)** *Pcdh19* null cells were detected by X-Gal staining and were located in the cortex and hippocampus of $Pcdh19^{+/\beta\text{-}Geo}$ (**E**) and $Pcdh19^{Y/\beta\text{-}Geo}$ (**F**) adult brains. $Pcdh19^{+/\beta\text{-}Geo}$ brains showed less staining consistent with X-inactivation. No signal was detected in $Pcdh19^{Y/+}$ brains (**D**). Scale bar represents 500μm. Three animals were analysed for each genotype and age. **(G)** *Pcdh19* null cells are predominantly expressed in layer II/III and V of the adult cortex. Scale bar represents 100μm.

In summary, our characterization of *Pcdh19* null mice reveals that *Pcdh19* is widely expressed in the CNS but not required for brain development *per se*. However, given the significantly increased motility of *Pcdh19* null neurons *in vitro* and the identification of *Pcdh19* mutant phenotypes in other species, further detailed analysis of this mouse model may reveal subtle abnormalities in *Pcdh19* null brains.

Methods

Animals. *Pcdh19* null mice (TF2108) were purchased from Taconic Biosciences. Both male and female animals were used in this study. The day the vaginal plug was detected was designated as embryonic day 0.5 (0.5 dpc). The day of birth was designated postnatal day 0 (P0). Each group subjected to analysis contained at least three mice. All of the experiments were approved by The University of Adelaide Animal Ethics Committee and performed according to their ethical guidelines.

Genotyping. Genotyping was performed by PCR amplification using three primers: one primer common to both *Pcdh19* WT and *Pcdh19* null alleles F-5′-AGTCCACTACCGACTCTGCTG -3′, one specific to the *Pcdh19* WT allele R-5′-CAAAGTTAGCCAGGCGGGAC-3′ and one specific to the *Pcdh19* null allele R-5′-AACTCACAACGTGGCACTGG-3′. PCR products were separated on a 1% agarose gel. *Pcdh19* WT and null allele products were 102 bp and 471 bp, respectively.

Protein extraction, synaptosome fractionation and western blotting. Cortex, hippocampi and cerebellum for protein extraction were minced in extraction buffer (50 mM Tris, 150 mM NaCl, 1% NP40 (Roche) and 1% Triton X-100 (Sigma) and incubated at 4 degrees C for 30 minutes. Synaptosome fractions were isolated using Syn-PER synaptic protein extraction reagent (ThermoFisher Scientific) according to the manufacturer's instructions. Lysates and fractions were separated on Invitrogen Bolt™ precast 4–12% polyacrylamide gels and transferred to PVDF membrane before being blotted. Antibodies and their corresponding dilutions were: mouse anti-*PCDH19* 1:100 (Abcam, ab57510) and rabbit anti-3-ACTIN 1:1000 (Cell Signalling Technology, #4967), mouse anti-PSD95 1:2000 (ThermoScientific, 7E3-1138) and rabbit anti-SYNAPTOPHYSIN 1:5000 (Abcam, ab32127). Membranes were blocked in 5% BSA+5% Skim milk in Tris-buffered saline−0.1% Tween 20 (TBST) and antibodies were incubated with the membrane in 5% BSA in TBST. Membranes were developed using Bio-Rad Clarity Western ECL substrate and imaged using a Bio-Rad ChemiDoc.

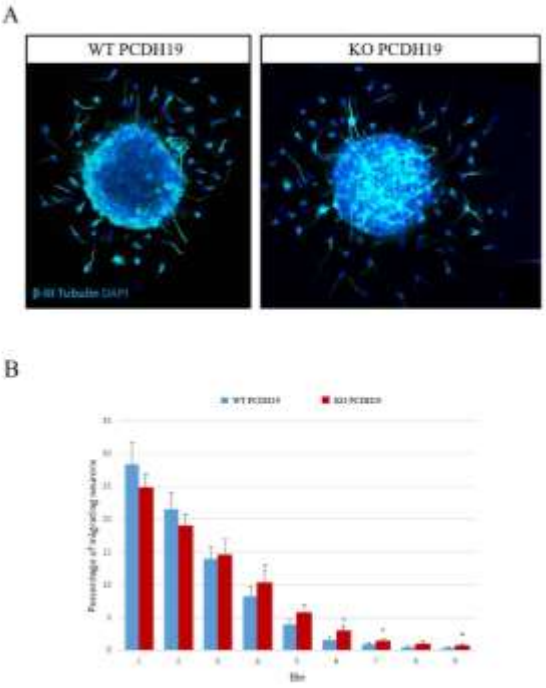

Figure 7. Loss of *Pcdh19* leads to an increase in neuronal migration. Neural progenitor cells (NPCs) were isolated from the telencephalic vesicles of *Pcdh19* WT or *Pcdh19* null E14.5 embryos and grown as non-adherent neurospheres. Neurospheres were plated on a Poly-L-Lysine substrate and cells were allowed to attach and migrate. (**A**) Neuronal migration was scored at 48 hrs by co-staining with a neuronal specific antibody 3-III Tubulin (Cyan) and DAPI. (**B**) Neuronal migration was determined by drawing concentric circles around the contiguous boundary of the neurosphere and counting the number of neurons within each circle. Differences in the number of migrating neurons was determined by the percentage of neurons within each circle (bin). The percentage of neurons is greater in the more distal circles in the KO *Pcdh19* neurospheres compared to the WT *Pcdh19* neurospheres. Each data point represents 7 embryos collected from 3 litters with at least 20 neurospheres scored for each embryo. Error bars = SEM, *differs from WT; $P < 0.05$, Student's T-test.

Primary Hippocampal Neuron Culture, Nucleofection and Immunohistochemistry. 18.5 dpc hippocampi were dissected from wild type embryos and neurons dissociated with 0.5% Trypsin. 1×10^5 neurons were nucleofected with 1 μg *PCDH19*-FLAG using the Neon Transfection System (Invitrogen) and seeded onto poly-D-lysine coated coverslips. Primary neurons were maintained in Neurobasal medium + B27 supplement (Life Technologies). Primary neurons were cultured for 12 days then fixed in 4% PFA for 15-30 minutes. For immunofluorescence, cells were block permeablised with 0.1% Tween20 (PBST) and 10% foetal calf serum for 1 hour at room temperature. Primary neurons were then incubated overnight with anti-FLAG (1:1000, Sigma Aldrich) and anti-SYNAPSIN (1:500, Millipore) at 4 °C and then with secondary antibody (donkey anti-mouse Cy3 and donkey anti-rabbit Cy5; JacksonImmunoResearch). Images were acquired on a Nikon Eclipse Ti microscope.

X-gal staining. 15.5 dpc embryonic heads and dissected P42 brains were fixed in 4% paraformaldehyde at 4 °C, cryoprotected in 30% sucrose and frozen in OCT embedding medium. Embryos were fixed in 4% paraformaldehyde in PBS. Whole embryos or cryosections were incubated in staining solution: 19 mM Sodium dihydrogen phosphate, 81 mM Disodium hydrogen phosphate, 2 mM $MgCl_2$, 5 mM EGTA, 0.01% Sodium deoxycholate, 0.02% NP-40, 5 mM Potassium ferricyanide, 5 mM Potassium ferrocyanide, and 1 mg/ml X-gal substrate, at 37 °C until blue staining was sufficient. Images were acquired on a Nikon Eclipse Ti microscope, compiled and minimally processed (adjusted for color and light/dark) using Adobe Photoshop CS.

Histological analysis. Embryos for histological examination were fixed in 4% PFA, embedded in paraffin, cut at 5μm and stained with Mayer's haematoxylin and Eosin using standard approaches. Images were acquired on a Nikon Eclipse Ti Microscope and measurements taken using Nikon Imaging Software (NIS Elements). Three animals were analysed for each genotype with cortical measurements being made in the visual cortex and hippocampal measurements in the CA1 region. A total of ten measurements for each region was recorded for each individual animal and averaged. The mean was then determined from the average of the three animals in each group.

***In situ* hybridisation.** 15.5 dpc embryonic heads and dissected P42 brains were fixed in 4% paraformaldehyde at 4 °C, cryoprotected in 30% sucrose and frozen in OCT embedding medium. *In situ* hybridization of 16-μM sections was performed as described previously[24]. The *Pcdh19* probe was a digoxigenin-labeled antisense RNA probe prepared as described[21]. The *LacZ* probe sequence (500 bp) was generated by PCR using the following primers F-5′-ATGTGCGGCGAGTTGCGTGA-3′ R-5′-CGCTCATCGCCGGAGCCAGC-3′. At least three independent samples of each group were analyzed and representative sections are shown. No signal was detected using a sense control probe. Images were acquired on a Nikon Eclipse Ti microscope, compiled and minimally processed (adjusted for color and light/dark) using Adobe Photoshop CS.

Neurosphere Migration Assay. NPCs were isolated from the 14.5 dpc embryonic mouse cortex (telencephalic vesicles) and grown as non-adherent neurospheres in the presence of 20 ng/mL bFGF and EGF as previously described[25]. Passage 4 neurospheres were cultured for 5 days and seeded onto a poly-L-lysine substrate at a density of 100 neurospheres/9.5 cm^2 with the removal of growth factors. Cells were allowed to migrate for 48 hrs before being fixed in 4% paraformaldehyde (PFA) in phosphate buffered saline (PBS) for 15 minutes at room temperature. For immunofluorescence analysis, cells were block permeablised in 0.2% tween20 (PBST) and 5% horse serum for 1 hour at room temperature. To identify neurons, cells were stained overnight with β-III tubulin primary antibody (1:300, Sigma Aldrich) in PBST with 0.5% horse serum at 4 °C and then with secondary antibody, donkey anti-mouse AlexaFluor647 (1:700, Invitrogen) for 1 hr at room temperature. Cells were counterstained with 300 nM 4′,6-diamidino-2-phenylindole (DAPI) to identify single cells and mounted with Slow-fade mounting media (Invitrogen) for microscopy. Fluorescence was viewed using the Zeiss AxioImager M2 fluorescent microscope (Carl Zeiss, Germany). Images of isolated single neurospheres and migrating cells were captured at 20× magnification using an Axiocam Mrm camera and Vs4.9.1.0 software (Axiovision, Carl Zeiss). Neurospheres were reconstructed using the Image J Stitching plugin[26] and migration analysis preformed using the ImageJ2 software[27]. Briefly, the neurosphere boundary was identified and the radius of the neurosphere determined. The concentric circles plugin was used to draw 10 concentric circles (ie. migration zones) around the boundary of the sphere, with an outer radius calculated by the radius of the neurosphere+600 pixels (307 μM). Using the cell counter plugin the number of migrating neurons within each concentric circle was determined by counting co-stained β-III tubulin and DAPI cells. The migration distance was then calculated as a percentage of total migrating cells within each circle (bin). Each data point represents 7 embryos collected from 3 litters with at least 20 neurospheres scored for each embryo. Analysis conducted by Student's two-tailed, unpaired t test, assuming equal variance.

Real time PCR. RNA was extracted from P14 hippocampi by using an RNeasy mini column (Qiagen) according to the manufacturer's instructions. Reverse transcription was performed on 1μg of RNA using a High Capacity RNA to cDNA synthesis kit (Life Technologies). Real time PCR was performed on a Step One Plus thermocycler (Life Technologies) using Fast Sybr green master mix (Life Technologies) according to manufacturer's instructions on a two-step program. Primers and product sizes were as follows; *Pcdh19* (130 bp) F-5′ -TGGCAATCAAATGCAAGCGT-3′ R-5′ ACCGAGATGCAATGCAGACA-3′, β-Galactosidase (85 bp) F-5′ TACGATGCGCCCATCTACAC-3′ R5′ AACAACCCGTCGGATTCTCC-3′ β-actin (89 bp) F-5′-CTGCCTGACGGCCAGG-3′ R-5′-GATTCCATACCCAAGAAGGAAGG-3′.

References

1. Frank, M. & Kemler, R. Protocadherins. *Curr. Opin. Cell Biol.* **14,** 557–562 (2002).
2. Junghans, D., Haas, I. G. & Kemler, R. Mammalian cadherins and protocadherins: about cell death, synapses and processing. *Curr. Opin. Cell Biol.* **17,** 446–452 (2005).
3. Morishita, H. & Yagi, T. Protocadherin family: diversity, structure, and function. *Curr. Opin. Cell Biol.* **19,** 584–592 (2007).
4. Redies, C., Vanhalst, K. & Roy, F. van. delta-Protocadherins: unique structures and functions. *Cell. Mol. Life Sci. CMLS* **62,** 2840–2852 (2005).
5. Dibbens, L. M. *et al.* X-linked protocadherin 19 mutations cause female-limited epilepsy and cognitive impairment. *Nat. Genet.* **40,** 776–781 (2008).
6. Emond, M. R., Biswas, S., Blevins, C. J. & Jontes, J. D. A complex of Protocadherin-19 and N-cadherin mediates a novel mechanism of cell adhesion. *J. Cell Biol.* **195,** 1115–1121 (2011).
7. Tai, K., Kubota, M., Shiono, K., Tokutsu, H. & Suzuki, S. T. Adhesion properties and retinofugal expression of chicken protocadherin-19. *Brain Res.* **1344,** 13–24 (2010).
8. Hayashi, S. *et al.* Protocadherin-17 mediates collective axon extension by recruiting actin regulator complexes to interaxonal contacts. *Dev. Cell* **30,** 673–687 (2014).
9. Hoshina, N. *et al.* Protocadherin 17 regulates presynaptic assembly in topographic corticobasal Ganglia circuits. *Neuron* **78,** 839–854 (2013).
10. Uemura, M., Nakao, S., Suzuki, S. T., Takeichi, M. & Hirano, S. OL-protocadherin is essential for growth of striatal axons and thalamocortical projections. *Nat. Neurosci.* **10,** 1151–1159 (2007).
11. Biswas, S., Emond, M. R. & Jontes, J. D. Protocadherin-19 and N-cadherin interact to control cell movements during anterior neurulation. *J. Cell Biol.* **191,** 1029–1041 (2010).
12. Cooper, S. R. *et al.* Protocadherins control the modular assembly of neuronal columns in the zebrafish optic tectum. *J. Cell Biol.* **211,** 807–814 (2015).
13. Emond, M. R., Biswas, S. & Jontes, J. D. Protocadherin-19 is essential for early steps in brain morphogenesis. *Dev. Biol.* **334,** 72–83 (2009).
14. Kok, F. O. *et al.* Reverse genetic screening reveals poor correlation between morpholino-induced and mutant phenotypes in zebrafish. *Dev. Cell* **32,** 97–108 (2015).
15. Ryan, S. G. *et al.* Epilepsy and mental retardation limited to females: an X-linked dominant disorder with male sparing. *Nat. Genet.* **17,** 92–95 (1997).
16. Depienne, C. & LeGuern, E. *PCDH19*-related infantile epileptic encephalopathy: an unusual X-linked inheritance disorder. *Hum. Mutat.* **33,** 627–634 (2012).
17. Scheffer, I. E. *et al.* Epilepsy and mental retardation limited to females: an under-recognized disorder. *Brain* **131,** 918–927 (2008).
18. Terracciano, A. *et al. PCDH19*-related epilepsy in two mosaic male patients. *Epilepsia* **57,** e51–e55 (2016).

19. Cotton, A. M. *et al.* Landscape of DNA methylation on the X chromosome reflects CpG density, functional chromatin state and X-chromosome inactivation. *Hum. Mol. Genet.* **24,** 1528–1539 (2015).
20. Homan, C. C. *et al.* Mutations in USP9X are associated with X-linked intellectual disability and disrupt neuronal cell migration and growth. *Am. J. Hum. Genet.* **94,** 470–478 (2014).
21. Gaitan, Y. & Bouchard, M. Expression of the δ-protocadherin gene *Pcdh19* in the developing mouse embryo. *Gene Expr. Patterns* **6,** 893–899 (2006).
22. Rossi, A. *et al.* Genetic compensation induced by deleterious mutations but not gene knockdowns. *Nature* **524,** 230–233 (2015).
23. Depienne, C. *et al.* Sporadic Infantile Epileptic Encephalopathy Caused by Mutations in *PCDH19* Resembles Dravet Syndrome but Mainly Affects Females. *PLoS Genet* **5,** e1000381 (2009).
24. Wilson, L. D. *et al.* Developmentally regulated expression of the regulator of G-protein signaling gene 2 (Rgs2) in the embryonic mouse pituitary. *Gene Expr. Patterns* **5,** 305–311 (2005).
25. Basak, O. & Taylor, V. Identification of self-replicating multipotent progenitors in the embryonic nervous system by high Notch activity and Hes5 expression. *Eur. J. Neurosci.* **25,** 1006–1022 (2007).
26. Preibisch, S., Saalfeld, S. & Tomancak, P. Globally optimal stitching of tiled 3D microscopic image acquisitions. *Bioinforma. Oxf. Engl.* **25,** 1463–1465 (2009).
27. Schneider, C. A., Rasband, W. S. & Eliceiri, K. W. NIH Image to ImageJ: 25 years of image analysis. *Nat. Methods* **9,** 671–675 (2012).

Acknowledgements

This study was supported by the Australian National Health and Medical Research Council and the *PCDH19* Alliance.

Author Contributions

P.Q.T., D.T.P., J.G., J.N.H., L.A.J., B.T.B., E.J.J. and C.C.H. conceived and designed the experiments. P.Q.T., J.N.H., L.A.J., B.P.H., D.T.P. and C.C.H. interpreted the data. D.T.P., C.C.H. and S.G.P. performed the experiments. D.T.P., P.Q.T. and C.C.H. wrote the manuscript. P.Q.T. and J.G. obtained the funding.

Additional Information

Supplementary information accompanies this paper at http://www.nature.com/srep

Competing financial interests: The authors declare no competing financial interests.

How to cite this article: Pederick, D. T. *et al.* *Pcdh19* Loss-of-Function Increases Neuronal Migration *In Vitro* but is Dispensable for Brain Development in Mice. *Sci. Rep.* **6,** 26765; doi: 10.1038/srep26765 (2016).

Supplementary Information

Pcdh19 Loss-of-Function Increases Neuronal Migration *In Vitro* but is Dispensable for Brain Development in Mice

Daniel T. Pederick, Claire C. Homan, Emily J. Jaehne, Sandra G. Piltz, Bryan P. Haines, Bernhard T. Baune, Lachlan A. Jolly, James N. Hughes, Jozef Gecz and Paul Q. Thomas

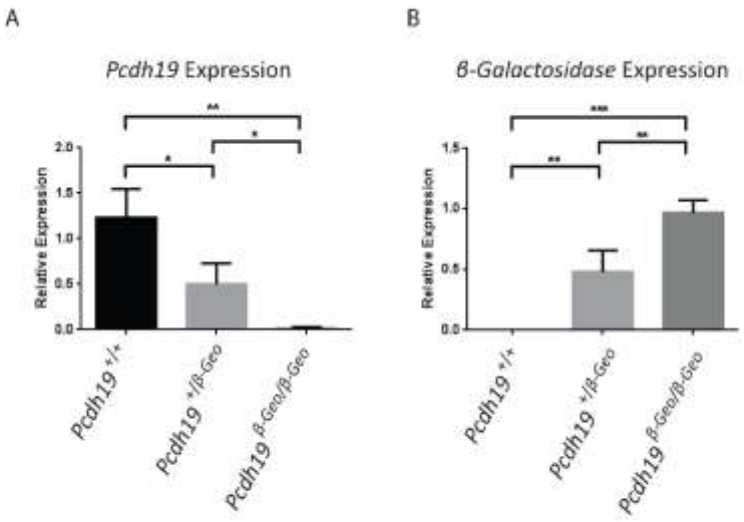

Supplementary Figure 1 Validation of Pcdh19 KO allele by quantitative PCR
A) Pcdh19 WT cDNA could be detected in P14 hippocampal cDNA extracted form Pcdh19+/+and Pcdh19+/β-Geo brains. A significant decrease in Pcdh19 WT cDNA was observed in Pcdh19+/β-Geo brains. Pcdh19 β-Geo/β-Geo samples had no detectable Pcdh19 WT cDNA. Statistical significance was analysed by one way ANOVA. Pcdh19+/+ vs Pcdh19+/β-Geo $p<0.05$, Pcdh19+/+ vs Pcdh19 β-Geo/β-Geo $p<0.01$ and Pcdh19+/β-Geo vs Pcdh19 β-Geo/β-Geo $p<0.05$. Performed with three biological samples of each genotype and in technical triplicates. Normalised to ActB.
B) β-Galactosidase cDNA could be detected in P14 hippocampal cDNA extracted form Pcdh19+/β-Geo and Pcdh19 β-Geo/β-Geo brains. A significant decrease in β-Galactosidase cDNA was observed in Pcdh19+/β-Geo brains. Pcdh19+/+ samples had no detectable β-Galactosidase cDNA. Statistical significance was analysed by one way ANOVA. Pcdh19+/+ vs Pcdh19+/β-Geo $p<0.01$, Pcdh19+/+ vs Pcdh19 β-Geo/β-Geo $p<0.001$ and Pcdh19+/β-Geo vs Pcdh19 β-Geo/β-Geo $p<0.01$. Performed with three biological samples of each genotype and in technical triplicates. Normalised to ActB.

A

+/- (F)	+/Y (M)	
	+	Y
+	+/+ 24.3% [26]	+/Y 22.4% [24]
-	+/- 29.0% [31]	-/Y 24.3% [26]

TOTAL 100%
(107)

B

+/- (F)	-/Y (M)	
	-	Y
+	+/- 22.0% [17]	+/Y 24.7% [19]
-	-/- 28.6% [22]	-/Y 24.7% [19]

TOTAL 100%
(77)

Supplementary Figure 2 Breeding of Pcdh19 null Mice produced all genotypes at the expected frequencies

A) A random sample of offspring generated from a Pcdh19+/β-Geo crossed with a Pcdh19Y/+ generated all genotypes at expected frequencies. Statistical significance was analysed by a Chi Square test p=0.8013.

B) A random sample of offspring generated from a Pcdh19+/β-Geo female crossed with a Pcdh19Y/β-Geo generated all genotypes at expected frequencies. Statistical significance was analysed by a Chi Square test p= 0.8820.

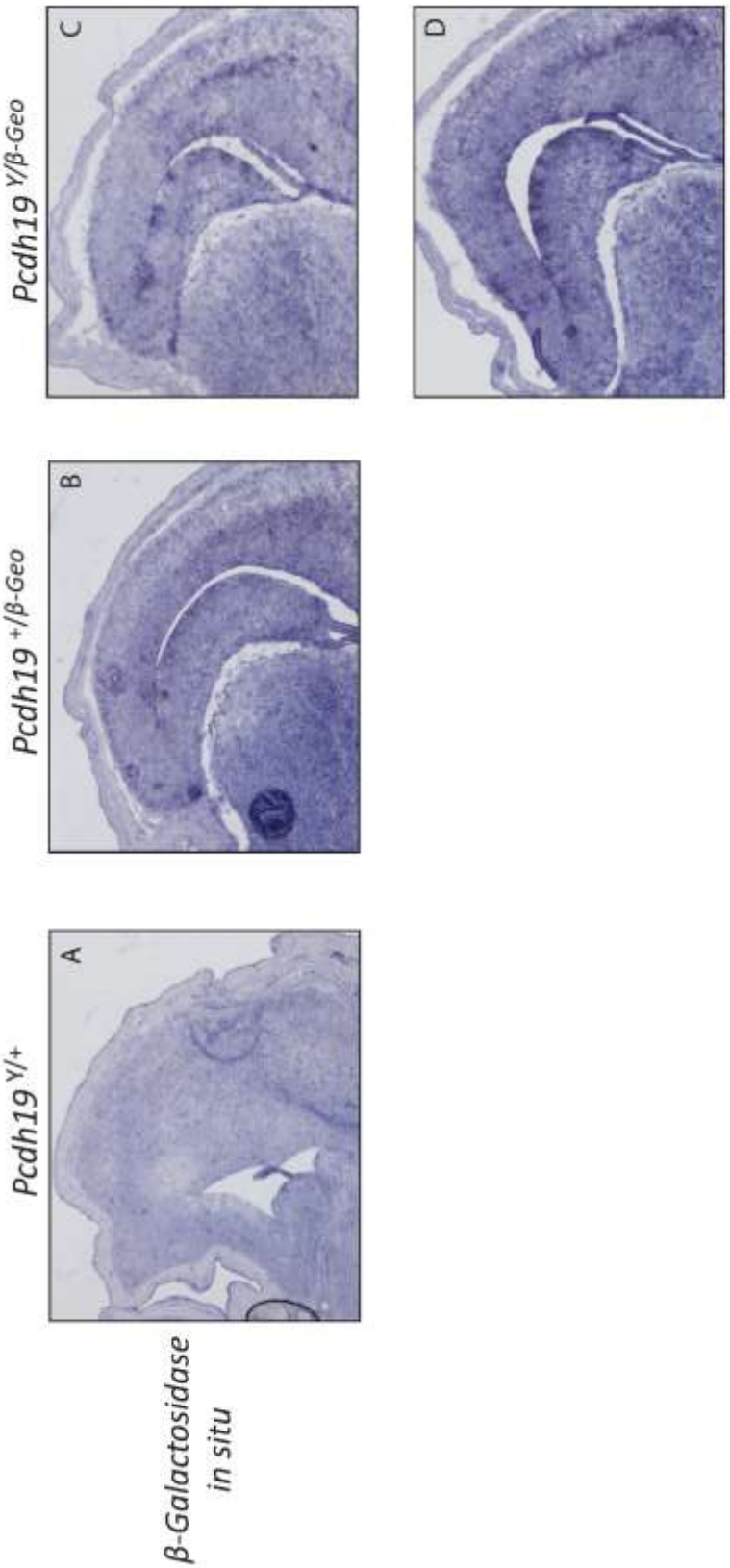

Supplementary Figure 3 Pcdh19 null cells were identified using in situ hybrisation and expressed in the developing cortex and hippocampus (E15.5)
A) Pcdh19 null cells were not present in Pcdh19Y/+ brains.
B) Pcdh19 null cells were present in the developing cortex and hippocampus of Pcdh19Y/β-Geo brains.
C-D) Pcdh19 null cells were the present in the developing cortex and hippocampus of Pcdh19+/β-Geo brains. Pcdh19+/β-Geo brains exhibited less staining consistent with X-inactivation.

CHAPTER 3

Abnormal cell sorting is associated with the unique X-linked inheritance of *PCDH19* epilepsy

Daniel T. Pederick, Kay L. Richards, Sandra G. Piltz, Simone A. Mandelstam, Russell C. Dale, Ingrid E. Scheffer, Jozef Gecz, Steven Petrou, James N. Hughes and Paul Q. Thomas

Submitted to: *Science* on 27.1.2017

3.1 Summary

The most intriguing characteristic of *PCDH19*-GCE is its unique pattern of X-linked inheritance. To date there is no experimental evidence providing insight into the molecular and cellular mechanisms underlying the unique inheritance. Therefore, this was addressed in the submitted manuscript presented in this chapter entitled "Abnormal cell sorting is associated with the unique X-linked inheritance of Protocadherin 19 epilepsy".

To begin investigating the cellular mechanism that underlies the unique X-linked inheritance of *PCDH19*-GCE we used an *in vitro* system to investigate the role of PCDH19 in dictating specific cell-cell interactions and how disease causing missense mutations impact normal function. K562 cells were used to perform these experiments as they do not express endogenous protocadherins or classical cadherins (Ozawa and Kemler, 1998; Schreiner and Weiner, 2010), meaning all cell-cell interactions we observed were dependent on the PCDHs we exogenously expressed.

Two populations of cells co-expressing the same combination of NC PCDHs displayed extensive mixing but when one of these populations had a NC PCDH deleted, added or substituted, the two cell populations displayed significant sorting into two groups dependent on the NC PCDHs they expressed. We also performed aggregation assays using K562 cells and confirmed that three disease causing missense mutations lack adhesive activity. We next mixed cells expressing WT PCDH19/PCDH10 with mutant PCDH19/PCDH10 and observed significant segregation of the two cell populations. These experiments provide the first evidence that NC PCDHs can cooperate to determine adhesion specificities which are sensitive to single PCDH differences.

Next, we sought to investigate how perturbation of these adhesion codes would manifest in the developing mammalian brain where complex arrays of adhesion molecules direct

morphogenesis. We showed that young adult heterozygous mice display abnormally elevated neuronal activity and that this phenotype is not present in homozygous mice, consistent with the unique X-linked inheritance of *PCDH19*-GCE in humans.

To determine the impact of mosaic PCDH19 expression at the cellular level *in vivo* we required reporter alleles for *Pcdh19*-expressing WT and null cells. To label *Pcdh19* null cells, we used the previously validated *Pcdh19* null mice from Chapter 2. In Chapter 3 we describe the generation of a mouse model allowing unequivocal identification of PCDH19 WT cells. Specifically, we utilised CRISPR-Cas9 genome engineering to insert a HA-FLAG epitope tag at the C-terminus of PCDH19 allowing detection of endogenous protein using commercially-available antibodies. We show for the first time PCDH19 spatial expression which was widely expressed in the developing brain, becoming restricted in the postnatal cortex.

To investigate the phenotype resulting from disruption of PCDH19-dependent cell adhesion codes, we generated female mice with both $Pcdh19^{HA\text{-}FLAG}$ and *Pcdh19* null alleles. Simultaneous staining with HA antibodies and X-gal revealed striking segregation of PCDH19-positive and PCDH19-null cortical neuroprogenitors. Abnormal cell sorting observed in heterozygous mice demonstrates that mosaic expression of PCDH19 generates distinct cell populations with incompatible adhesion codes. Furthermore, we show that the cell sorting phenotype could be removed by deleting the remaining PCDH19 WT allele in heterozygous female embryos. This confirms that the complete absence of PCDH19 rescues abnormal cell sorting and provides a clear cellular phenotype that is associated with *PCDH19*-GCE.

Finally, analysis of MRI scans from a cohort of *PCDH19*-GCE patients revealed variable cortical folding abnormalities in four patients with commonly occurring *PCDH19*-GCE mutations.

Overall Chapter 3 describes how the mosaic expression of *Pcdh19* leads to the generation of differential adhesion codes in neural progenitor cells and appears to be the underlying cellular mechanism responsible for the unique X-linked inheritance pattern of *PCDH19*-GCE.

Statement of Authorship

Title of Paper	Abnormal cell sorting is associated with the unique X-linked inheritance of *PCDH19* epilepsy
Publication Status	☐ Published ☐ Accepted for Publication ☑ Submitted for Publication ☐ Unpublished and Unsubmitted work written in manuscript style
Publication Details	Pederick, D. T., Richards, K. L., Piltz, S. G., Mandelstam, S. A., Dale, R. C., Scheffer, I. E., Gecz, J., Petrou, S., Hughes, J. N., Thomas, P. T. (2017) Abnormal cell sorting is associated with the unique X-linked inheritance of *PCDH19* epilepsy. Submitted to *Science* 27.1.2017

Principal Author

Name of Principal Author (Candidate)	Daniel Pederick
Contribution to the Paper	Conceived, designed and performed experiments, generated reagents, analysed data and wrote manuscript.
Overall percentage (%)	80
Certification:	This paper reports on original research I conducted during the period of my Higher Degree by Research candidature and is not subject to any obligations or contractual agreements with a third party that would constrain its inclusion in this thesis. I am the primary author of this paper.
Signature	Date 9.2.17

Co-Author Contributions

By signing the Statement of Authorship, each author certifies that:

i. the candidate's stated contribution to the publication is accurate (as detailed above);
ii. permission is granted for the candidate in include the publication in the thesis; and
iii. the sum of all co-author contributions is equal to 100% less the candidate's stated contribution.

Name of Co-Author	Kay L. Richards
Contribution to the Paper	Performed and analysed ECoG experiments
Signature	Date 9.2.17

Name of Co-Author	Sandra G. Piltz
Contribution to the Paper	Performed micro-injection of mouse zygotes
Signature	Date 9/2/17

Name of Co-Author	Simone A. Mandelstam
Contribution to the Paper	Analysed patient MRI images
Signature	Date 15.2.17

Name of Co-Author	Russell C. Dale
Contribution to the Paper	Patient phenotyping
Signature	Date 9.2.17

Name of Co-Author	Ingrid E. Scheffer
Contribution to the Paper	Patient phenotyping
Signature	Date 10.2.17

Name of Co-Author	Jozef Gecz
Contribution to the Paper	Supervised, conceived and designed experiments.
Signature	Date 9/2/17

Name of Co-Author	Steve Petrou
Contribution to the Paper	Conceived and designed experiments
Signature	Date 15.2.17

Name of Co-Author	James N. Hughes
Contribution to the Paper	Supervised, conceived and designed experiments, analysed data and wrote manuscript.
Signature	Date 9/2/17

Name of Co-Author	Paul Q. Thomas
Contribution to the Paper	Supervised, conceived and designed experiments, analysed data and wrote manuscript.
Signature	Date 9/2/17

This page has been left blank intentionally.

Submitted Manuscript: Confidential

Title: Abnormal cell sorting is associated with the unique X-linked inheritance of *PCDH19* Epilepsy

Authors: Daniel T. Pederick[1, 2], Kay L. Richards[3], Sandra G. Piltz[1, 2], Simone A. Mandelstam[4, 5, 6], Russell C. Dale[7], Ingrid E. Scheffer[3, 8], Jozef Gecz[1, 2, 9, 10], Steven Petrou[3], James N. Hughes[1, 2] and Paul Q. Thomas[1, 2, 10]*

Affiliations:

[1]School of Biological Sciences, The University of Adelaide, Adelaide, South Australia 5005, Australia

[2]Robinson Research Institute, The University of Adelaide, Adelaide, South Australia 5005, Australia

[3]Florey Institute of Neuroscience and Mental Health, The University of Melbourne, Melbourne, Victoria 3010, Australia

[4]Department of Paediatrics, The University of Melbourne, Melbourne, Victoria 3010, Australia

[5]Department of Radiology, The University of Melbourne, Melbourne, Victoria 3010, Australia

[6]Department of Medical Imaging, Royal Children's Hospital, Florey Neurosciences Institute, Parkville, Victoria 3052, Australia

[7]Institute for Neuroscience and Muscle Research, University of Sydney[8]University of Melbourne, Austin Health and Royal Children's Hospital, Victoria, 3084, Australia

[9]School of Medicine, The University of Adelaide, Adelaide, South Australia 5005, Australia

[10] South Australian Health and Medical Research Institute, Adelaide, South Australia 5000, Australia

*Correspondence to: paul.thomas@adelaide.edu.au

Abstract:

X-linked diseases typically exhibit more severe phenotypes in males than females. In contrast, *Protocadherin 19* (*PCDH19*) mutations cause epilepsy in heterozygous females but spare hemizygous males. The cellular mechanism responsible for this unique pattern of X-linked inheritance is unknown. We show that PCDH19 contributes to highly specific combinatorial adhesion codes such that mosaic expression of *Pcdh19* in heterozygous female mice leads to striking sorting between WT PCDH19- and null PCDH19-expressing cells in the developing cortex, correlating with altered network activity. In addition, we identify variable cortical malformations in PCDH19 epilepsy patients. Our results highlight the role of PCDH19 in determining specific adhesion codes during cortical development and how disruption of these codes is associated with the unique X-linked inheritance of *PCDH19* epilepsy.

One Sentence Summary: A single difference in PCDH expression disrupts complex adhesion codes present within the developing mammalian cortex.

Main Text:

Protocadherins (PCDHs) are the largest family of adhesion molecules and regulate axon guidance/sorting, neurite self-avoidance and synaptogenesis (*1–3*). Mutations in PCDH family members have been associated with a variety of neurological disorders including epilepsy, autism and schizophrenia (*4–7*). Notably, mutations in Protocadherin 19 (*PCDH19)* cause *PCDH19* Girls Clustering Epilepsy (*PCDH19*-GCE) which is reported to be the second most common cause of monogenic epilepsy (*8*, *9*). *PCDH19*-GCE is an X-linked disorder with a unique pattern of inheritance whereby heterozygous females are affected while hemizygous males are spared (*8*, *10*). It has been proposed that the coexistence of WT and mutant *PCDH19* neurons that arise through random X-inactivation underpins the unique inheritance (*8*, *11*). This hypothesis is supported by the existence of affected males who are mosaic carriers of somatic *PCDH19* mutations (*11*). However, it is currently unclear what processes are regulated by PCDH19 in the brain and how these are disrupted by mosaic expression but not by the complete absence of functional protein.

PCDH19 has been shown to function as a homotypic cell adhesion molecule in vitro (*12*) and recently published data indicate that PCDH19 has a virtually identical structure to members of the closely-related clustered PCDH family (*13*). Interestingly, clustered PCDHs have been shown to form combinatorial adhesion codes that are likely to play a role in vertebrate neuronal self-avoidance (*14–16*). Given the overlapping expression of non-clustered (NC) PCDHs in vivo (*17*, *18*), we hypothesized that PCDH19, in combination with other NC PCDH family members, could contribute to complex adhesion codes and that perturbation of these codes underpins the unique X-linked inheritance pattern of *PCDH19*-GCE.

To investigate the adhesion activity of PCDH19 in combination with other NC PCDHs we performed mixing experiments using K562 cells which ordinarily do not aggregate during culture due to a lack of endogenous PCDHs and classical cadherins (*16*, *19*). PCDH17 and PCDH10 were selected for these experiments due to their ability to interact in cis with PCDH19 when co-expressed in the same cell in a co-immunoprecipitation assay (Fig. 1A) and overlapping expression with *Pcdh19* in the embryonic mammalian brain (*17*). K562 cells transfected with different fluorescently-labelled PCDH combinations were mixed in a 1:1 ratio and quantitatively assessed for the presence/absence of sorting between the two populations (Fig. 1B). When both cell populations expressed the same combination of PCDHs random mixing was observed (Fig. 1C). In contrast, populations expressing different PCDH combinations exhibited significant cell sorting indicating that cells with matching PCDH profiles preferentially adhere (Fig. 1C). Notably, significant sorting occurred between populations that differed by a single PCDH. We next assessed the impact of *PCDH19*-GCE missense mutations on combinatorial PCDH adhesion. We first individually expressed PCDH19 containing one of three commonly occurring missense mutations in K562 cells and found that each lacked adhesive function (Fig. S1), consistent with previously reported data for other missense mutations (*13*). When PCDH10 was co-expressed with either WT PCDH19 or mutant PCDH19.N340S, significant sorting occurred between the two populations (Fig. 1C). Taken together, these data suggest that PCDH19 forms heterotypic cis interactions with NC PCDHs and contributes to combinatorial adhesion codes that are sensitive to single PCDH differences.

Next, we sought to investigate how perturbation of these adhesion codes would manifest in the developing mammalian brain where complex arrays of adhesion molecules direct morphogenesis. For these experiments we used mice carrying a null allele (*Pcdh19*$^{\beta\text{-}Geo}$)

(*20*) to generate female heterozygous mice with mosaic expression of *Pcdh19.* Given the seizures and elevated neural activity of *PCDH19*-GCE affected females (*21*, *22*), we initially performed electrocorticogram (ECoG) analysis on young adult mice to investigate if a phenotype exists in heterozygous mice that does not manifest in homozygote animals. ECoG traces from $Pcdh19^{+/\beta\text{-}Geo}$ (*+/β-Geo*) postnatal day 42 (P42) mice showed a consistent increase in amplitude compared to $Pcdh19^{+/+}$ (+/+) and $Pcdh19^{\beta\text{-}Geo/\beta\text{-}Geo}$ (*β-Geo/β-Geo*) animals, which were themselves indistinguishable (Fig. 2A). Strikingly, ECoG signatures for *+/β-Geo* mice showed a significant increase in mean number of spike-wave discharge (SWD) events per hour and event duration compared with +/+ mice (Fig. 2B, C and S2). In contrast, the mean number of SWDs per hour and the mean duration of a SWD event for *β-Geo/β-Geo* animals was not significantly different to +/+ mice (Fig. 2B, C and S2). This indicates that mosaic expression of *Pcdh19* in mice results in altered brain network activity. In contrast, this phenotype is not present in mice completely lacking PCDH19, consistent with the unique X-linked inheritance of *PCDH19*-GCE in humans.

To determine the impact of mosaic PCDH19 expression at the cellular level in vivo we required reporter alleles for *Pcdh19*-expressing WT and null cells. To label *Pcdh19*-expressing null cells, we used the $Pcdh19^{\beta\text{-}Geo}$ *β-galactosidase* knock-in reporter allele, which we had previously validated using X-Gal staining (*20*). To enable unequivocal identification of WT PCDH19-expressing cells, we employed CRISPR-Cas9 genome editing to insert an HA-FLAG epitope sequence at the C-terminus of the PCDH19 ORF (Fig. S3A). Successful insertion was validated via PCR, sequencing, western blot and HA immunohistochemistry (Fig. S3B, C and D, respectively). Consistent with previously published mRNA in situ hybridization data (*8*, *20*, *23*), we detected PCDH19 expression in

many brain regions, including prominent expression in the developing cortex that became more restricted in the postnatal brain (Fig. S3D, E and S4).

Simultaneous labelling of PCDH19 positive (HA) and negative (X-gal) cells in *Pcdh19*$^{HA\text{-}FLAG/\beta\text{-}Geo}$ (*HA-FLAG/β-Geo*) brains enabled us to investigate the phenotype resulting from disruption of PCDH19-dependent cell adhesion codes. HA immunostaining of *HA-FLAG/β-Geo* brains revealed a striking alternating pattern of PCDH19-positive and PCDH19-negative cells that extended from the ventricular zone to the cortical plate. (Fig. 2D, left). X-gal staining of *HA-FLAG/*β*-Geo* brains revealed a complementary and non-overlapping pattern to HA immunostaining (Fig. 2D, left), suggesting this pattern is due to segregation of PCDH19-positive and PCDH19-null cells To confirm that this pattern did not arise due to random X-inactivation and subsequent clonal expansion, we examined HA-staining in "wild type" *Pcdh19*$^{HA\text{-}FLAG/+}$ (*HA-FLAG/+*) control embryos (Fig. 2D, right). This allowed us to identify the pattern of PCDH19-positive HA labelled cells in the presence of PCDH19-positive unlabelled cells. Within the cortex, X-inactivation manifested as small interspersed patches of HA-positive and HA-negative staining along the ventricle and overlying neural progenitors in the ventricular zone, with only subtle variations in HA staining within the cortical plate (Fig. 2D, right). The significantly increased percentage of HA-negative regions in *HA-FLAG/*β*-Geo* embryos compared with *HA-FLAG/+* controls confirms that PCDH19-positive and PCDH19-null cells coalesced into distinct groups (Fig. 2E). We also noted significantly increased variation of HA-immunostaining across different *HA-FLAG/*β*-Geo* animals, suggesting differences in abnormal cell sorting phenotypes are due to unique patterns of X-inactivation in each embryo (Fig. 2F, S5 and S6). Consistent with an active role in cell sorting, PCDH19 was present at interfaces between PCDH19 expressing radial glial cells but not between PCDH19-positive and negative cells, supporting its role as a

homotypic cell-cell adhesion molecule in vivo (Fig. S7). Cell body redistribution was independently confirmed by staining for nuclear-localised SOX3 in *Pcdh19*$^{+/\beta\text{-}Geo}$; *Sox3*$^{+/-}$ trans-heterozygous mice (Fig. S8). Taken together, these data suggest that mosaic expression of *Pcdh19* in neuroprogenitors generates distinct cell populations with incompatible adhesion codes that abnormally segregate during cortical development.

The absence of pathology in hemizygous males and the normal brain activity of mice completely lacking functional PCDH19 (Fig. 2A, B and C) suggests that the removal of differential adhesion codes dictated by mosaic PCDH19 expression will restore normal cell sorting during cortical development. To test this hypothesis we developed a method to assess in vivo cell sorting by visualising *Pcdh19* allele-specific expression in functionally null PCDH19 female mice. Using CRISPR-Cas9 genome editing, we deleted the *Pcdh19*$^{HA\text{-}FLAG}$ allele in *HA-FLAG/β-Geo* zygotes to create *DEL/β-Geo* null embryos (Fig. 2F). Deletion of exon 1 and lack of functional PCDH19 was validated by sequencing and HA immunostaining (Fig. 2G and data not shown). X-gal staining of *DEL/β-Geo* embryos at 14 days post embryo transfer demonstrated that the two populations of null cells readily intermix, thereby rescuing the abnormal cell sorting phenotype observed in *HA-FLAG/β-Geo* embryos (Fig. 2G). Quantification of X-gal staining variation confirmed that the abnormal cell sorting was rescued in *DEL/β-Geo* cortices (Fig. 2I and S4). This provides further evidence that the differential adhesion codes of PCDH19-positive and PCDH19-negative cells leads to abnormal cell sorting. Importantly, the lack of abnormal cell sorting in *DEL/β-Geo* null embryos provides a clear cellular phenotype that correlates with and likely explains the unique X-linked inheritance of *PCDH19*-GCE.

Given that cortical neuroprogenitor cells predominantly undergo radial as opposed to lateral movement (*24*), the presence of large blocks of cells in *HA-FLAG/β-Geo* embryos at 14.5dpc suggests that abnormal cell sorting must occur at an earlier stage in development. We were also interested to determine whether abnormal cell sorting persists in post-mitotic neurons. Initially, we established that PCDH19 expression in the developing brain commences at 9.5 dpc (Fig. S9). Comparison of *HA-FLAG/+* and *HA-FLAG/β-Geo* embryos at 9.5 dpc revealed a similar pattern of highly interspersed PCDH19-positive and -negative cells (Fig. 3A) indicating that segregation had not yet occurred. In contrast, at 10.5 dpc abnormal cell sorting was evident in *HA-FLAG/β-Geo* embryos but not in *HA-FLAG/+* controls (Fig. 3A). In addition, abnormal cell sorting was observed in postnatal neurons that express PCDH19 (Fig. 3B). The rapid onset and persistence of abnormal cell sorting demonstrates that cortical progenitors are acutely sensitive to disruptions in specific adhesion codes and that these embryonic cellular rearrangements are maintained in postmitotic neurons.

Although central nervous system (CNS) abnormalities have not previously been described in *+/β-Geo* mice (*20*) we hypothesized that abnormal cell sorting caused by mosaic expression of PCDH19 during human cortical development could result in morphological defects due to the prolonged expansion of neuroprogenitors and extensive sulcation relative to mice (*25*). Using data from the Allen Brain Atlas we confirmed *PCDH19* is highly expressed in human embryonic CNS including the cortex during the key neurogenic period of 8-16 weeks post conception (*26*, *27*) (Fig. S10A). *PCDH19* expression is reduced postnatally, but is still detectable, with the brain remaining the predominant site of expression in the adult (Fig. S10B). We then reviewed MRI images from a cohort of *PCDH19*-GCE girls. We identified abnormal cortical sulcation in four patients with common causative mutations in *PCDH19* (p.N340S, p.S671X and p.Y366LfsX10; Fig.4, S11 and Table S2) (*21*). The patients presented with variably positioned cortical defects that included

bottom of the sulcus dysplasias, abnormal cortical folding, cortical thickening and blurring of the grey/white junction. These data suggest that subtle CNS abnormalities are a feature of *PCDH19*-GCE, which is supported by previous observations of dysplastic neurons (*10*). While it is not known how abnormal cell sorting could generate these defects, their variability is consistent with the random nature of X-inactivation and phenotypes observed in *PCDH19*-GCE patients.

In summary, the generation of differential adhesion codes in neural progenitor cells caused by mosaic expression of *Pcdh19* appears to be the underlying cellular mechanism responsible for the unique X-linked inheritance pattern of *PCDH19*-GCE. Furthermore, our data suggests that uniform removal of PCDH19, as seen in hemizygous males, does not lead to the formation of incompatible adhesion codes allowing for normal positioning of neuroprogenitor cells and neural activity (Fig. S12). The abnormal rearrangement of neuroprogenitor cells in the incipient cortex of heterozygous brains indicates that at least some of their neuronal progeny will be aberrantly positioned, regardless of whether they maintain expression of *Pcdh19* postnatally. This rearrangement has the potential to perturb functional boundaries within the cortex and alter connectivity between cortical and subcortical regions.

More broadly, our data suggests that neurodevelopmental disorders associated with mutation of other NC PCDH family members (*4–7*) may be caused by disruption of adhesion codes. Since all other NC PCDHs are autosomal, mosaic disruption of adhesion codes would have to occur through a process other than X-inactivation. There is strong evidence that NC PCDHs are subject to random monoallelic expression (RMAE) (*28*). Individuals with a

heterozygous germ line mutation in a given autosomal NC PCDH would have a proportion of their cells expressing either the functional or non-functional allele, resulting in disrupted adhesion codes. The proportion of RMAE affected cells would likely impact the penetrance or expressivity of any resultant phenotype.

Although both clustered and NC PCDHs can function in combinatorial adhesion complexes, our data indicates that the interaction of matching adhesion codes for each of these closely-related protein families in vivo can lead to different outcomes. Matching codes of clustered PCDHs are thought to result in repulsion which has been implicated in neuronal self avoidance. In contrast, our data indicate that cells expressing matching NC PCDH codes selectively associate in vivo. Given the complex and overlapping expression pattern of NC PCDHs throughout development it seems likely that this property may direct spatial positioning of neuroprogenitors and could conceivably be utilized during morphogenesis of other organs.

The ability of cells with different identities to self-associate and form discrete populations was first identified in the early 1900s by mixing sponge cells from different colored species (*29–31*). We now appreciate the critical role of adhesion molecules in regulating cell identity and directing tissue morphogenesis in many developmental contexts including in the brain (*32–35*). Our findings advance this field by providing evidence that perturbation of cellular adhesion codes underlies the unique X-linked inheritance pattern of *PCDH19*-GCE and suggests that just a single difference in PCDH expression is enough to disrupt the complex adhesion codes present within the developing mammalian cortex.

References:

1. A. M. Garrett, J. A. Weiner, Control of CNS synapse development by γ-protocadherin-mediated astrocyte-neuron contact. *J. Neurosci. Off. J. Soc. Neurosci.* **29**, 11723–11731 (2009).

2. M. Uemura, S. Nakao, S. T. Suzuki, M. Takeichi, S. Hirano, OL-protocadherin is essential for growth of striatal axons and thalamocortical projections. *Nat. Neurosci.* **10**, 1151–1159 (2007).

3. J. L. Lefebvre, D. Kostadinov, W. V. Chen, T. Maniatis, J. R. Sanes, Protocadherins mediate dendritic self-avoidance in the mammalian nervous system. *Nature*. **488**, 517–521 (2012).

4. K. Ishizuka *et al.*, Investigation of Rare Single-Nucleotide PCDH15 Variants in Schizophrenia and Autism Spectrum Disorders. *PLOS ONE*. **11**, e0153224 (2016).

5. E. M. Morrow *et al.*, Identifying autism loci and genes by tracing recent shared ancestry. *Science*. **321**, 218–223 (2008).

6. N. J. Bray *et al.*, Screening the human protocadherin 8 (PCDH8) gene in schizophrenia. *Genes Brain Behav.* **1**, 187–191 (2002).

7. Genetic determinants of common epilepsies: a meta-analysis of genome-wide association studies. *Lancet Neurol.* **13**, 893–903 (2014).

8. L. M. Dibbens *et al.*, X-linked protocadherin 19 mutations cause female-limited epilepsy and cognitive impairment. *Nat. Genet.* **40**, 776–781 (2008).

9. K. Duszyc, I. Terczynska, D. Hoffman-Zacharska, Epilepsy and mental retardation restricted to females: X-linked epileptic infantile encephalopathy of unusual inheritance. *J. Appl. Genet.* (2014), doi:10.1007/s13353-014-0243-8.

10. S. G. Ryan *et al.*, Epilepsy and mental retardation limited to females: an X-linked dominant disorder with male sparing. *Nat. Genet.* **17**, 92–95 (1997).

11. C. Depienne *et al.*, Sporadic Infantile Epileptic Encephalopathy Caused by Mutations in PCDH19 Resembles Dravet Syndrome but Mainly Affects Females. *PLoS Genet*. **5**, e1000381 (2009).

12. K. Tai, M. Kubota, K. Shiono, H. Tokutsu, S. T. Suzuki, Adhesion properties and retinofugal expression of chicken protocadherin-19. *Brain Res.* **1344**, 13–24 (2010).

13. S. R. Cooper, J. D. Jontes, M. Sotomayor, Structural determinants of adhesion by Protocadherin-19 and implications for its role in epilepsy. *eLife*. **5** (2016), doi:10.7554/eLife.18529.

14. C. A. Thu *et al.*, Generation of single cell identity by homophilic interactions between combinations of α, β and γ protocadherins. *Cell*. **158**, 1045–1059 (2014).

15. R. Rubinstein *et al.*, Molecular Logic of Neuronal Self-Recognition through Protocadherin Domain Interactions. *Cell*. **163**, 629–642 (2015).

16. D. Schreiner, J. A. Weiner, Combinatorial homophilic interaction between gamma-protocadherin multimers greatly expands the molecular diversity of cell adhesion. *Proc. Natl. Acad. Sci. U. S. A.* **107**, 14893–14898 (2010).

17. S.-Y. Kim, H. S. Chung, W. Sun, H. Kim, Spatiotemporal expression pattern of non-clustered protocadherin family members in the developing rat brain. *Neuroscience*. **147**, 996–1021 (2007).

18. C. R. Krishna-K, Expression of cadherin superfamily genes in brain vascular development. *J. Cereb. Blood Flow Metab.* **29**, 224–229 (2009).

19. M. Ozawa, R. Kemler, Altered cell adhesion activity by pervanadate due to the dissociation of alpha-catenin from the E-cadherin.catenin complex. *J. Biol. Chem.* **273**, 6166–6170 (1998).

20. D. T. Pederick *et al.*, Pcdh19 Loss-of-Function Increases Neuronal Migration In Vitro but is Dispensable for Brain Development in Mice. *Sci. Rep.* **6**, 26765 (2016).

21. I. E. Scheffer *et al.*, Epilepsy and mental retardation limited to females: an under-recognized disorder. *Brain*. **131**, 918–927 (2008).

22. N. Higurashi *et al.*, PCDH19-related female-limited epilepsy: further details regarding early clinical features and therapeutic efficacy. *Epilepsy Res.* **106**, 191–199 (2013).

23. Y. Gaitan, M. Bouchard, Expression of the δ-protocadherin gene Pcdh19 in the developing mouse embryo. *Gene Expr. Patterns*. **6**, 893–899 (2006).

24. S. C. Noctor, A. C. Flint, T. A. Weissman, R. S. Dammerman, A. R. Kriegstein, Neurons derived from radial glial cells establish radial units in neocortex. *Nature*. **409**, 714–720 (2001).

25. T. Sun, R. F. Hevner, Growth and folding of the mammalian cerebral cortex: from molecules to malformations. *Nat. Rev. Neurosci.* **15**, 217–232 (2014).

26. J. A. Miller *et al.*, Transcriptional landscape of the prenatal human brain. *Nature*. **508**, 199–206 (2014).

27. B. D. Semple, K. Blomgren, K. Gimlin, D. M. Ferriero, L. J. Noble-Haeusslein, Brain development in rodents and humans: Identifying benchmarks of maturation and vulnerability to injury across species. *Prog. Neurobiol.* **0**, 1–16 (2013).

28. V. Savova, J. Patsenker, S. Vigneau, A. A. Gimelbrant, dbMAE: the database of autosomal monoallelic expression. *Nucleic Acids Res.*, gkv1106 (2015).

29. H. V. Wilson, On some phenomena of coalescence and regeneration in sponges. *J. Exp. Zool.* **5**, 245–258 (1907).

30. P. S. Galtsoff, The awœboid movement of dissociated sponge cells. *Biol. Bull.* **45**, 153–161 (1923).

31. P. S. Galtsoff, Regeneration after dissociation (an experimental study on sponges) I. Behavior of dissociated cells of microciona prolifera under normal and altered conditions. *J. Exp. Zool.* **42**, 183–221 (1925).

32. D. Duguay, R. A. Foty, M. S. Steinberg, Cadherin-mediated cell adhesion and tissue segregation: qualitative and quantitative determinants. *Dev. Biol.* **253**, 309–323 (2003).

33. R. A. Foty, M. S. Steinberg, The differential adhesion hypothesis: a direct evaluation. *Dev. Biol.* **278**, 255–263 (2005).

34. S. M. Bello, H. Millo, M. Rajebhosale, S. R. Price, Catenin-dependent cadherin function drives divisional segregation of spinal motor neurons. *J. Neurosci. Off. J. Soc. Neurosci.* **32**, 490–505 (2012).

35. S. R. Price, N. V. De Marco Garcia, B. Ranscht, T. M. Jessell, Regulation of Motor Neuron Pool Sorting by Differential Expression of Type II Cadherins. *Cell*. **109**, 205–216 (2002).

Acknowledgments: We thank Dr L. Luo (Stanford University) and members of the Thomas lab for discussion and comments on the manuscript. We thank the patients and their families for participating in our research, together with their referring clinicians. D.T.P was supported by an Australian Government Research Training Program Scholarship. This work was supported by an NHMRC Program Grant (400121) and the PCDH19 Alliance. The supplementary materials contain additional data. Author contributions: D. T. P., J.G., J. N. H. and P. Q. T. conceived and designed the study; D.T.P. performed and analysed all experiments except the ECoG recordings which were performed by K. L. R. and S. P; S. G. P. performed the microinjection of mouse zygotes; recruitment and phenotyping of the patient cohort was performed by R.C.D. and I. E. S. and S. A. M. analysed the MRI images.; D. T. P. prepared all figures; D. T. P. , J. N. H., and P. Q. T. wrote the manuscript; and all authors revised the manuscript.

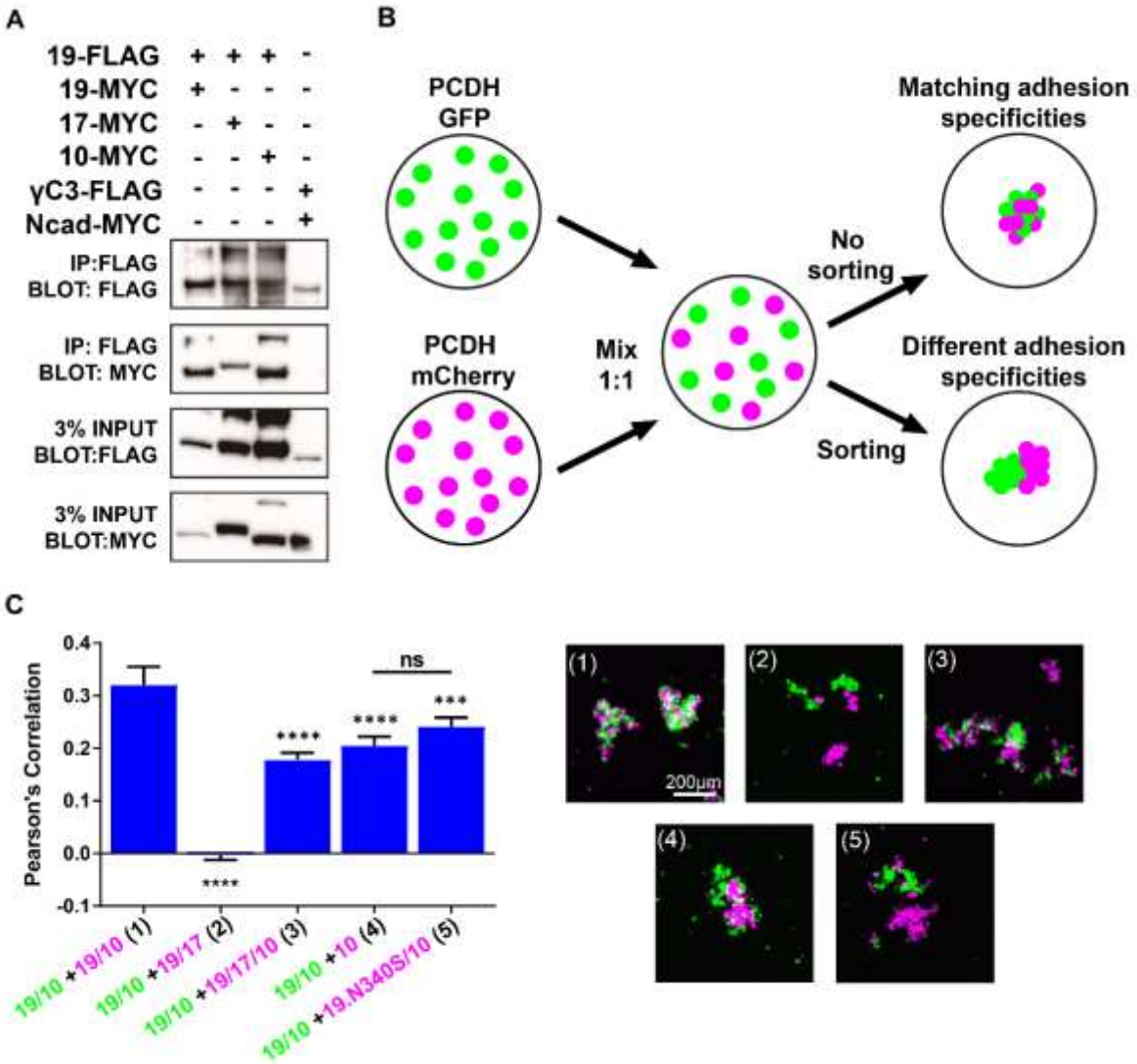
A
19-FLAG + + + -
19-MYC + - - -
17-MYC - + - -
10-MYC - - + -
γC3-FLAG - - - +
Ncad-MYC - - - +
IP:FLAG BLOT: FLAG
IP: FLAG BLOT: MYC
3% INPUT BLOT:FLAG
3% INPUT BLOT:MYC
B
PCDH GFP
PCDH mCherry
Mix 1:1
No sorting
Sorting
Matching adhesion specificities
Different adhesion specificities
C
Pearson's Correlation
0.4
0.3
0.2
0.1
0.0
-0.1
ns
****
****
****
***
19/10 +19/10 (1)
19/10 +19/17 (2)
19/10 +19/17/10 (3)
19/10 +10 (4)
19/10 +19.N340S/10 (5)
(1)
(2)
(3)
(4)
(5)
200μm

Fig. 1. δ2 non-clustered PCDHs form combinatorial codes which dictate adhesion specificity. **(**A) Co-immunoprecipitation of K562 cell lysates expressing PCDH combinations indicated by the + symbol. Lysates were pulled-down with FLAG Ab and subsequent blotting was performed with MYC Ab (*N*=3 experiments). Cis interaction of FLAG-PCDH19 with MYC-PCDH19, MYC-PCDH17 and MYC-PCDH10 was detected. Cells transfected with PCDHγC3-FLAG and Ncad-MYC served as a negative control for cis-interaction as previously reported (*14*). (B) Schematic diagram describing mixing assays performed to assess adhesion specificity. Fluorescently-labelled K562 cells expressing different NC PCDH combinations were mixed in a 1:1 ratio, allowed to aggregate and quantitatively assessed for the degree of mixing/sorting between the two populations. (C) Quantification of the degree of mixing using Pearson's correlation coefficient. Expression constructs are indicated by 19 (PCDH19), 17 (PCDH17), 10 (PCDH10) and 19.N340S (PCDH19 N340S missense mutation) (***$P < 0.001$, ****$P <$ 0.0001, ns=not significant, one-way analysis of variance (ANOVA) with Tukey's multiple comparison test against 19/10 +19/10 unless otherwise indicated). Representative images of quantified K562 mixing assays. Cell sorting is observed when populations differ by just one NC PCDH (panels (2), (3), (4), (5)), in contrast to mixing which occurs in populations express the same NC PCDHs (panel (1)). See Table S1 for additional information including *N* for each experiment.

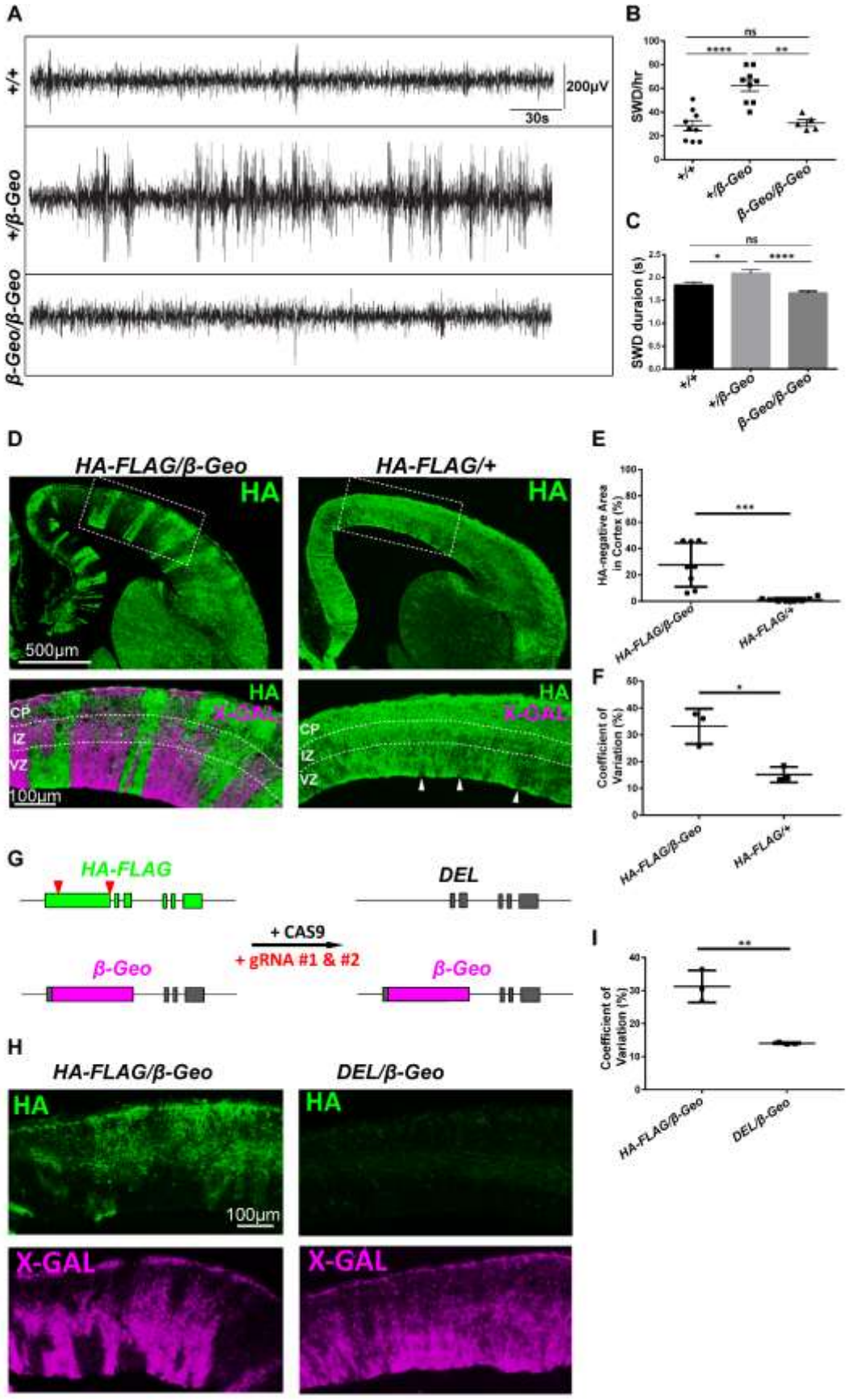
A
+/+
+/β-Geo
β-Geo/β-Geo
200μV
30s
B
SWD/hr
ns
****
**
+/+
+/β-Geo
β-Geo/β-Geo
C
SWD duration (s)
ns
*
****
D
HA-FLAG/β-Geo
HA-FLAG/+
HA
500μm
X-GAL
CP
IZ
VZ
100μm
E
HA-negative Area in Cortex (%)
***
F
Coefficient of Variation (%)
*
G
HA-FLAG
DEL
+ CAS9
+ gRNA #1 & #2
β-Geo
H
HA-FLAG/β-Geo
DEL/β-Geo
I
Coefficient of Variation (%)
**

Fig. 2. Mosaic expression of *Pcdh19* causes altered network brain activity and abnormal cell sorting between PCDH19 positive and PCDH19 negative cells in the developing cortex. (A) Representative 5 minute traces from ECoG recordings of +/+, *+/β-Geo* and *β-Geo/β-Geo* P42 mice. (B) Quantification of SWD/hr of +/+, *+/β-Geo* and *β-Geo/β-Geo* P42 mice (*****P* < 0.0001, ***P* < 0.01, ns=not significant, student's two-tailed, unpaired *t* test p values). (C) Quantification of mean SWD duration of +/+, *+/β-Geo* and *β-Geo/β-Geo* P42 mice (*****P* < 0.0001, **P* < 0.05, ns=not significant, two-way ANOVA with Tukey's multiple comparisons test). (D) Representative HA and X-gal immunostaining of 14.5 dpc *HA-FLAG/+* and *HA-FLAG/β-Geo* brains. Large blocks of HA-positive and HA-negative cells are present in the ventricular zone (VZ) of the cortex which extended into the intermediate zone (IZ) and cortical plate (CP) of *HA-FLAG/β-Geo* embryos (left). In contrast, small patches of HA-negative cells were present along the ventricle of *HA-FLAG/+* (indicated by arrowheads) which did not extend into the intermediate zone (IZ) and cortical plate (CP) (right). (E) Quantification of HA-negative regions in the cortex of 14.5 dpc *HA-FLAG/β-Geo* and *HA-FLAG/+* and brains (***P* < 0.01, unpaired *t* test). (F) Quantification HA-immunostaining intensity throughout the cortex revealed a higher degree of variability in *HA-FLAG/β-Geo* compared with *HA-FLAG/+* (**P* < 0.05, unpaired *t* test). (G) Schematic describing CRISPR-Cas9-induced conversion of *HA-FLAG/β-Geo* embryos to DEL/β-Geo. Two gRNAs targeting exon1 flanking sequences (red arrows) were injected into *HA-FLAG/β-Geo* zygotes in combination with CAS9 protein. Zygotes were transferred into pseudopregnant female mice and harvested 14 days post transfer. (H) HA and X-gal immunostaining of *HA-FLAG/β-Geo* and *DEL/β-Geo* 14 day post transfer embryonic brains). Normal redistribution of PCDH19 null cells was observed in the cortex of *DEL/β-Geo* embryos indicating that preventing the disruption of PCDH19-dependent adhesion codes abolishes abnormal cell sorting. (I) Quantification of X-gal staining intensity throughout the ventricle revealed a higher degree of variability in *HA-FLAG/β-Geo* brains compared to *HA-FLAG/+* brains (***P* < 0.01, unpaired *t* test). Also see Table S1.

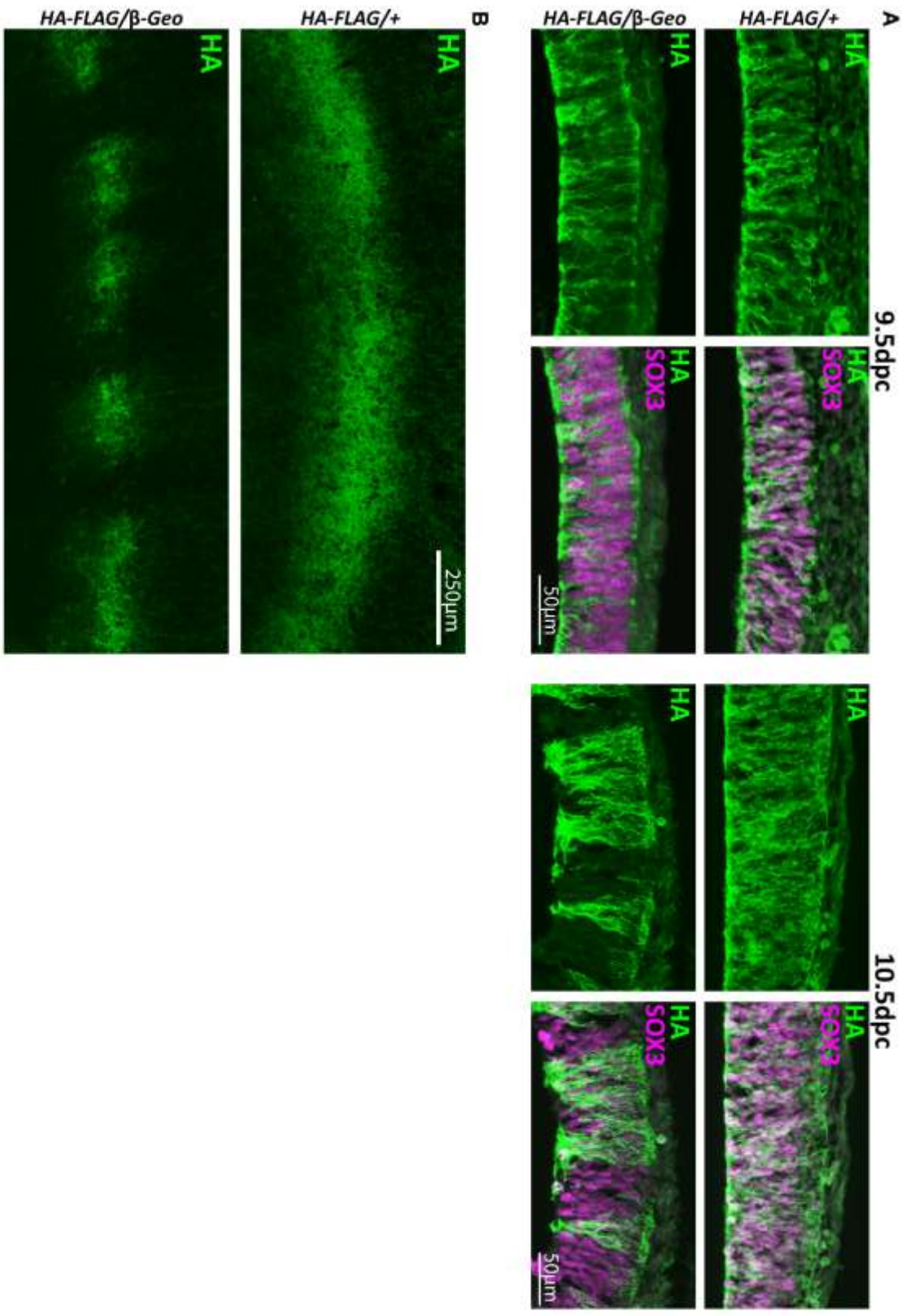
A
HA-FLAG/β-Geo
HA-FLAG/+
9.5dpc
10.5dpc
HA
SOX3
50μm
B
HA-FLAG/β-Geo
HA-FLAG/+
HA
250μm

Fig. 3. Early cortical progenitor cells are acutely sensitive to mosaic expression of *Pcdh19*. (A) Representative images of HA and SOX3 (neuroprogenitor marker) co-immunostaining of 9.5dpc and 10.5dpc *HA-FLAG/+* and *HA-FLAG/β-Geo* heads (*N*=3 of each genotype). Abnormal cell sorting is not apparent at 9.5dpc (right) but one day later the segregation of PCDH19-postive and PCDH19-null cells has occurred (left). (B) HA immunostaining of P7 *HA-FLAG/+* and *HA-FLAG/β-Geo* brains (*N*=3 of each genotype) highlights the persistence of abnormal cell sorting in the postnatal cortex.

PATIENT A

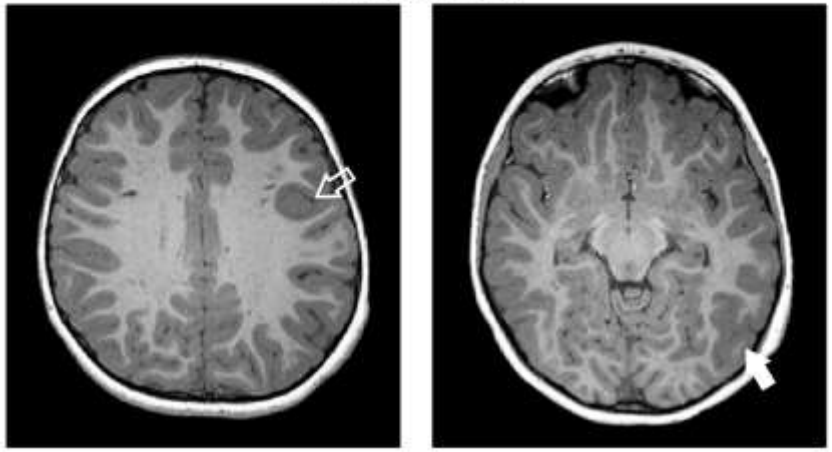

PATIENT B

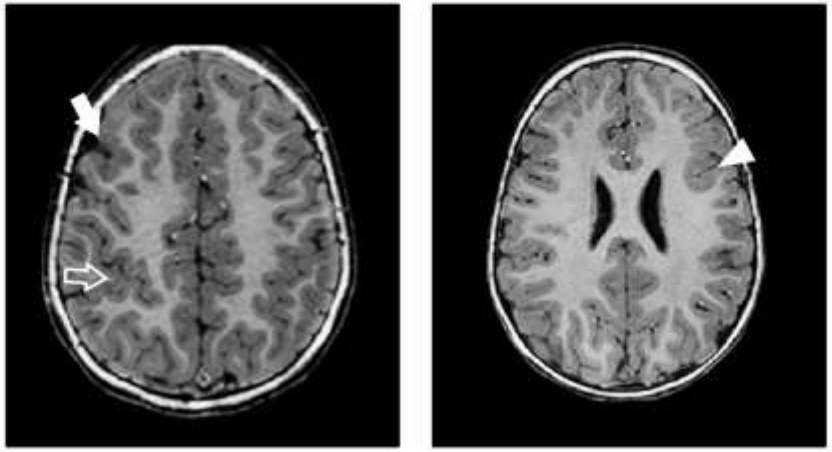

PATIENT C

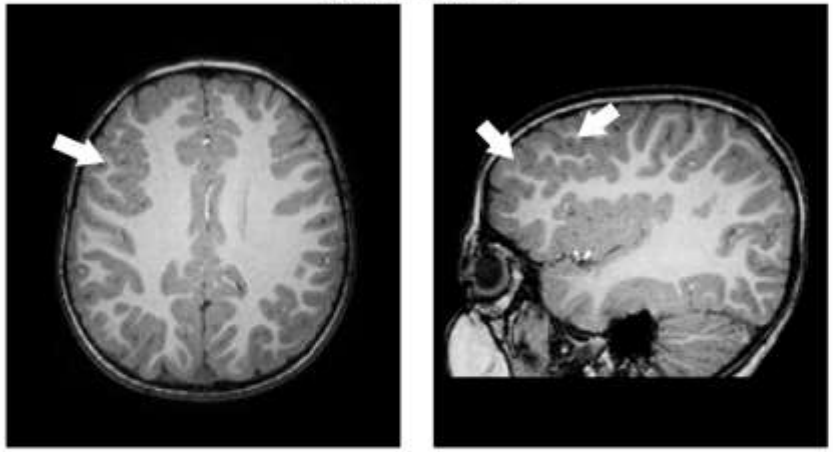

PATIENT D

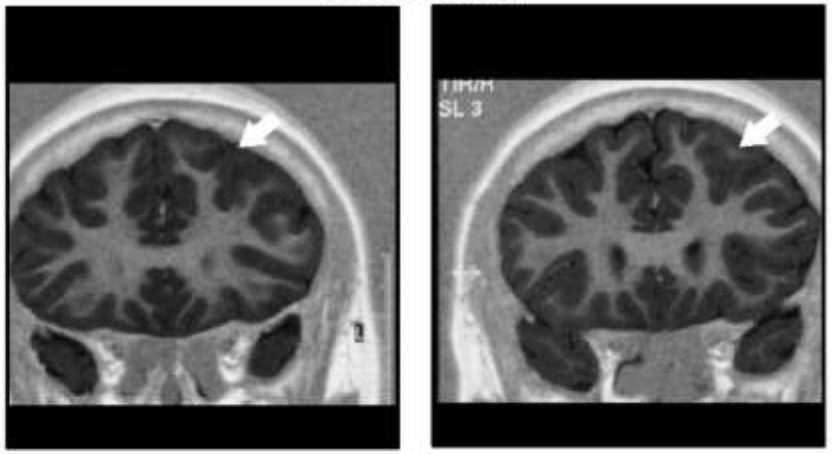

Fig. 4. Mosaic expression of *PCDH19* results in variable cortical folding abnormalities in *PCDH19*-GCE patients. Patient A: A focal area of cortical thickening in the left mid frontal lobe (open arrow) and mild cortical thickening and blurring of the grey/white interface in the left posterior temporal lobe was observed in axial T1 weighted MRI images (closed arrow). Patient B: Axial T1 weighted MRI images show an unusual stellate configuration to the right central sulcus with loss of cortical clarity (open arrow) and a focal retraction/puckered appearance of right lateral frontal cortex with complex sulcation and deep cortical thickening suggesting a likely bottom of the sulcus dysplasia (closed arrow). A focal area of suspected cortical dysplasia was identified in the left mid frontal region in addition to cortical thickening (arrowhead). Patient C: Axial and sagittal images show an unusual complex sulcal arrangement present in the right frontal lobe with 2 parallel sulci forming an ovoid ring configuration (closed arrows). Patient D: Contiguous coronal T1 images reveal cortical thickening with blurring of the grey/white junction which is highly suggestive of a left cortical dysplasia (closed arrows).

This page has been left blank intentionally.

Supplementary Materials for

Abnormal cell sorting is associated with the unique X-linked inheritance of *PCDH19* Epilepsy

Daniel T. Pederick[1, 2], Kay L. Richards[3], Sandra G. Piltz[1, 2], Simone A. Mandelstam[4, 5, 6], Russell C. Dale, Ingrid E. Scheffer[3, 7], Jozef Gecz[1, 2, 8, 9], Steven Petrou[3], James N. Hughes[1, 2] and Paul Q. Thomas[1, 2, 9]*

This PDF file includes:

Materials and methods:

Plasmids

Open reading frames (ORF) were purchased from either Vector Builder (PCDH10 and PCDH17) or Promega (PCDH19). Tagged ORFs were generated by PCR and point mutations were created using overlap extension PCR. All ORFs were cloned into GFP or Mcherry containing expression plasmids using restriction enzymes. Primer sequences used for PCR amplifications will be provided upon request.

Co-immunoprecipitation and western blotting

K562 cells (human leukemia cell line, ATCC CCL243) were transfected with 5µg of each plasmid using the Neon Transfection System (Invitrogen) and harvested 48 hours later. Transfected cells were homogenized in IP lysis buffer (25mM Tris-HCl (pH7.4), 150 mM NaCl, 1 mM EDTA, 1% NP-40, and 5% glycerol) in addition to cOmplete mini EDTA-free Protease Inhibitor Cocktail (Roche) and the PhosSTOP Phosphatase Inhibitor Cocktail (Roche). Cells were incubated in lysis buffer for 30 minutes at 4˚C, followed by brief sonication and another 30 minutes at 4˚C. The supernatant was collected by centrifugation at 13,200 rpm for 30 minutes at 4˚C. 1uL of mouse anti-FLAG (Sigma, F3165), was added to each supernatant and incubated overnight at 4˚C. 30µL of Dynabeads™ Protein G (Invitrogen) was added to each sample and incubated for 2 hours at 4˚C. Beads were washed 3x in IPP150 wash buffer (150mM NaCl, 10mM Tris/HCl, 0.1% Igepal (Sigma) and 5% glycerol) and resuspended in 2X SDS load buffer. Lysates were separated on Invitrogen Bolt™ precast 4-12% polyacrylamide gels and transferred to PVDF membrane before being blotted. Antibodies and their corresponding dilutions were: mouse anti-FLAG 1:5000 (Sigma, F3165) and rabbit anti MYC (Cell Signalling Technology #2272S) Membranes were blocked in 5% BSA + 5% skim milk in tris-buffered saline + 0.1% Tween20 (TBST)

and antibodies were incubated with the membrane in 5% BSA in TBST at 4°C overnight. Membranes were developed using Bio-Rad Clarity Western ECL substrate and imaged using a Bio-Rad ChemiDoc.

K562 Aggregation Assay

$2x10^6$ K562 (human leukaemia cell line, ATCC CCL243) cells were nucleofected with 10µg of plasmid DNA using the Neon Transfection System (Invitrogen) and incubated for 24 hours. Cells were harvested, treated with DNase (1mg/mL) and passed through a 40µm cell strainer (Falcon) to obtain a single cell suspension. $2x10^5$ cells were added to each well of a 12 well tray and allowed to aggregate for 2-4 hours on a nutator at 37˚C/5% CO_2. Aggregated cells were imaged using a Nikon Eclipse Ti microscope. To quantify aggregate size images were exported to ImageJ where they were subjected to an equal threshold transformation and aggregate size was assessed using the "analyse particle" function. Raw data was transferred to GraphPad Prism 7 where a Kruskal-Wallis test was performed.

Cytospin immunofluorescence

K562 cell aggregates were fixed in 2% PFA for 2 hours at RT, washed in PBS and resuspended in 30% sucrose. Aggregate suspensions were then adhered to superfrost slides (ThermoFisher) using a Shandon Cytospin 3 (1000rpm, 10 minutes)**.** Immunofluorescence was performed by blocking with 10% foetal calf serum for 1 hour and then incubating with mouse anti-FLAG (Sigma, F3165) 1/1000 overnight at 4˚C and then secondary antibody for 2 hours at room temperature (donkey anti-mouse 488 (Jackson ImmunoResearch)). Images were acquired on a Leica SP5 Confocal microscope.

K562 Mixing Assay

$2x10^6$ K562 cells were nucleofected with 5µg of each plasmid DNA (10µg total for co-nucleofections) and incubated for 24 hours. Cells were harvested, treated with DNase (1mg/mL) and passed through a 40µm cell strainer (Falcon) to obtain a single cell suspension. $1x10^5$ cells from each sample were pooled and added to each well of a 12 well tray and allowed to aggregate for 3 hours on a nutator at 37˚C/5% CO_2. Aggregated cells were imaged using a Nikon Eclipse Ti microscope. Each condition was performed in biological triplicate with four technical repeats. Pearson's correlation coefficient was calculated using NIS Elements Advanced Research Software (Nikon). Raw data was transferred to GraphPad Prism 7 where a one way ANOVA test was performed.

Electrocorticogram (ECoG) recordings

ECoG recordings were obtained from 6-week-old female mice for wild type (WT), heterozygote (Het) and knock-out (KO) animals in DBA/2J background (>N9). Surgery for ECoG electrode placement was performed as described previously (*36*). In brief, mice were anesthetized with 2-4% isoflurane and 2 epidural silver "ball" electrodes implanted on each hemisphere above the somatosensory cortices using the following co-ordinates with respect to bregma: (ML $\pm$ 3 mm and AP -0.7 mm). A ground electrode was positioned 2.5 mm rostral and 1 mm lateral from bregma. Mice were allowed to recover for at least 72 hours post-surgery. Continuous ECoGs were then recorded in freely moving animals for 3-hour epochs during daylight hours following a standard 30-minute habituation period; a minimum of 9 hours recording was obtained for data analysis. Signals were band pass filtered at 0.1 to 200 Hz and sampled at 1 kHz using Powerlab 16/30 (AD Instruments Pty. Ltd., Sydney, NSW, Australia). In a subset of mice simultaneous video/ECoG recordings were also obtained to correlate behaviour. The spike wave discharge (SWD) signature of +/+, *+/β-Geo* and *β-Geo/ β-Geo* mice on a DBA/2J background was 5-8Hz as previously reported for this genetic background (*37*, *38*). 5 Quantification of spike wave discharges (SWD) was done for each

genotype based on rhythmic biphasic spikes with voltage at least two-fold higher than mean background. Measurements for SWD duration were made for a total of 350 events, defined as time from the first spike peak to final peak with a minimum of one-second duration.

Generation and Genotyping of *Pcdh19*$^{HA\text{-}FLAG}$ Mice

CRISPR gRNA was designed to target near the stop codon of PCDH19 (5'-TATCGTTCTCTAAAGCCATC-3') using CRISPR Design tool (crispr.mit.edu) and generated in house by cloning 20 nt oligos into pX330-U6-Chimeric_BB-CBh-hSpCas9, which was a gift from Feng Zhang (Addgene plasmid # 42230) according to the protocol described in (*39*). The ssDNA HA-FLAG oligo was designed to insert HA-FLAG 5' of the *Pcdh19* stop codon with 60bp of homology either side (5'-CGGAAGGATGGTCGTGACAAGGAATCTCCTAGCGTGAAGCGTCTGAAGGATATCGTTCTCTACCCATACGATGTTCCAGATTACGCTGACTACAAAGACGATGACGACAAGTAAAGCCATCTGGGTTCGAGGAAGAGAGAACAGAAACCACACTGGCTAGTGAAGATGTAGCAG-3') (Integrated DNA Technologies (IDT)). Cas9 mRNA was generated by IVT (mMessage) from pCMV/T7-hCas9 (Toolgen) digested with XhoI. The gRNA (50ng/µL), Cas9 mRNA (100ng/µL) and ssDNA HA-FLAG donor oligo (100ng/µL) (IDT) were injected into C57BL/6N zygotes, transferred to pseudopregnant recipients and allowed to develop to term. Founder pups were screened for HA-FLAG insertions by PCR across targeted region (F 5'-TAGCGTGAAGCGTCTGAAGG-3', R 5'-CAGGCAGTAGGGGTGTTCAG-3') and run on an agarose gel. A larger product of 281bp represented the HA-FLAG allele, while a smaller 230bp product represented the wild type allele. Positive samples were Sanger sequenced to verify the correct insertion of the HA-FLAG sequence. Routine genotyping was performed by agarose gel electrophoresis in which PCR products generated with the above primers were separated. The gender of embryos was

identified by PCR amplification of SRY (F 5'-CAGTTTCATGACCACCACCA-3' and R 5'-CATGAGACTGCCAACCACAG-3') and the gender of postnatal mice was assessed by analysis of external genitalia. All animal work was conducted following approval by The University of Adelaide Animal Ethics Committee (approval number S-2013-187, S-2014-068, S-2014-199A) in accordance with the Australian code for the care and use of animals for scientific purposes.

Protein Extraction and western blotting

Hippocampi for protein extraction were minced in extraction buffer (50mM Tris, 150mM NaCl, 1% NP40 (Roche) and 1% Triton X-100 (Sigma)) and incubated at 4˚C for 30 minutes. Lysates were separated on Invitrogen Bolt™ precast 4-12% polyacrylamide gels and transferred to PVDF membrane before being blotted. Antibodies and their corresponding dilutions were: mouse anti-PCDH19 1:200 (Abcam, ab57510), mouse anti-FLAG 1:5000 (Sigma, F3165), mouse anti-HA 1:1000 (Cell Signalling Technology #2367) and rabbit anti-β-ACTIN 1:1000 (Cell Signalling Technology, #4697). Membranes were blocked in 5% BSA + 5% skim milk in tris-buffered saline + 0.1% Tween20 (TBST) and antibodies were incubated with the membrane in 5% BSA in TBST at 4°C overnight. Membranes were developed using Bio-Rad Clarity Western ECL substrate and imaged using a Bio-Rad ChemiDoc.

Immunofluorescence

8.5dpc, 9.5 dpc and 10.dpc whole embryos were dissected and fixed for 2-6 hours in 4% paraformaldehyde (PFA) at 4˚C. To collect 13.5dpc, 14.5dpc and 15.5dpc embryonic brains pregnant dams were cardiacally perfused with 4% PFA. Embryonic brains were dissected and post fixed in 4% PFA at 4˚C for 4-6 hours. To collect P7 brains mice were cardiacally

perfused with 4% PFA, brains dissected and post fixed in 4% PFA at 4˚C for 4-6 hours. Embryos and brains were then cryoprotected in 30% sucrose and frozen in OCT embedding medium. 16µm sections were cut using a Leica CM1900 cryostat. Sections were blocked with 0.3% TritonX-100 and 10% horse serum in PBS for 1 hour at room temperature. Sections were then incubated overnight with rabbit anti-HA 1:300 (Cell Signalling Technology, #3724), goat anti-SOX3 1:300 (R&D Systems, AF2569), rat anti-CTIP2 1:400 (Abcam, ab18465) and rabbit anti-CUX1 1:400 (Santa Cruz, sc-13024) at 4˚C and then secondary antibody for 2 hours at room temperature (donkey anti-rabbit TxRed (Life Tehcnologies), donkey anti-goat 488 (Life Technologies), donkey anti-guinea pig 488 (Jackson ImmunoResearch) and goat anti-rat 488 (Jackson ImmunoResearch). Images were acquired on a Nikon Eclipse Ti microscope false coloured using Adobe Photoshop.

X-Gal staining

14.5dpc brains were collected as described above. Staining was performed as previously described (*20*). Images were acquired on a Nikon Eclipse Ti microscope and false coloured using Adobe Photoshop.

X-gal and immunofluorescence co-staining

X-gal staining was performed then followed by immunofluorescence staining as described above. Images were acquired on a Nikon Eclipse Ti microscope and false coloured using Adobe Photoshop.

Quantification of HA negative areas

Images from *HA-FLAG/β-Geo* transformed until HA-negative regions in *HA-FLAG/β-Geo* cortices became blank pixels. Equal thresholding was performed on *HA-FLAG/+* images. Regions of interest were drawn around the cortex of all images and the percent of HA-negative area (blank pixels) was assessed. Raw data was transferred to GraphPad Prism 7 where a Student's T-test was performed.

Quantification of HA immunostaining intensity variability

21 regions of interest (50µm x 50µm) were placed throughout the cortex and intensity measured using NIS Elements Advance Research Software (Nikon). Raw data was transferred to GraphPad Prism 7 where the coefficient of variation was calculated.

Generation of *DEL/β-Geo* embryos from *HA-FLAG/β-Geo* zygotes

CRISPR gRNAs were designed to target immediately after the Pcdh19 ATG and the 3' end of exon 1 (5'-CGGGACGGTGATCGCTAACG-3') and (5'-AGATCCGGACCTACAATTGC) respectively and generated as above. The gRNA (25ng/µL each) and CAS9 protein (50ng/µL) were combined and incubated for 10 minutes on ice before being injected into *Pcdh19*$^{HA\text{-}FLAG/\beta\text{-}Geo}$ zygotes which were then transferred to pseudopregnant recipients. 14 days post transfer embryonic brains were collected and fixed for 4-6 hours in 4% PFA at 4˚C.

Embryos were screened for the presence of HA-FLAG alleles by PCR as described above to confirm *Pcdh19*$^{HA\text{-}FLAG/\beta\text{-}Geo}$ identity. *Pcdh19*$^{HA\text{-}FLAG/\beta\text{-}Geo}$ embryos were then screened for large deletions of exon1 by PCR (F 5'-GCAATCTCAGCATTGGAGCC-3') (R 5'-GGGGTTTTTAGACCGACCGA-3'). Large deletions of exon 1 were confirmed via Sanger sequencing. *Pcdh19*$^{HA\text{-}FLAG/\beta\text{-}Geo}$ embryos positive for large deletions were then processed

for HA and X-Gal staining as described above, along with *Pcdh19*$^{HA\text{-}FLAG/\beta\text{-}Geo}$ embryos to serve as controls.

Quantification of X-gal staining intensity variability

14 regions of interest (50µm x 50µm) were placed throughout the ventricular zone of the cortex and intensity measured using NIS Elements Advance Research Software (Nikon). Raw data was transferred to GraphPad Prism 7 where the coefficient of variation was calculated.

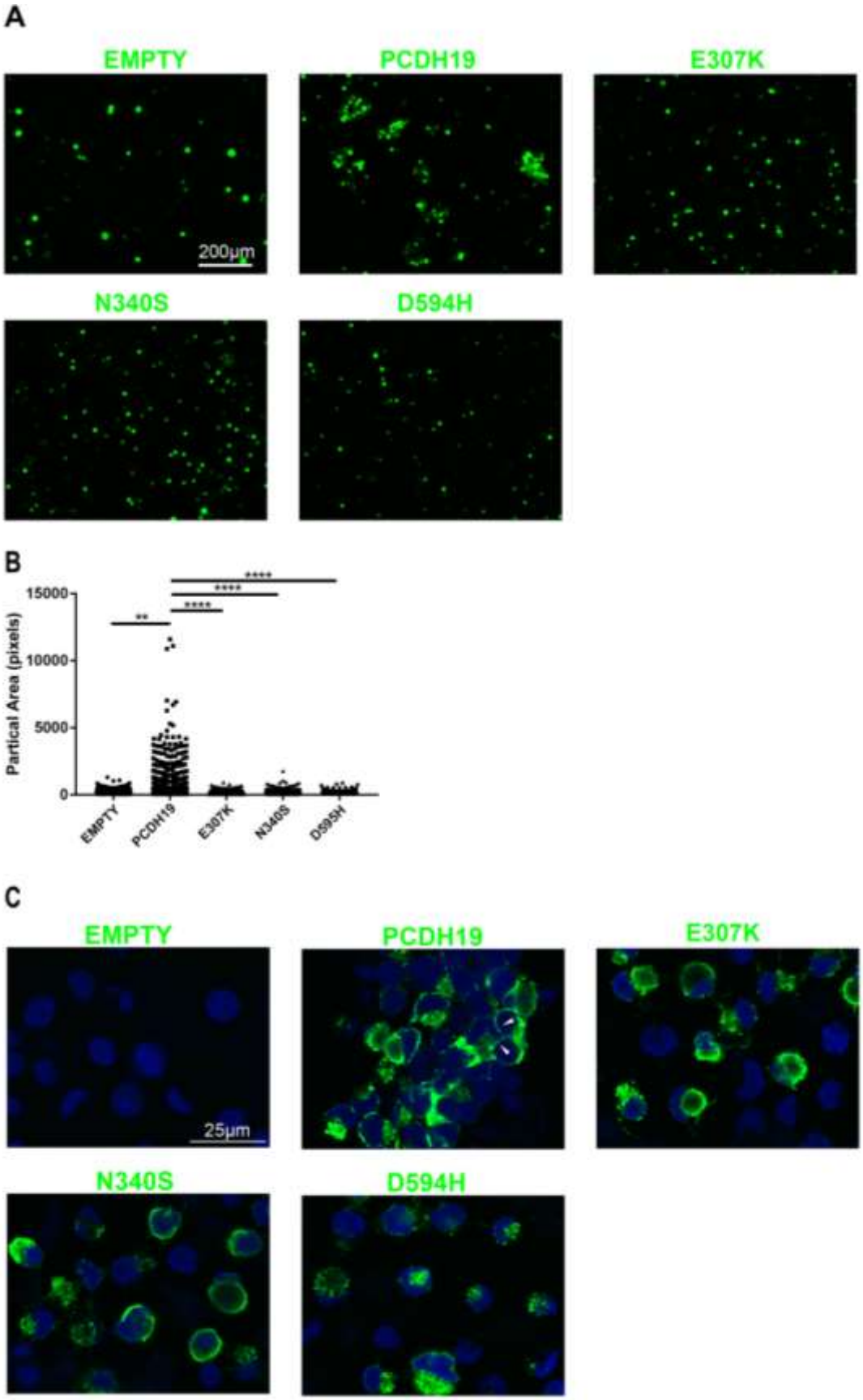
A
EMPTY
PCDH19
E307K
200µm
N340S
D594H
B
Partical Area (pixels)
15000
10000
5000
0
**
****
****
****
EMPTY
PCDH19
E307K
N340S
D595H
C
EMPTY
PCDH19
E307K
25µm
N340S
D594H

Fig. S1. *PCDH19*-GCE missense mutations lack adhesive function. (A) K562 cells transiently expressing PCDH19 form aggregates whereas cells K562 cells expressing *PCDH19*-GCE mutations do not. (B) Quantification of aggregate particle size confirms the lack of adhesive function in *PCDH19*-GCE missense mutations. (n=2 biological repeats with 10 technical replicates, **, $p<0.01$, ****, $p<0.0001$). (B) FLAG immunohistochemistry of K562 cells, white arrows indicate enrichment of PCDH19 at cell-cell interfaces (n=2 biological repeats with 4 technical replicates).

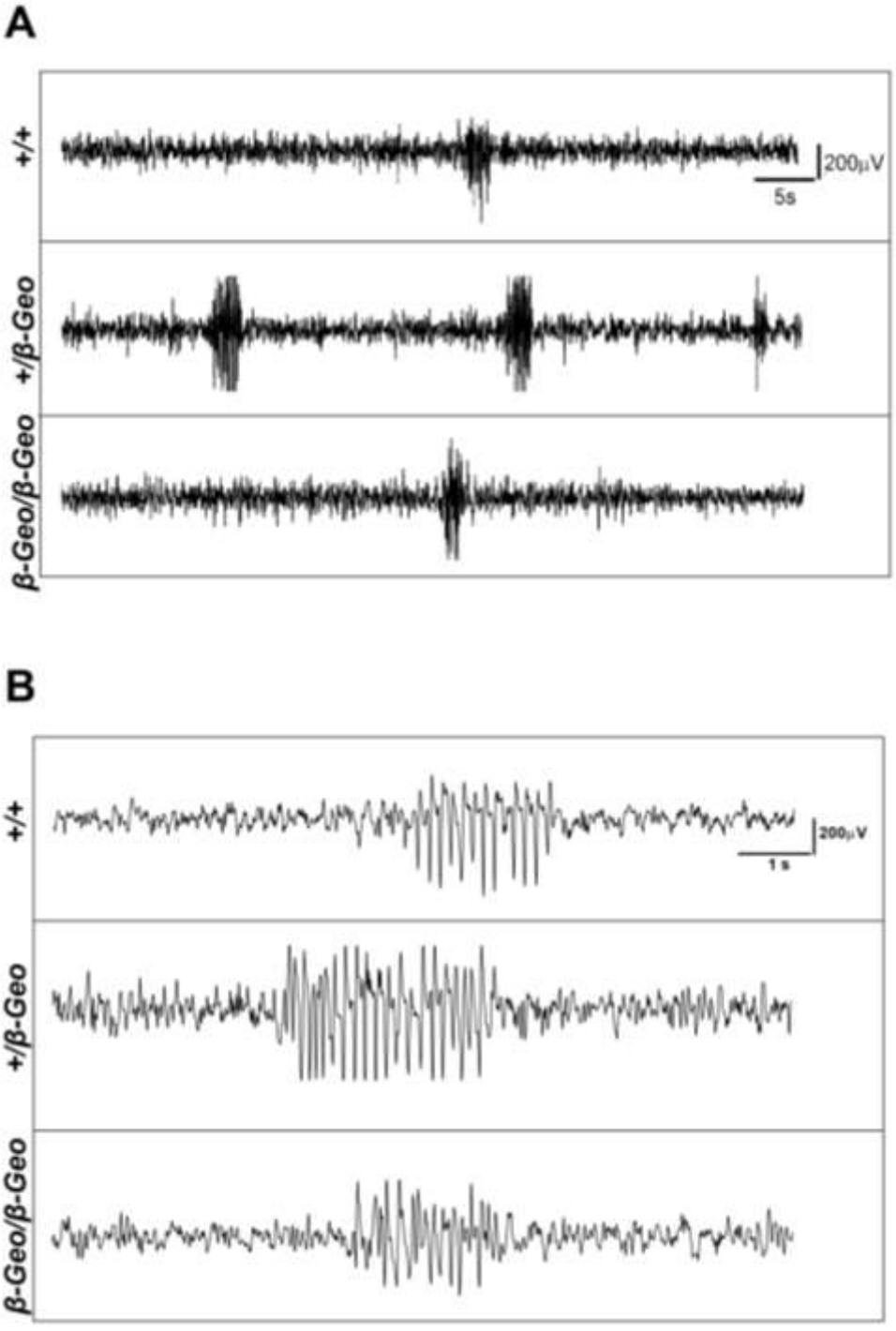
A
+/+
200μV
5s
+/β-Geo
β-Geo/β-Geo
B
+/+
200μV
1 s
+/β-Geo
β-Geo/β-Geo

Fig. S2. *+/ß-geo* mice display increased SWD frequency, duration and epileptiform events during sleep. (A) Representative trace showing multiple SWDs highlighting the increased frequency of SWDs in *+/ß-Geo* mice. (B) Single representative SWDs highlighting the increased duration of SWDs in *+/ß-Geo* mice.

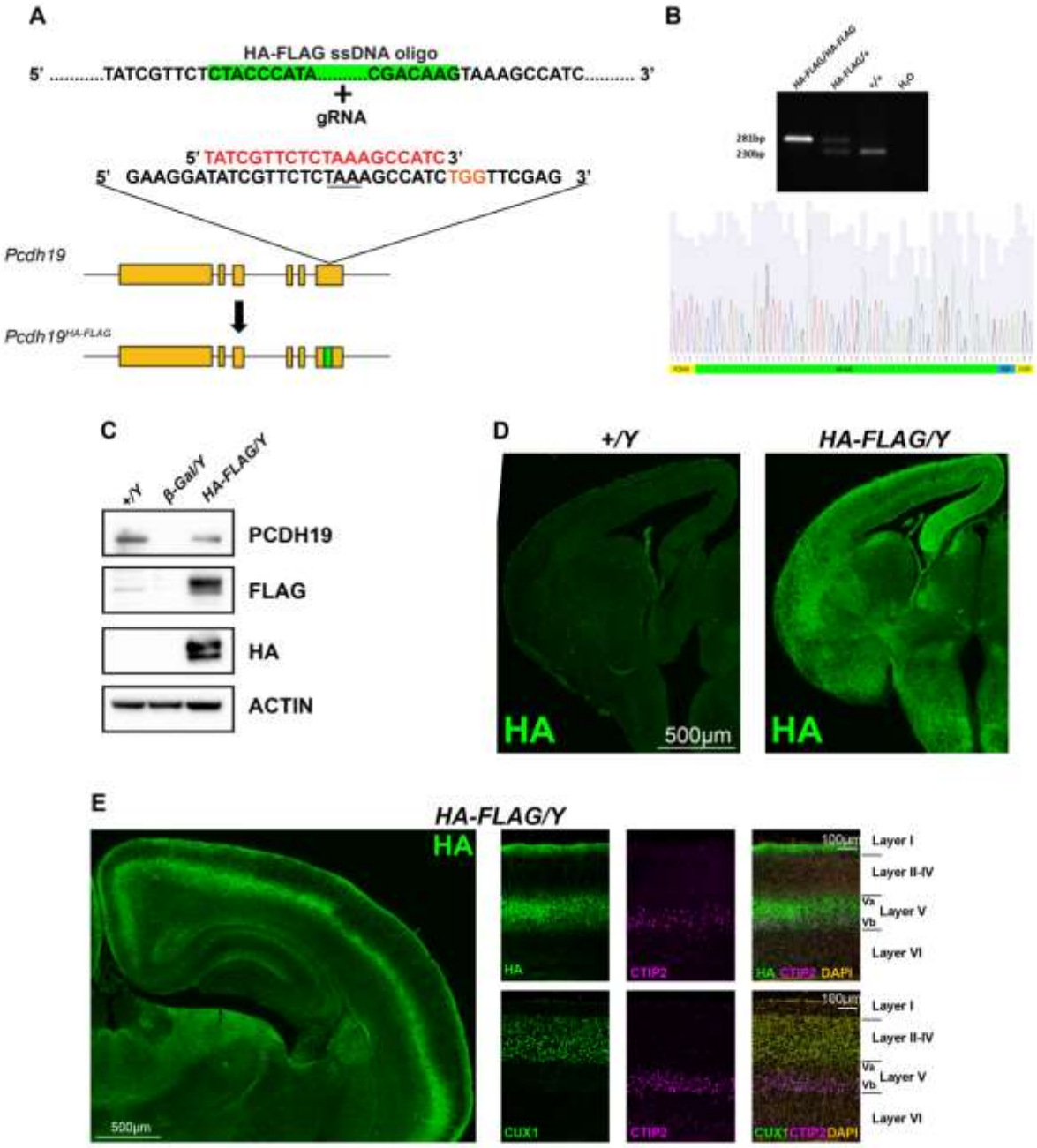
A
HA-FLAG ssDNA oligo
5' .....TATCGTTCTCTACCCATA.....CGACAAGTAAAGCCATC..... 3'
+
gRNA
5' TATCGTTCTCTAAAGCCATC 3'
5' GAAGGATATCGTTCTCTAAAGCCATCTGGTTCGAG 3'
Pcdh19
Pcdh19HA-FLAG
B
HA-FLAG/HA-FLAG
HA-FLAG/+
+/+
H2O
281bp
230bp
C
+/Y
β-Gal/Y
HA-FLAG/Y
PCDH19
FLAG
HA
ACTIN
D
+/Y
HA-FLAG/Y
HA
500µm
HA
E
HA-FLAG/Y
HA
500µm
HA
CTIP2
HA CTIP2 DAPI
CUX1
CTIP2
CUX1 CTIP2 DAPI
Layer I
Layer II-IV
Va
Vb
Layer V
Layer VI

Fig. S3. Generation of *Pcdh19*$^{HA\text{-}FLAG}$ mice using CRISPR-Cas9 editing reveals PCDH19 expression in the developing and postnatal brain. (A) *Pcdh19*$^{HA\text{-}FLAG}$ targeting strategy showing the HA-FLAG epitope (green), gRNA (red), PAM site (orange) and endogenous STOP codon (underlined). (B) PCR amplification was used to identify the insertion of the HA-FLAG epitope tag. (C) Protein extracts from P14 hippocampus were immunoblotted with PCDH19, FLAG, HA and β-ACTIN antibodies. (D) HA-immunostaining of 14.5 dpc *Pcdh19*$^{+/Y}$ and *Pcdh19*$^{HA\text{-}FLAG/Y}$ (n=3). (E) HA immunostaining of P7 *Pcdh19*$^{HA\text{-}FLAG}$ brains and co-staining with layer markers CTIP2 (layer Vb) and CUX1 (layer II-IV) (n=3), reveals PCDH19 expression predominantly in layers I and V.

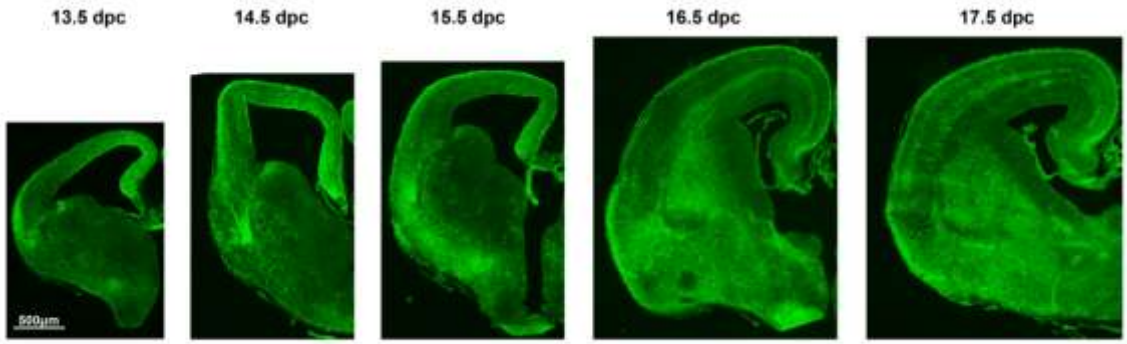

Fig. S4. PCDH19 has widespread expression throughout brain development. HA-immunostaining of HA-FLAG/Y embryonic brains revealed PCDH19 expression in the cortex, hippocampus, ganglionic eminence and sub-cortical regions. Representative images of *N*=3 for each time point.

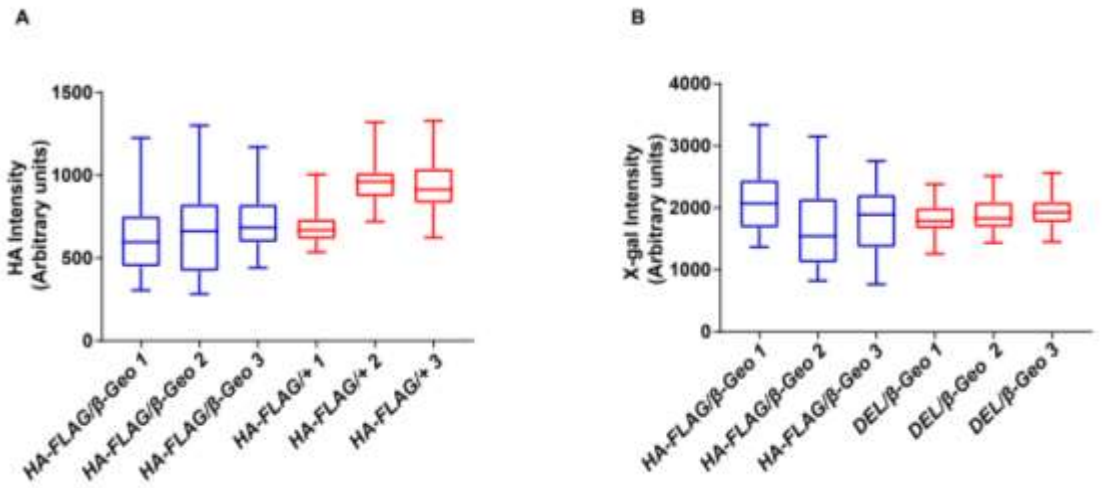

Fig. S5. Raw data used to quantify the variation seen between *HA-FLAG/β-Geo* animals. (A) Box and whisker plot demonstrating range of HA immunostaining intensity values for each independent animal. (B) Box and whisker plot demonstrating range of X-gal staining intensity values for each independent animal.

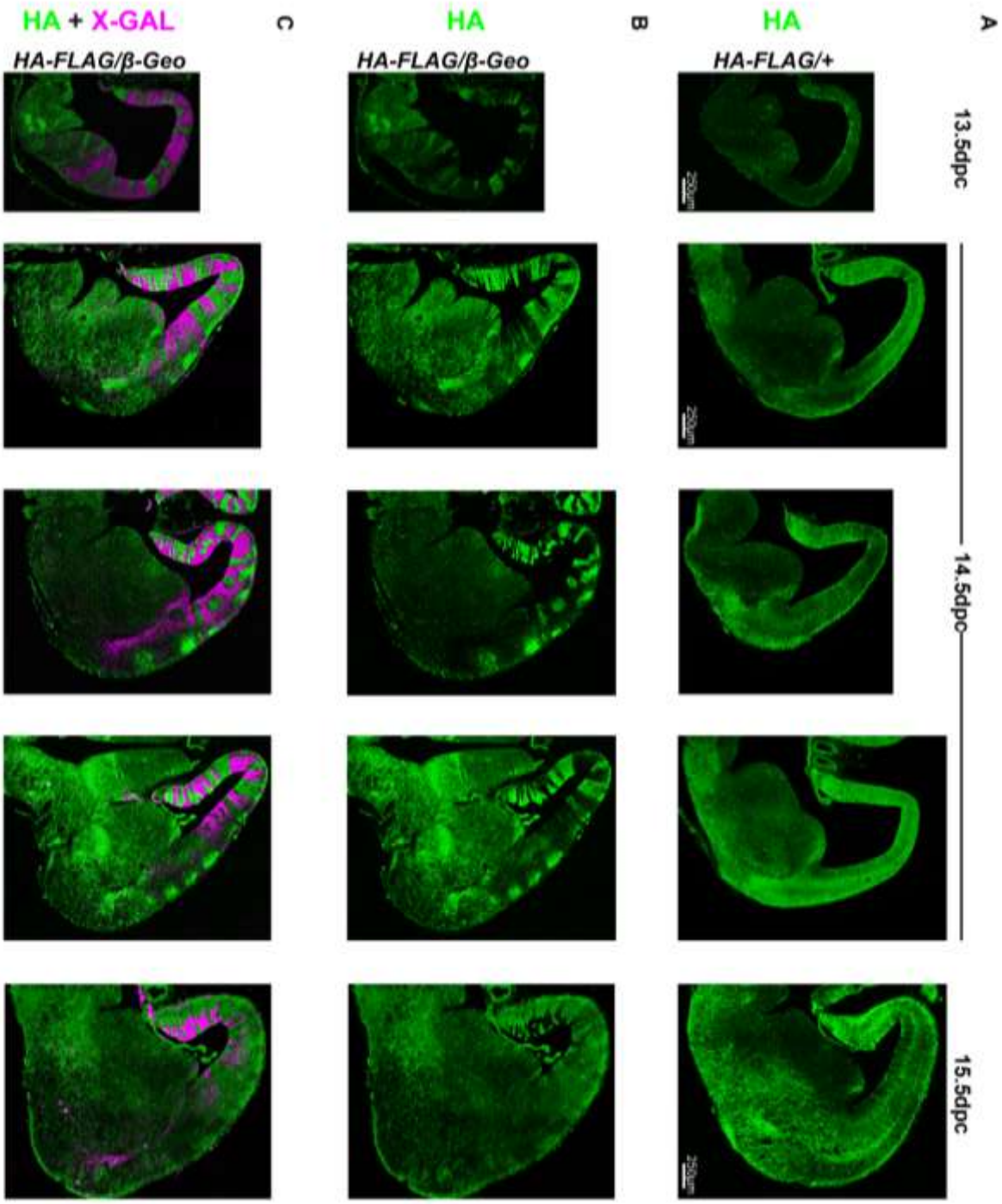
HA + X-GAL
HA-FLAG/β-Geo
C
HA
HA-FLAG/β-Geo
B
HA
HA-FLAG/+
A
13.5dpc
14.5dpc
15.5dpc

Fig. S6. Abnormal cell sorting patterns in *HA-FLAG/β-Geo* brains is variable. (A) HA immunostaining of *HA-FLAG/+* brains at 13.5, 14.5 and 15.5 dpc. (B) HA immunostaining of *HA-FLAG/β-Geo* brains at 13.5, 14.5 and 15.5 dpc. (C) X-Gal staining of *HA-FLAG/β-Geo* brains from (B) merged with HA images.

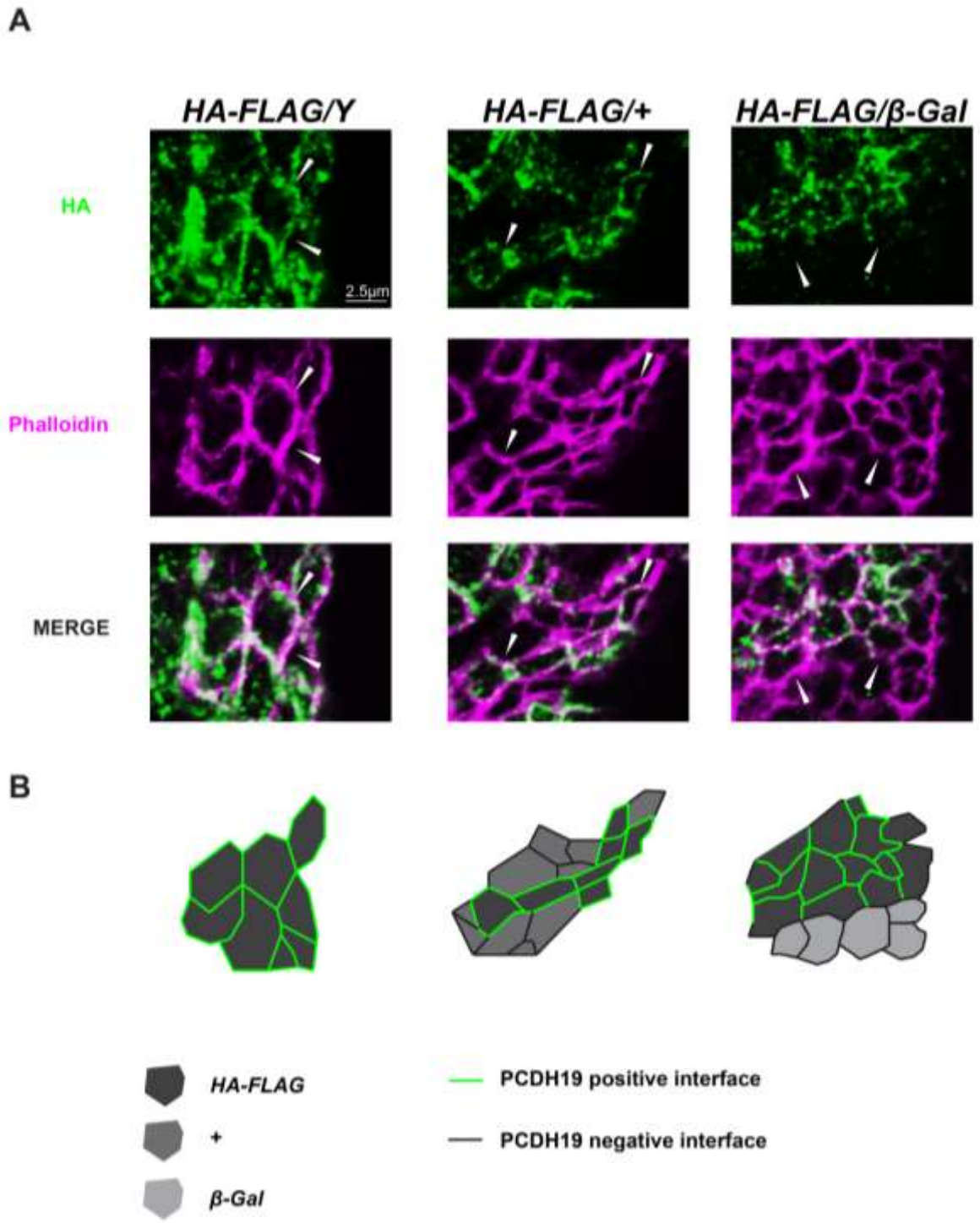
A
HA-FLAG/Y
HA-FLAG/+
HA-FLAG/β-Gal
HA
Phalloidin
MERGE
2.5μm
B
HA-FLAG
+
β-Gal
PCDH19 positive interface
PCDH19 negative interface

Fig. S7. PCDH19 is not present at cell-cell interfaces between WT PCDH19 and null PCDH19 radial glial cells. (A) HA and Phalloidin staining of the ventricular lining of 10.5 dpc cortex (*N*=3 of each genotype). PCDH19 is present at all cell-cell boundaries in HA-FLAG/Y brains (left, arrowheads) and at boundaries between HA-positive and HA-negative cells in HA-FLAG/+ brains (middle, arrowheads). In contrast, PCDH19 is not present at boundaries between HA-positive and HA-negative cells providing further evidence of its homotypic nature in vivo (right, arrowheads). (B) Schematic representation of PCDH19 location (green lines) overlapping with Phalloidin positive cell-cell interfaces (black lines).

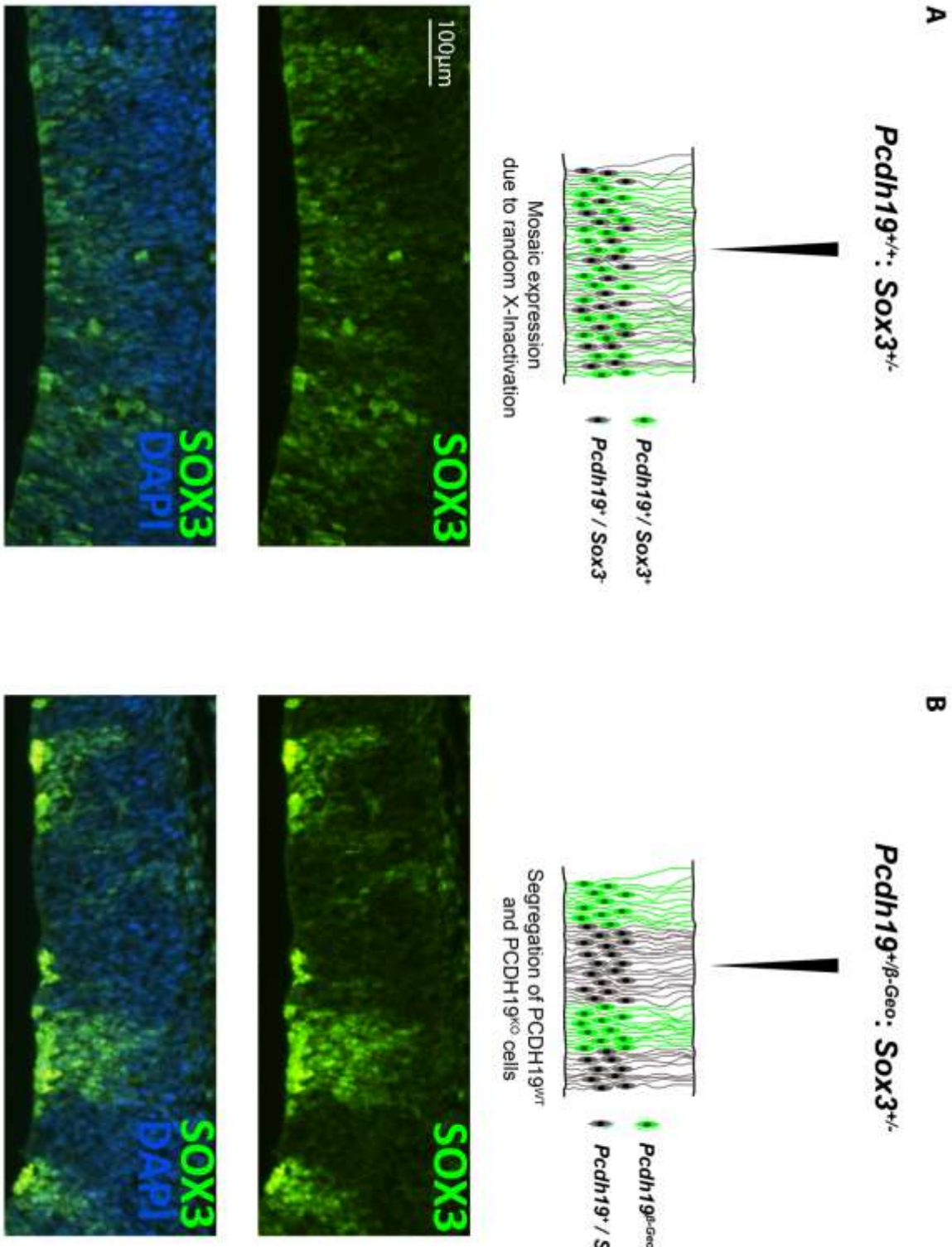
A
Pcdh19+/+: Sox3+/-
Pcdh19+/ Sox3+
Pcdh19- / Sox3-
Mosaic expression
due to random X-Inactivation
100µm
SOX3
SOX3
DAPI
B
Pcdh19+/β-Geo: Sox3+/-
Pcdh19β-Geo / Sox3+
Pcdh19- / Sox3-
Segregation of PCDH19WT
and PCDH19KO cells
SOX3
SOX3
DAPI

Fig. S8. Cell segregation in the developing cortex is due to the redistribution of cell bodies. (A) SOX3 immunostaining of *Pcdh19*$^{+/+}$: *Sox3*$^{+/-}$ 13.5 dpc cortex shows normal X-inactivation *(N*=3). (B) SOX3 staining of *Pcdh19*$^{+/\beta\text{-Geo}}$:*Sox3*$^{+/-}$ in 13.5 dpc cortex shows abnormal cell sorting of SOX3 +ve and SOX3 –ve neural progenitor cells *(N*=3). SOX3 null mice were generated by CRISPR-Cas9 mediated deletion of the whole ORF (unpublished data).

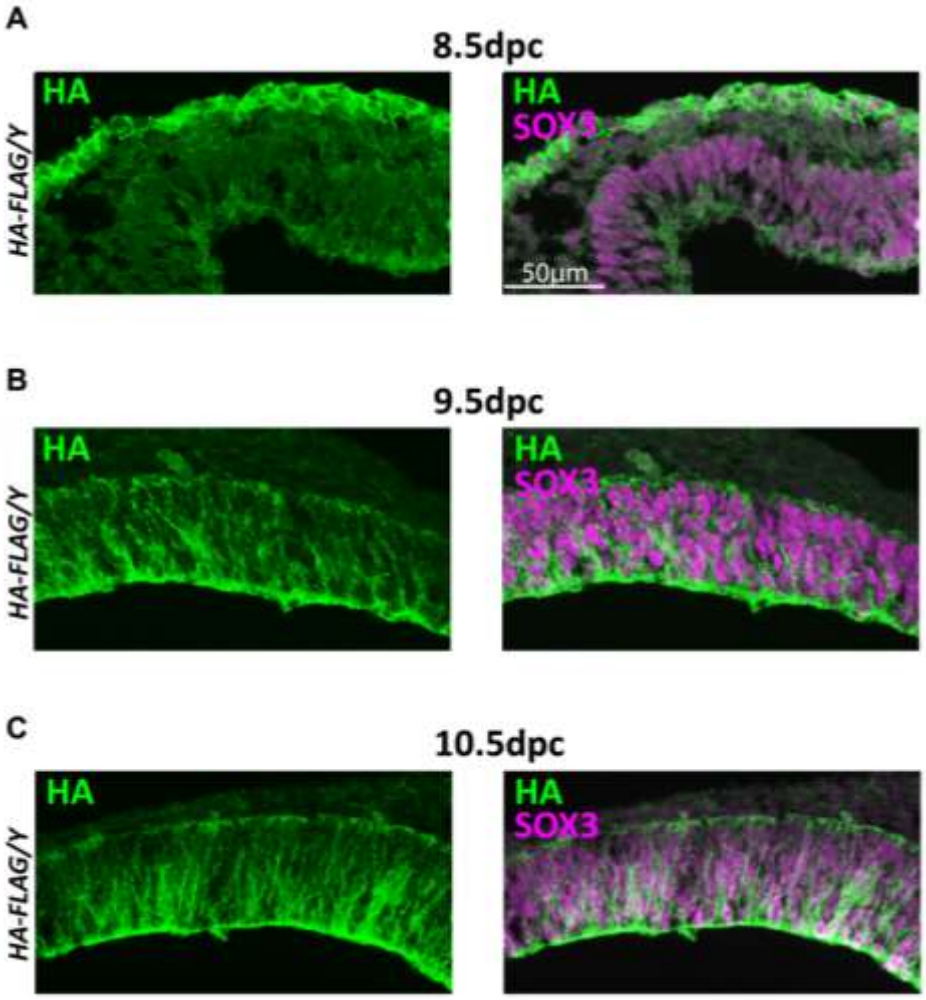

Fig. S9. PCDH19 is first expressed at 9.5dpc in the developing cortex. (A) At 8.5dpc PCDH19 expression is present in the surface ectoderm but no in the SOX3 +ve neuroepithelial cells *(N*=3) (B) PCDH19 expression is present in the developing cortex at 9.5dpc and 10.5 dpc (*N*=3 of each time point).

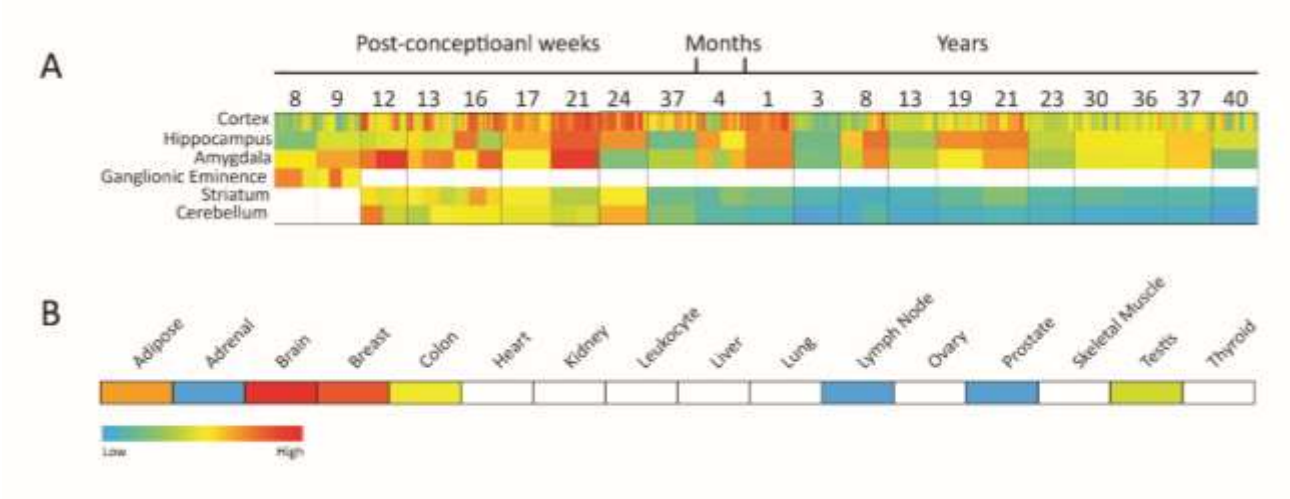

Fig. S10. *PCDH19* expression is enriched in the human cortex throughout embryonic development. (A) RNA-seq data from the Allen Brain Atlas highlighting the differential expression of *PCDH19* in brain regions throughout development (*26*). (B) Data from RNA-Seq of human individual tissues and mixture of 16 tissues (Illumina Body Map) was retrieved from EMBL-EBI ArrayExpress database under accession number E-MTAB-513 (http://www.ebi.ac.uk/arrayexpress/experiments/E-MTAB-513/) on 09/01/2016 highlighting the differential expression of *PCDH19* across different regions of the adult human. (White boxes represent no data available).

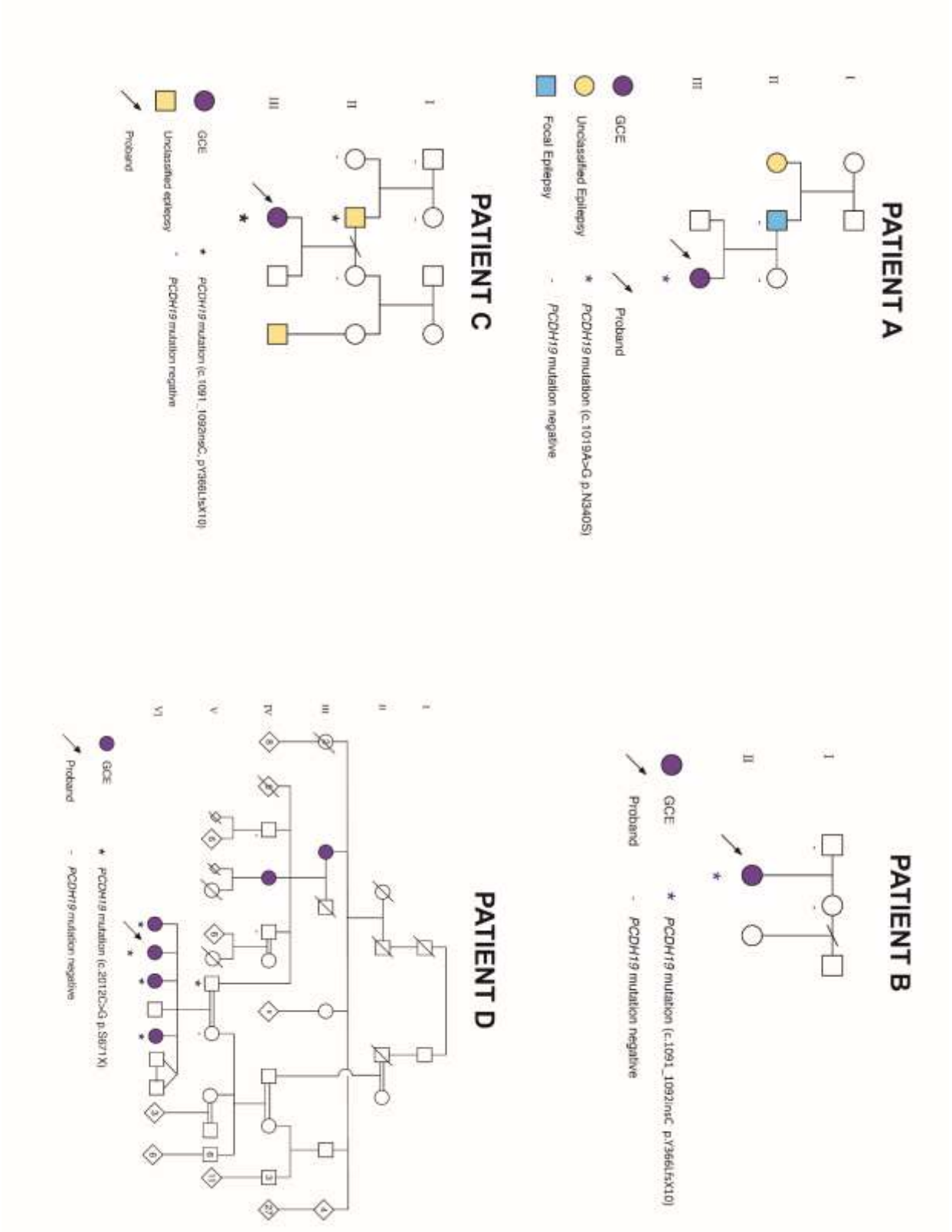
PATIENT A
I
II
III
GCE
Proband
Unclassified Epilepsy
* PCDH19 mutation (c.1019A>G, p.N340S)
Focal Epilepsy
- PCDH19 mutation negative
PATIENT B
I
II
GCE
* PCDH19 mutation (c.1091_1092insC, p.Y366LfsX10)
Proband
- PCDH19 mutation negative
PATIENT C
I
II
III
GCE
* PCDH19 mutation (c.1091_1092insC, pY366LfsX10)
Unclassified epilepsy
- PCDH19 mutation negative
Proband
PATIENT D
I
II
III
IV
V
VI
GCE
* PCDH19 mutation (c.2012C>G p.S671X)
Proband
- PCDH19 mutation negative

Fig. S11. Pedigrees of *PCDH19*-GCE patients which present with cortical folding abnormalities. (A) Acquired mutation through paternal inheritance (*21*). (B) Mutation was de novo (unpublished data). (C) Mutation was de novo (unpublished data). (D) Acquired mutation through paternal inheritance (unpublished data).

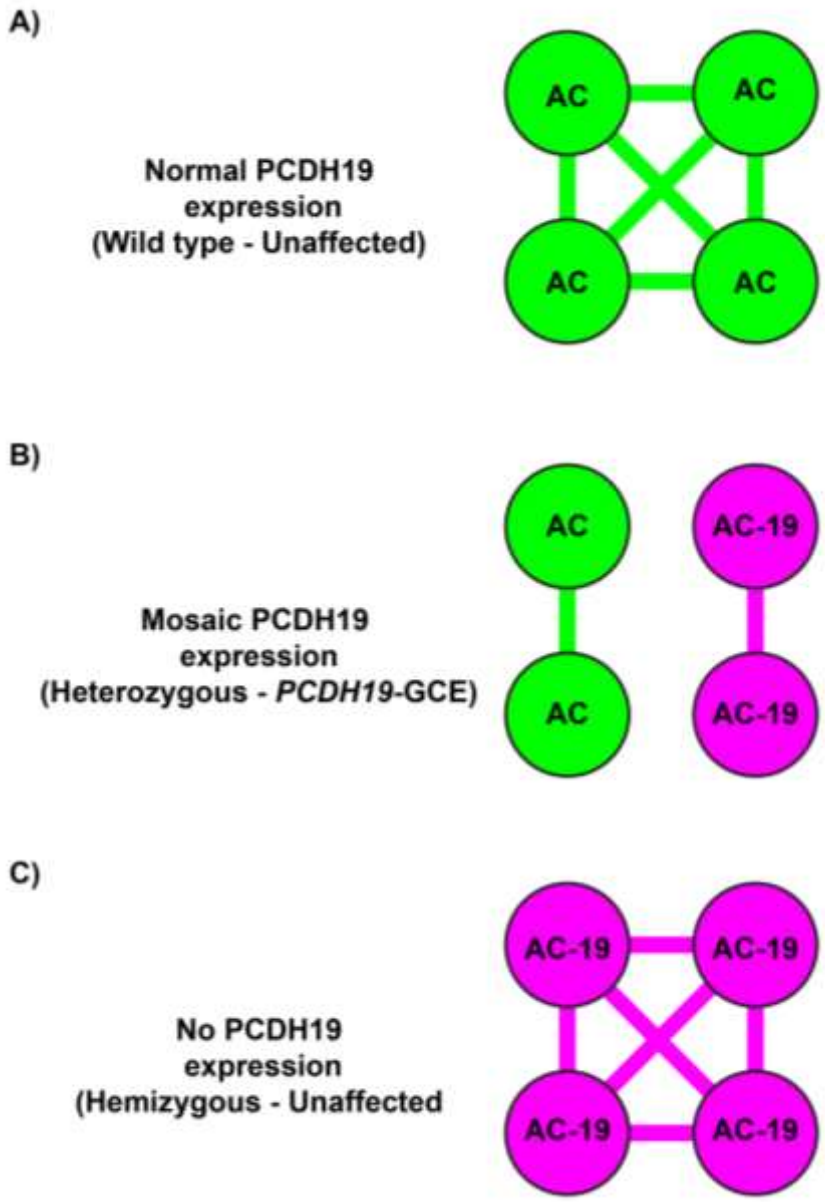

Fig. S12. Mosaic expression but not the complete loss of PCDH19 leads to incompatible adhesion codes. (A) Wild type cells in normal individuals have a complementary adhesion code (AC) which contains PCDH19, allowing interaction between cells. (B) Mosaic expression of PCDH19 leads to a mixture of cells that contain different adhesion codes. This causes wild type (AC) and null (AC-19) cells to have different adhesion codes and interact with cells that have a complementary adhesion code. (C) The complete loss of PCDH19 uniformly removes PCDH19 from all cells and therefore does not affect complementary adhesion codes.

Fig. 1. Mean ± SEM (3 biological repeats, 4 replicates in each)				
19/10 + 19/10	19/10 + 19/17	19/10 + 19/17/10	19/10 + 10	19/10 + 19.N340S/10
0.3206 ± 0.02001	0.2052± 0.009815	-0.003057 ± 0.005415	0.1784 ± 0.007573	0.2413 ± 0.01005

Fig. 2B Mean ± SEM (# animals)		
+/+ (9)	*+/β-Geo (9)*	*β-Geo/β-Geo (5)*
29 ± 4	62 ± 5	31 ± 3

Fig. 2C Mean ± SEM (# animals)		
+/+ (9)	*+/β-Geo (9)*	*β-Geo/β-Geo (5)*
1.8 ± 0.06	2.09 ±0.08	1.66 ± 0.05

Fig. 2E Mean ± SEM (3 animals of each)	
HA-FLAG/β-Geo	*HA-FLAG/+*
27.6 ± 5.9	1.2 ± 0.5

Fig. 2F Mean ± SEM (3 animals of each)	
HA-FLAG/β-Geo	*HA-FLAG/+*
33.2 ± 3.8	15.1 ± 1.7

Fig. 2I Mean ± SEM (3 animals of each)	
HA-FLAG/β-Geo	*DEL/β-Geo*
31.3 ± 2.8	14.1 ± 0.1

Table S1. Raw data from quantitative analysis, Fig. 1-2.

Patient	Mutation	Current age; sex	Age at seizure onset & offset	Seizure types	Febrile at seizure onset	Seizure clusters	Seizure triggers	Developmental and ID	Regression	ASD	Psychiatric features	EEG Features	AEDs	Other features
A	de novo c.1019A>G p.N340S	9y; F	9m Ongoing	GTCS, T, FBTC, FIAS	Yes	Yes		Normal at 18m Language concerns by 2y3m Moderate ID	No	Yes	None	At 18m: 2 GTCS captured, fast rhythms in central regions with rapid evolution to GSW, right posterior quadrant discharges	LEV, VPA, CLB, LTG, PHT	
B	de novo c.1091_1092insC p.Y368Lfs X10	7y; F	5m Ongoing	FT, FBTC, FIAS, GTCS, H, Ab, T, MJ, At. SE	No	Yes	Fever Vaccination	Normal at 8m Moderate DD from 8m Severe ID by 6y	At 8m	Yes	Behavioural problems	At 16-18m: generalised slowing with frequent unilateral & bilateral frontal & central epileptiform activity	Pyridoxine, folic acid, CBZ*, PB, LEV, CLB, VPA, TPM, Sistiperitol (Beneficial), PHT, paraldehyde, prednisolone, midazolam, KD, VNS	Significant sleep problems
C	Pat m/n c.1091_1092insC p.Y368Lfs X10	11y; F	10m Ongoing	FIAS, GTCS, FBTC, CSE	No	Yes	Illness	Normal until seizure onset Moderate ID	Speech regression at 13m	Yes	Extreme OCD Behavioural problems	At 11.5m: generalised slow wave, no definite epileptiform discharges At 12m: seizure captured with bilateral fast spike-wave, runs of occipital spike-wave At 3y3m: ictal recording with possible left fronto-temporal load in with rapid generalisation and fast spike-wave	LTG, PB, PHT, CBZ, TPM*, CZP, Pyridoxine, LEV	Strabismus
D	Pat m/n c.2012C>G p.S671X (21)	22y; F	6m 18y	GTCS, Ab	Yes	Yes	Fever	ID	Yes	Yes	Behavioural problems	At 1y, 3y and 6y: generalised slowing At 15y: generalised 10Hz PSW and 4-5Hz spike-wave	VPA, CBZ, CZP	

Table S1. Brief clinical description of *PCDH19*-GCE patients which have cortical folding abnormalities. FIAS, focal impaired awareness seizure; GTCS, generalised tonic-clonic seizure; FBTC, focal bilateral tonic-clonic seizure; T, tonic; FT, focal tonic; H, hemiclonic; Ab, absence; MJ, myoclonic jerks; At, atonic; m, months; y, years; F, female; M, male; GSW, generalised spike-wave; AED, anti-epileptic drug; PSW, polyspike-wave; w, weeks; SE, status epilepticus; DD, developmental delay; VEM, video EEG monitoring; CSE, convulsive status epilepticus; ID, intellectual disability; pat inh, paternally inherited; VNS, nagal nerve stimulator; LEV, levetiracetam; VPA, sodium valproate; LTG, lamotrigine; PB, phenobarbitone; PHT, phenytoin; CBZ, carbamazepine; CZP, clonazepam; CLB, clobazam; TPM, topiramate; KD, ketogenic diet; OCD, obsessive compulsive disorder. *exacerbated seizures. Current medications underlined.

Complete references:

1. A. M. Garrett, J. A. Weiner, Control of CNS synapse development by γ-protocadherin-mediated astrocyte-neuron contact. *J. Neurosci. Off. J. Soc. Neurosci.* **29**, 11723–11731 (2009).

2. M. Uemura, S. Nakao, S. T. Suzuki, M. Takeichi, S. Hirano, OL-protocadherin is essential for growth of striatal axons and thalamocortical projections. *Nat. Neurosci.* **10**, 1151–1159 (2007).

3. J. L. Lefebvre, D. Kostadinov, W. V. Chen, T. Maniatis, J. R. Sanes, Protocadherins mediate dendritic self-avoidance in the mammalian nervous system. *Nature*. **488**, 517–521 (2012).

4. K. Ishizuka *et al.*, Investigation of Rare Single-Nucleotide PCDH15 Variants in Schizophrenia and Autism Spectrum Disorders. *PLOS ONE*. **11**, e0153224 (2016).

5. E. M. Morrow *et al.*, Identifying autism loci and genes by tracing recent shared ancestry. *Science*. **321**, 218–223 (2008).

6. N. J. Bray *et al.*, Screening the human protocadherin 8 (PCDH8) gene in schizophrenia. *Genes Brain Behav.* **1**, 187–191 (2002).

7. Genetic determinants of common epilepsies: a meta-analysis of genome-wide association studies. *Lancet Neurol.* **13**, 893–903 (2014).

8. L. M. Dibbens *et al.*, X-linked protocadherin 19 mutations cause female-limited epilepsy and cognitive impairment. *Nat. Genet.* **40**, 776–781 (2008).

9. K. Duszyc, I. Terczynska, D. Hoffman-Zacharska, Epilepsy and mental retardation restricted to females: X-linked epileptic infantile encephalopathy of unusual inheritance. *J. Appl. Genet.* (2014), doi:10.1007/s13353-014-0243-8.

10. S. G. Ryan *et al.*, Epilepsy and mental retardation limited to females: an X-linked dominant disorder with male sparing. *Nat. Genet.* **17**, 92–95 (1997).

11. C. Depienne *et al.*, Sporadic Infantile Epileptic Encephalopathy Caused by Mutations in PCDH19 Resembles Dravet Syndrome but Mainly Affects Females. *PLoS Genet*. **5**, e1000381 (2009).

12. K. Tai, M. Kubota, K. Shiono, H. Tokutsu, S. T. Suzuki, Adhesion properties and retinofugal expression of chicken protocadherin-19. *Brain Res.* **1344**, 13–24 (2010).

13. S. R. Cooper, J. D. Jontes, M. Sotomayor, Structural determinants of adhesion by Protocadherin-19 and implications for its role in epilepsy. *eLife*. **5** (2016), doi:10.7554/eLife.18529.

14. C. A. Thu *et al.*, Generation of single cell identity by homophilic interactions between combinations of α, β and γ protocadherins. *Cell*. **158**, 1045–1059 (2014).

15. R. Rubinstein *et al.*, Molecular Logic of Neuronal Self-Recognition through Protocadherin Domain Interactions. *Cell*. **163**, 629–642 (2015).

16. D. Schreiner, J. A. Weiner, Combinatorial homophilic interaction between gamma-protocadherin multimers greatly expands the molecular diversity of cell adhesion. *Proc. Natl. Acad. Sci. U. S. A.* **107**, 14893–14898 (2010).

17. S.-Y. Kim, H. S. Chung, W. Sun, H. Kim, Spatiotemporal expression pattern of non-clustered protocadherin family members in the developing rat brain. *Neuroscience*. **147**, 996–1021 (2007).

18. C. R. Krishna-K, Expression of cadherin superfamily genes in brain vascular development. *J. Cereb. Blood Flow Metab.* **29**, 224–229 (2009).

19. M. Ozawa, R. Kemler, Altered cell adhesion activity by pervanadate due to the dissociation of alpha-catenin from the E-cadherin.catenin complex. *J. Biol. Chem.* **273**, 6166–6170 (1998).

20. D. T. Pederick *et al.*, Pcdh19 Loss-of-Function Increases Neuronal Migration In Vitro but is Dispensable for Brain Development in Mice. *Sci. Rep.* **6**, 26765 (2016).

21. I. E. Scheffer *et al.*, Epilepsy and mental retardation limited to females: an under-recognized disorder. *Brain*. **131**, 918–927 (2008).

22. N. Higurashi *et al.*, PCDH19-related female-limited epilepsy: further details regarding early clinical features and therapeutic efficacy. *Epilepsy Res.* **106**, 191–199 (2013).

23. Y. Gaitan, M. Bouchard, Expression of the δ-protocadherin gene Pcdh19 in the developing mouse embryo. *Gene Expr. Patterns*. **6**, 893–899 (2006).

24. S. C. Noctor, A. C. Flint, T. A. Weissman, R. S. Dammerman, A. R. Kriegstein, Neurons derived from radial glial cells establish radial units in neocortex. *Nature*. **409**, 714–720 (2001).

25. T. Sun, R. F. Hevner, Growth and folding of the mammalian cerebral cortex: from molecules to malformations. *Nat. Rev. Neurosci.* **15**, 217–232 (2014).

26. J. A. Miller *et al.*, Transcriptional landscape of the prenatal human brain. *Nature*. **508**, 199–206 (2014).

27. B. D. Semple, K. Blomgren, K. Gimlin, D. M. Ferriero, L. J. Noble-Haeusslein, Brain development in rodents and humans: Identifying benchmarks of maturation and vulnerability to injury across species. *Prog. Neurobiol.* **0**, 1–16 (2013).

28. V. Savova, J. Patsenker, S. Vigneau, A. A. Gimelbrant, dbMAE: the database of autosomal monoallelic expression. *Nucleic Acids Res.*, gkv1106 (2015).

29. H. V. Wilson, On some phenomena of coalescence and regeneration in sponges. *J. Exp. Zool.* **5**, 245–258 (1907).

30. P. S. Galtsoff, The awœboid movement of dissociated sponge cells. *Biol. Bull.* **45**, 153–161 (1923).

31. P. S. Galtsoff, Regeneration after dissociation (an experimental study on sponges) I. Behavior of dissociated cells of microciona prolifera under normal and altered conditions. *J. Exp. Zool.* **42**, 183–221 (1925).

32. D. Duguay, R. A. Foty, M. S. Steinberg, Cadherin-mediated cell adhesion and tissue segregation: qualitative and quantitative determinants. *Dev. Biol.* **253**, 309–323 (2003).

33. R. A. Foty, M. S. Steinberg, The differential adhesion hypothesis: a direct evaluation. *Dev. Biol.* **278**, 255–263 (2005).

34. S. M. Bello, H. Millo, M. Rajebhosale, S. R. Price, Catenin-dependent cadherin function drives divisional segregation of spinal motor neurons. *J. Neurosci. Off. J. Soc. Neurosci.* **32**, 490–505 (2012).

35. S. R. Price, N. V. De Marco Garcia, B. Ranscht, T. M. Jessell, Regulation of Motor Neuron Pool Sorting by Differential Expression of Type II Cadherins. *Cell*. **109**, 205–216 (2002).

36. H. O. Tan *et al.*, Reduced cortical inhibition in a mouse model of familial childhood absence epilepsy. *Proc. Natl. Acad. Sci. U. S. A.* **104**, 17536–17541 (2007).

37. V. A. Letts, B. J. Beyer, W. N. Frankel, Hidden in plain sight: spike-wave discharges in mouse inbred strains. *Genes Brain Behav.* **13**, 519–526 (2014).

38. C. A. Reid *et al.*, Multiple molecular mechanisms for a single GABAA mutation in epilepsy. *Neurology*. **80**, 1003–1008 (2013).

39. L. Cong *et al.*, Multiplex genome engineering using CRISPR/Cas systems. *Science*. **339**, 819–823 (2013).

CHAPTER 4

General Discussion

Together the data presented from Chapters 2 and 3 indicate that loss of *Pcdh19* does not overly affect mouse brain development but when expressed in a mosaic fashion causes abnormal cell sorting between *Pcdh19* WT and *Pcdh19* null cells. Furthermore, we show that abnormal cell sorting in the developing cortex correlates with altered network brain activity consistent with changes that can underlie seizures which is not observed in mice completely lacking *Pcdh19*. We also provide evidence supporting the combinatorial activity of NC PCDHs contributing to specific cell-cell interactions, which when disrupted leads to abnormal cell sorting. Overall we provide a long sought after cellular mechanism for the unique X-linked inheritance pattern of *PCDH19*-GCE. However, the examination of results from Chapters 2 and 3 together raise additional discussion points which are addressed below.

In Chapter 2 we reported no gross morphological abnormalities in *Pcdh19*$^{+/\beta\text{-}Geo}$ and *Pcdh19*$^{\beta\text{-}Geo/\beta\text{-}Geo}$ brains and identified no spontaneous seizures in *Pcdh19*$^{+/\beta\text{-}Geo}$ mice. This may be due to the inherent difficulty of observing seizures in neonatal mice (the equivalent age where clusters of seizures present in *PCDH19*-GCE patients) or genetic differences between mice and humans. In fact, attempts to model epilepsy in mice do not always genetically match the corresponding human disorder. For example, heterozygous *TSC1/2* mutations in humans lead to Tuberous Sclerosis and seizures but an epilepsy phenotype is not observed in mice with heterozygous *Tsc1/2* loss of function mutations (European Chromosome 16 Tuberous Sclerosis Consortium, 1993; Fryer et al., 1987; Kobayashi et al., 2001; Onda et al., 1999). Similarly, heterozygous mutations in *PRRT2* cause a range of epileptic and movement disorders that has recently been modelled using a *Prrt2* null mouse (Michetti et al., 2017). Phenotypes representing epilepsy and movement disorders were only reported in *Prrt2* homozygous mice and no pathogenic phenotype was observed in *Prrt2* heterozygous null mice. Despite the lack of seizures in *Pcdh19*$^{+/\beta\text{-}Geo}$ mice, it is important to

note that ECoG analysis identified an epileptic like phenotype. Therefore, the *PCDH19*-GCE mouse model does follow the human inheritance pattern since *Pcdh19*$^{+/\beta\text{-}Geo}$ mice display epileptiform brain activity and *Pcdh19*$^{\beta\text{-}Geo/\beta\text{-}Geo}$ mice do not. We therefore conclude that heterozygous mice are an appropriate informative model to investigate the cellular mechanisms that underlie the disease. It appears likely that inherent differences in human and mouse brain development are the reason for the presentation of different phenotypes.

We also show that the loss of *Pcdh19* leads to a subtle increase in the migration potential of neurons *in vitro*. This was not seen in *vivo* as there were no ectopically positioned *Pcdh19* null neurons present in both the developing and adult brain. This was further supported by our findings in Chapter 3, where *Pcdh19* WT and *Pcdh19* null cells were both correctly positioned when simultaneously identified within the same brain. We therefore believe it is unlikely that the subtle migration defect seen in cultured *Pcdh19* null neurons contributes to pathogenesis as we confirmed mice completely lacking *Pcdh19* have normal brain activity. Instead the slightly increased migration potential may highlight another endogenous role of *Pcdh19* that does not contribute to *PCDH19*-GCE.

The abnormal cell sorting of neuroepithelial progenitors and radial glia raises the intriguing possibility that the entire mature cortex segregates according to their developmental expression of *Pcdh19*. If the entire cortex is subjected to rearrangement due to mosaic *Pcdh19* expression, it is possible the epileptiform brain activity observed in adult *Pcdh19*$^{+/\beta\text{-}Geo}$ is not only caused by defective connectivity between *Pcdh19* WT and *Pcdh19* null neurons but also contributed to by abnormal connections and spatial arrangement of other neurons. If the entire cortex was to undergo segregation it is likely this would result in abnormal organisation of functional cortical columns. Interestingly, cortical column organisation has been reported in gyrencephalic (folded) brains such as apes, monkeys and ferrets but there is little evidence supporting cortical column organisation in the

lissencephalic (smooth) brains of mice and rats (Chow et al., 1971; Shaw et al., 1975; Tiao and Blakemore, 1976). If abnormal cell sorting does occur throughout the entire cortex this neuronal architecture difference between humans and mice may contribute to the more severe phenotype seen in *PCDH19*-GCE patients. Furthermore, the identification of abnormal cortical sulcation in multiple *PCDH19*-GCE patients, suggests that aberrant cell sorting may generate different morphological phenotypes in gyrencephalic brains compared to lissencephalic brains. The cortical folding of human brains is largely caused by variable proliferation of basal radial glia, a cell type which is not present in the lissencephalic brain of mice. Proliferation of basal radial glia cause "wedges" of cell dense areas, which ultimately cause the brain to fold. It is possible that if segregation occurred within the basal radial glial cells in the developing human brain then abnormal folding may occur due to irregular formation of "wedges". These hypothesises could be investigated by using CRISPR-Cas9 technology to generate a *Pcdh19*$^{+/-}$ ferret (Kou et al., 2015), a gyrencephalic animal model, allowing any roles of PCDH19 specific to folded brains to be examined.

X-Gal staining of *Pcdh19*$^{+/\beta\text{-}Geo}$ mice in Chapter 2 revealed "patchy" staining of *Pcdh19* null cells which we attributed to normal X-inactivation. Due to the clonal and radial nature of excitatory neuron migration in the cortex we predicted X-inactivation would manifest as "columns" of either *Pcdh19* WT or *Pcdh19* null cells. This was in agreement with previous studies that utilised an X-linked β-galactosidase reporter where predominant columns of X-Gal staining were present in the mouse cortex (Tan et al., 1995). At the time this research was undertaken the normal X-inactivation pattern of neurons in the cortex was not well understood. More recently, experiments have been performed to conduct a detailed analysis of X-inactivation in the mouse brain, by labelling both X-chromosomes with either GFP or tdTomato (Wu et al., 2014). It was reported that although there were regions in the cortex

predominantly originating from one X-chromosome there was always a degree of intermingling of both GFP and tdTomato positive cells. This agrees with the HA staining of control *Pcdh19*$^{HA\text{-}FLAG/+}$ brains which showed that normal X-inactivation leads to grossly even distribution of PCDH19. Furthermore, these results highlight the significance of our finding that normal cell distribution is dramatically affected by mosaic expression of *Pcdh19.* The fact that we misinterpreted the "patchy" staining in heterozygous mice highlights the importance of controls. In our case it was not until we had generated a HA tagged mouse and stained HA/+ control mice that we were able to properly interpret the "patchy" staining in heterozygous mice as an abnormal cell sorting phenotype.

Using a combination of *in vitro* and *in vivo* techniques we have shown that the abnormal cell sorting is due to disruption of PCDH19 dependent adhesion interfaces between neuroprogenitors cells at 10.5 dpc. During cortical development neuroprogenitors located in the ventricular zone predominantly undergo radial migration. We envisage two potential cellular consequences downstream of incompatible adhesion codes that could lead to segregation of neuroprogenitors; 1) the incompatibility between cells prevents lateral mixing (passive segregation); or 2) the incompatibility between cells promotes active sorting of neuroprogenitors. Our results suggest that the cells undergo active sorting as we observe small "blocks" only a few cells wide in 14.5-17.5 dpc brains. If lateral mixing was prevented, we would expect to see a minimum "block" size that would represent proliferation of a single "trapped "cell at 10.5 dpc (32 cells at 14.5 dpc with an assumed cell cycle of 12 hours). One caveat of our experiment is the two-dimensional analysis. It is possible, the small blocks we see at later stages are because we have "shaved" the edges of larger blocks. Analysis of the segregation pattern in three-dimensions would clarify this mechanism.

We show that PCDH19 and other members of the NC PCDH family can function in combinatorial activity which dictates cell-cell interaction specificities. This is similar to the cooperative activity of clustered PCDHs which have been proposed to form lattice like structures that act to differentiate between self and non-self neuronal processes (Rubinstein et al., 2015). Structural studies have further elucidated this mechanism showing that clustered PCDHs form tetramers that are maintained by *trans* homodimers through EC domains 1-4 and *cis* heterodimers through EC6 (Goodman et al., 2016; Nicoludis et al., 2015; Rubinstein et al., 2015). The mechanism by which NC PCDHs act in combination is still to be determined and could potentially be similar to the lattice like structures formed by clustered PCDHs. This is supported by the recent structure analysis of zebrafish PCDH19 highlighting its similarity to clustered PCDHs (Cooper et al., 2016). In addition, using co-immunoprecipitation we showed that PCDH19 can interact with both PCDH17 and PCDH10 when expressed in the same cell, supporting the ability of NC PCDHs to form *cis* heterodimers. In the future disease causing mutations positioned in domains important for *trans* (EC1-4) and *cis* (EC6) interactions could be assessed to determine how they impact the formation of *trans* and *cis* interactions. Cooper et al., 2016 showed that missense mutations within EC1-4 are positioned in domains crucial for homotypic *trans* interactions and we would predict that missense mutations within EC6 will affect *cis* heterodimeric interactions.

Rubinstein et al., 2015 modelled the impact a single PCDH isoform mismatch has on the size of lattice structure between cells. They showed that a single mismatch between the PCDH profiles of two adjacent cells led to a dramatic decrease in lattice size, which they attributed to cause cell sorting in their *in vitro* experiments. We used the same modelling approach to determine if having one less PCDH between cells, as is the case *in vivo* using *Pcdh19*$^{HA\text{-}FLAG/\beta\text{-}Geo}$ mice, would result in the same dramatic decrease in lattice size. We show

that the lattice size between two cells where one cell has one less PCDH (N:N-1) modelling *Pcdh19*$^{HA\text{-}FLAG/\beta\text{-}Geo}$ mice, is dramatically reduced compared to a perfect match of PCDHs between two cells (N:N) (Figure 1-4). Furthermore, if both cells have the same PCDH removed (N-1:N-1), modelling *Pcdh19*$^{\beta\text{-}Geo/\beta\text{-}Geo}$, mice the lattice size returns to almost normal levels, which agrees with the absence of a phenotype observed in *Pcdh19*$^{\beta\text{-}Geo/\beta\text{-}Geo}$ (Figure 1-4). In agreement with this we showed that we could remove NC PCDH incompatibility between PCDH19 WT and PCDH19 null cells by deletion of the remaining functional *Pcdh19* allele in *Pcdh19*$^{HA\text{-}FLAG/\beta\text{-}Geo}$ mice which lead to reversal of abnormal cell sorting.

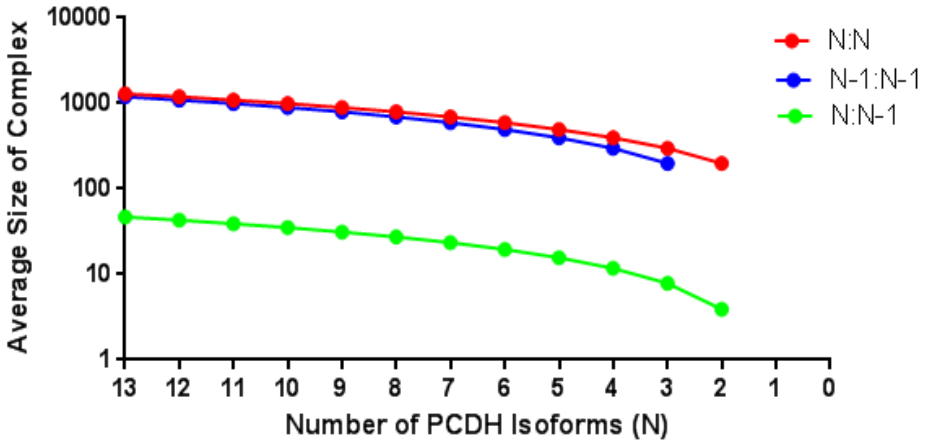

Figure 1-4. The predicted size of adhesion complexes between PCDH19 WT and PCDH19 KO cells is dramatically reduced. Mathematical modelling predicts the size of adhesion complexes is dramatically reduced between PCDH19 WT and PCDH19 KO cells (green line) when compared to adhesion complexes between PCDH19 WT and PCDH19 WT (red line) or PCDH19 KO and PCDH19 KO cells (green line). Modelling was performed with 100 isomers of each PCDH molecule. (Performed by Ian Dodd).

NC PCDHs could act in combination by determining the adhesive strength of cells. Cell sorting could then occur as cells with higher adhesion potential will cluster and the cells with lower adhesion potential will be excluded but still form their own cluster. We believe this mechanism is unlikely for multiple reasons; 1) cells in the developing cortex express many adhesion molecules, therefore it is unlikely the removal of just PCDH19 (a relatively weak adhesion molecule) would lead to a dramatic decrease in their adhesion potential; 2) the absence of a neurological phenotype in *Pcdh19*$^{\beta\text{-}Geo/\beta\text{-}Geo}$ mice suggests that cells completely lacking PCDH19 are largely normal and 3) *in vitro* experiments where two populations of cells expressed the same number but different NC PCDH molecules displayed cell segregation – we would expect many of these cells to have similar overall adhesion strength.

CHAPTER 5

Future Directions

Here we have shown that abnormal cell sorting underlies the unique X-linked inheritance pattern of *PCDH19*-GCE. This provides a platform to investigate how abnormal cell sorting leads to seizures, intellectual disability and autism spectrum disorder. A series of experiments is described below to identify additional neurological processes which are disrupted due to the mosaic expression of *Pcdh19* which may contribute to pathology.

5.1 Investigating Connectivity between PCDH19 WT and PCDH19 null neurons

Given the expression of PCDH19 at the synapse (Chapter 2) and the known roles for δ2 PCDHs in axon guidance and synaptogenesis (Hayashi et al., 2014; Uemura et al., 2007) we envisage that synaptic connections between PCDH19 WT and PCDH19 mutant cells will be disrupted in PCDH19 heterozygous females contributing to disease. Furthermore, the morphology of neurons positioned at boundaries between PCDH19 WT and PCDH19 KO cells may be affected. We hypothesise that abnormal cell sorting of PCDH19 WT and PCDH19 KO cells alters neuronal connectivity through disruption of lateral connections within the cortex. This can be investigated by generating a *Pcdh*19-P2A-CRE mouse (*Pcdh19*^{Cre}), permitting the expression of CRE in cells expressing functional PCDH19. *Pcdh19*^{Cre} mice could then be used in two ways to investigate morphology and arborisation of PCDH19 neurons. The first approach would cross *Pcdh19*^{Cre} mice to commercially available Brainbow 3.2 mice (Cai et al., 2013), which generate multi-coloured neurons in response to Cre recombination which variably activates three membrane-bound fluorophores to create a range of colours. This will allow individual PCDH19 expressing neurons to be traced even in large groups of PCDH19 positive cells allowing us to test the hypothesis that neuronal processes will also be segregated in addition to cell bodies. Secondly *in utero* electroporation of mouse embryos with a loxP-membrane_tdTomato-loxP-membrane_GFP

construct (pCA-mT/mG – Addgene plasmid #26123) will result in mGFP staining only in Pcdh19-Cre positive cells while Pcdh19-Cre negative cells will express mtdTomato. Comparing Scholl analysis of mGFP neurons in *Pcdh19*$^{Cre/+}$ and *Pcdh19*$^{Cre/\beta\text{-}Geo}$ brains will assess any reduction in arborisation formed at the boundaries of PCDH19 WT and PCDH19 KO cells in the cortex.

To investigate functional synaptic connectivity between PCDH19 WT and PCDH19 KO cells a modified rabies virus (EnvA-delta;G) (DeNardo et al., 2015) can be used to assess the degree of monosynaptic transmission. This approach would also utilise the *Pcdh19*^{Cre} mice as the modified rabies virus is expressed in a Cre-dependent fashion, allowing only *Pcdh19-Cre* cells to become competent for infection. Initially a cre-dependent helper AAV virus will be injected into the cortex to express TVA-mCherry, which is essential for rabies virus infection. 14 days later the rabies-GFP virus will be injected and brains analysed 5 days later. This approach marks "starter" cells in yellow and "input" cells in green allowing robust identification of cells which have received synaptic inputs. We would expect to see reduced connectivity in *Pcdh19*$^{Cre/\beta\text{-}Geo}$ brains compared to *Pcdh19*$^{Cre/+}$ brains. Furthermore, we would expect that connectivity when present in *Pcdh19*$^{Cre/\beta\text{-}Geo}$ brains will be restricted to cells within the same patch of Pcdh19-Cre cortex and will not propagate into PCDH19 null zones. The same technique could also be applied *in vitro* on cultured primary neurons from *Pcdh19*$^{Cre/+}$ and *Pcdh19*$^{Cre/\beta\text{-}Geo}$ embryos.

5.2 Is Interneuron Distribution Affected by Mosaic *Pcdh19* Expression?

Inhibitory neurons (interneurons) are responsible for keeping neuronal circuits "in check" and maintaining proper firing rates between excitatory neurons. It has been suggested that altered inhibition due to interneuron dysfunction is an underlying cause of epilepsy (Bernard et al., 2000; Holmes, 1997; Tasker and Dudek, 1991).

Cortical interneurons begin life in the ganglionic eminence and undergo a long range tangential migration path which relies on a large number of molecular cues. Physical, genetic or chemical disruptions in brain development can impair interneuron function resulting in unstable neural circuits, evolving into seizures. Due to the relatively low number of interneurons compared to excitatory neurons in the mammalian cortex (approximately 1:3 (Markram et al., 2004)) it is crucial that they are appropriately distributed to allow correct network inhibition.

We have evidence that PCDH19 is expressed in both interneuron progenitors in the ganglionic eminence and tangentially migrating interneurons in the marginal zone of the developing cortex (Figure 1-5A). Furthermore, segregation of PCDH19-positive and PCDH19-null interneurons is observed in both the ganglionic eminence and marginal zone (Figure 1-5B and C). Therefore, we hypothesise that segregation of PCDH19-positive and PCDH19-null interneuron precursors during tangential migration leads to abnormal distribution of cortical interneurons in the mature brain. In the future it would be interesting to test whether the final location of PCDH19-positive interneurons is segregated and whether this segregation corresponds with the abnormal cell sorting pattern observed in excitatory cells of the cortex. We feel there are two possible presentations of interneuron segregation; interneurons will segregate according to PCDH19 expression in excitatory cells, such that

PCDH19 expressing interneurons only populate PCDH19 expressing zones of the cortex (Figure 2-5, left); alternatively, segregation established during migration of interneurons is the determining factor in final distribution and not abnormal cell sorting in cortical excitatory cells (Figure 2-5, right). To investigate this, we will utilise the *Pcdh19*^{Cre} mouse described above to specifically label PCDH19 expressing interneurons in a heterozygous brain and see where they are finally positioned. We will specifically label PCDH19-Cre positive interneurons by *in utero* electroporation of mT/mG plasmid into the ganglionic eminence of *Pcdh19*$^{Cre/\beta\text{-}Geo}$ embryos. This technique will allow us to trace the lineage of mature interneurons expressing PCDH19 throughout development as they will be marked by mGFP due to Cre-recombination. Mature brains will be stained for HA to show the cortical cell sorting pattern and GFP to reveal the location of PCDH19-Cre positive interneurons.

If PCDH19-positive interneurons are restricted to PCDH19-positive patches of cortex we envisage a disturbance in the distribution of interneurons. We have evidence showing the X-inactivation ratio in the cortex can be vastly different from the X-inactivation pattern in the ganglionic eminence in the same hemisphere which could lead to a situation where there is an insufficient number of PCDH19-positive interneurons or PCDH19-negative interneurons to distribute amongst the appropriate patches in cortex. This would result in regions with increased excitation due to lack of interneurons. Alternatively, if interneuron distribution is unaffected it will result in PCDH19 WT interneurons being present in PCDH19 KO patches of the cortex and vice versa. As we suggested above, synaptic connections between PCDH19 WT and PCDH19 KO neurons may be perturbed, therefore inhibitory synapses in these regions may be disrupted, again leading to increased excitation.

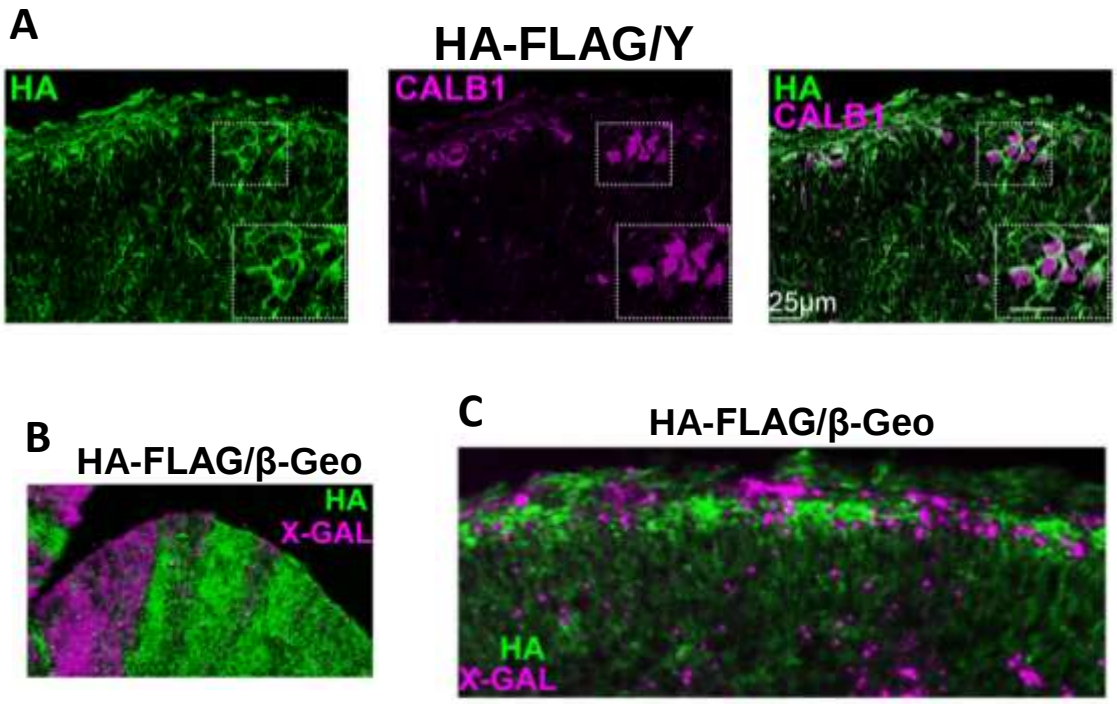

Figure 1-5. PCDH19 is expressed in tangentially migrating cortical interneurons which undergo abnormal cell sorting. A) Co-immunostaining of 15.5 dpc HA-FLAG/Y brains reveals PCDH19 expression in tangentially migrating cortical interneurons. B) HA and X-gal staining of 14.5 dpc HA-FLAG/β-Geo brains shows segregation of PCDH19 positive and PCDH19 null cells in the ganglionic eminence. C) HA and X-gal staining of 16.5 dpc brains confirms abnormal cell sorting of tangentially migrating interneurons in the marginal zone.

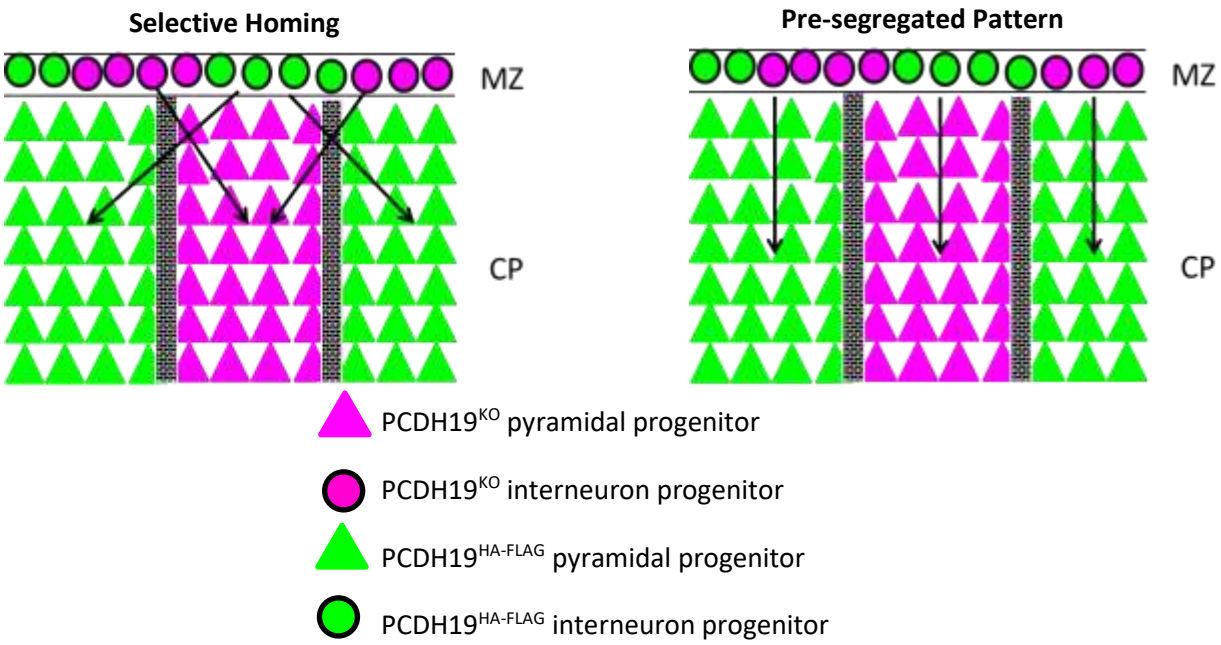

Figure 2-5. Schematic diagram describing different mechanisms that may lead to abnormal interneuron distribution. It is proposed that the final position of interneurons in the mature cortex is dictated by either their pre-segregation pattern (left) or selective homing to "PCDH19-like" regions of excitatory cells (right).

To complement the above experiments investigating the role of PCDH19 in the final positioning of interneurons we could generate a floxed *Pcdh19* allele (*Pcdh19*^{fl}) which would result in complete loss of PCDH19 in the presence of Cre. *Pcdh19*^{fl} mice will be crossed with Dlx-Cre mice which will lead to the deletion of *Pcdh19* in all cortical interneurons. We hypothesise that PCDH19 negative interneurons will fail to be positioned correctly in the cortex leading to decreased local inhibition of excitatory neurons. Furthermore, *Pcdh19*^{fl} mice could be crossed with Emx1-Cre mice which will delete *Pcdh19* from all excitatory pyramidal neurons of the cortex. Again we would hypothesise that *Pcdh19* positive interneurons will fail to be positioned correctly in the cortex. These experiments will investigate the importance of PCDH19 expression in both excitatory and inhibitory neurons of the cortex and its role in determining the final position of cortical interneurons. They could also highlight a role for PCDH19 in dictating specific cell-cell interactions not only within the same cell type as we described in Chapter 3, but also between different types of neurons.

5.3 Can Epileptiform Brain Activity be Rescued after Abnormal Cell Sorting has Occurred?

In Chapter 3 we show that deletion of PCDH19 in heterozygous female embryos reverses abnormal cell sorting. This experiment was performed in zygotes meaning that *Pcdh19* was deleted before its initial expression in the developing brain at 9.5dpc and consequently before abnormal cell sorting occurs. It would be interesting to investigate whether the deletion of *Pcdh19* after abnormal cell sorting has begun can rescue the phenotype. Furthermore, if PCDH19 is important in forming homotypic interactions during synaptogenesis, deletion of *Pcdh19* in the postnatal brain may restore some normal neural connectivity even though abnormal cell sorting occurred during development. We hypothesise that abnormal cell sorting will only be rescued if *Pcdh19* is deleted before 9.5dpc in the mouse brain, but deletion of *Pcdh19* in the postnatal brain will rescue abnormal synaptic connections that may occur between PCDH19 WT and PCDH19 KO cells. To test this, $Pcdh19^{fl}$ mice could be crossed with an inducible global CRE mouse line where Cre is activated in the presence of doxycycline (Dox). Dox will then be introduced to pregnant female mice at different stages to determine whether deletion of *Pcdh19* can rescue abnormal cell sorting. Furthermore, $Pcdh19^{fl/\beta\text{-}Geo}$ adult mice could be subject to ECoG analysis to assess their level of increased brain activity and then be administered with Dox followed by another ECoG analysis. This will determine if deletion of *Pcdh19* in the adult brain can restore neuronal connections between PCDH19 WT and PCDH19 KO cells returning circuit activity to normal.

The experiments outlined above will provide further insight into how abnormal cell sorting ultimately leads to epileptiform brain activity in $Pcdh19^{HA\text{-}FLAG/\beta\text{-}Geo}$ mice. This information will be critical in understanding the origin of seizures in *PCDH19*-GCE and the development of much needed novel treatments.

5.4 Investigating the Combinatorial Activity of Other NC PCDHs *In Vivo*

To support our data suggesting that NC PCDHs cooperate to dictate specific cell-cell interactions in the developing brain, it would be interesting to investigate whether cell sorting occurs with mosaic expression of other NC PCDH members. This experiment is particularly challenging as all other PCDHs are autosomal genes, unlike PCDH19 which is X-linked, and therefore undergoes X-inactivation generating a mosaic expression pattern. One approach to perform this experiment would be to utilise *Pcdh19*^{Cre} mice as a system that can recombine DNA in a manner resembling X-inactivation. This would also require the generation of a floxed gene of interest, for example *Pcdh10*. In order to label PCDH10 WT and PCDH10 KO cells the floxed allele would be generated using CRISPR-Cas9 technology in zygotes of mT/mG strain (Muzumdar et al., 2007). This mT/mG strain operates in the same way as the above described plasmid where cells express membrane-GFP in the presence of Cre, while cells are membrane-tdTomato positive in the absence of Cre. Mice would be generated that are homozygous for both the mT/mG allele and the floxed-PCDH10 allele. These mice could then be crossed with Pcdh19$^{Cre/+}$ mice to generate mosaic expression of PCDH10 WT and PCDH10 KO cells that are labelled with mtdTomato and mGFP respectively, allowing easy identification of a cell sorting phenotype (Figure 3-5).

Alternatively, PCDH10 KO mouse embryonic stem cells (mESC) that contain a GFP marker could be generated and injected into mouse blastocysts. The localisation of PCDH10 KO ESCs could be compared to that of PCDH10 WT ESCs in the developing cortex to investigate a cell sorting phenotype. Both of the describe techniques could be performed with multiple NC PCDHs to further strengthen a combinatorial role in the developing brain

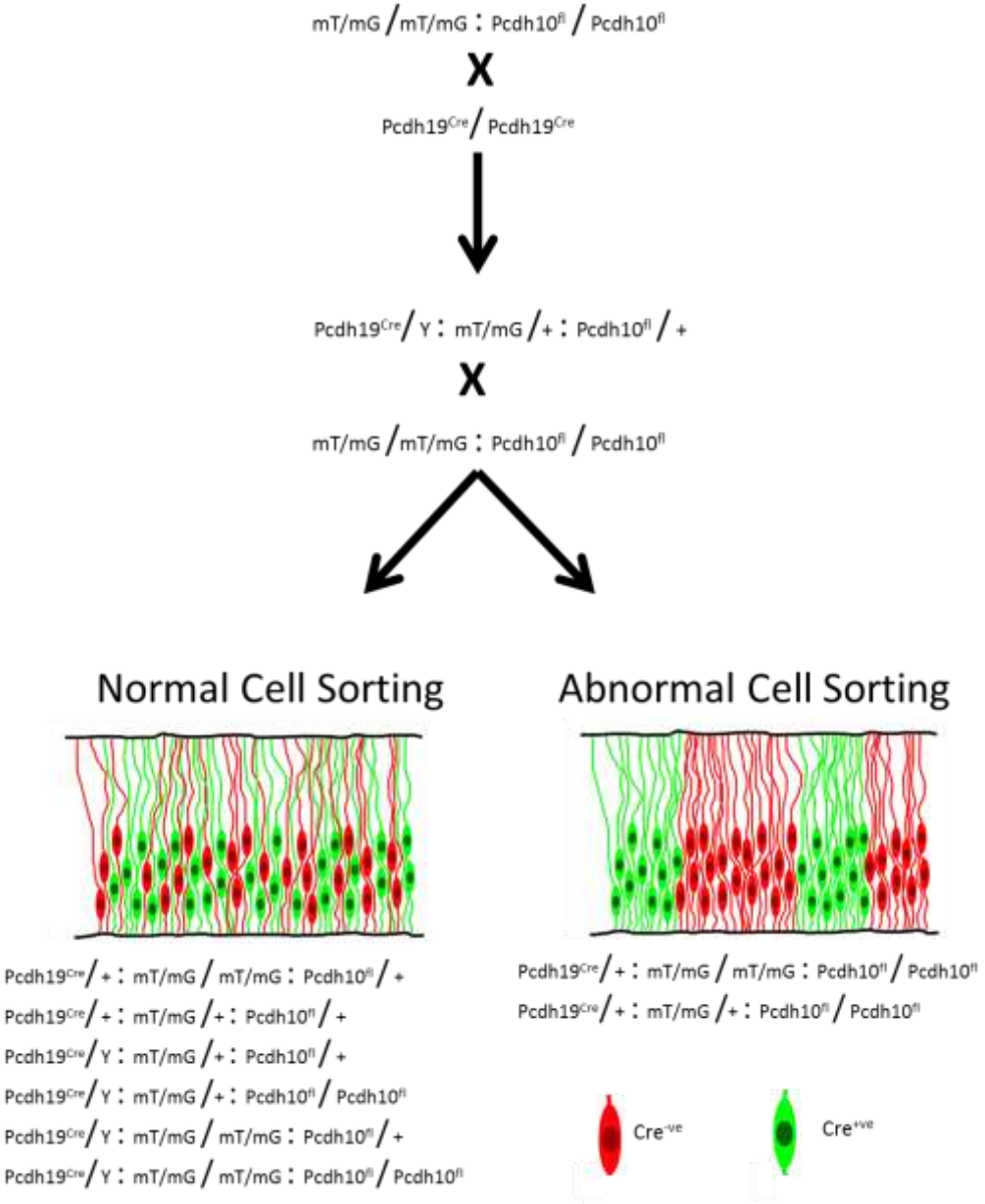

Figure 3-5. Experimental design to investigate the effect mosaic expression of PCDH10 has on cortical cell sorting. Mice will be generated that display mosaic expression of PCDH10 due to Cre recombination driven by the X-linked *Pcdh19*^{Cre} allele. We hypothesis that abnormal cell sorting will occur in animals with mosaic PCDH10 expression but normal cell sorting will occur in animals that are either complete KO or HET for PCDH10.

5.5 Concluding remarks

This study aimed to understand the cellular and molecular basis of the unique X-linked inheritance pattern associated with *PCDH19*-GCE.

Our data highlights the ability of PCDH19 to cooperate with other NC PCDHs and dictate adhesion specificities. *In vivo*, the generation of differential adhesion codes caused by mosaic expression of PCDH19 leads to abnormal cell sorting, such that PCDH19-positive and PCDH19-null neuronal progenitors segregate within the developing cortex. Furthermore, abnormal cell sorting is not present in animals completely lacking PCDH19. Our findings suggest that disruption of cellular adhesion codes is associated with the unique X-linked inheritance of *PCDH19*-GCE and that just a single difference in PCDH expression is enough to disrupt the complex adhesion codes present in the developing mammalian cortex.

Additional Methods

Immunofluorescence

Immunostaining was performed as described in chapter 3. Additional antibodies used

goat anti-SOX3 1:300 (R&D Systems, AF2569 and guinea pig anti-CALBINDIN 1:400 (Synaptic Systems,214004). Images were acquired on a Leica SP5 Confocal microscope.

Modelling Size of Lattice-Like Adhesion Complexes

Modelling was performed according to experimental procedures outlined in (Rubinstein et al., 2015).

References

Bernard, C., Cossart, R., Hirsch, J.C., Esclapez, M., and Ben-Ari, Y. (2000). What is GABAergic Inhibition? How Is it Modified in Epilepsy? Epilepsia *41*, S90–S95.

Boggon, T.J., Murray, J., Chappuis-Flament, S., Wong, E., Gumbiner, B.M., and Shapiro, L. (2002). C-cadherin ectodomain structure and implications for cell adhesion mechanisms. Science *296*, 1308–1313.

Buckmaster, P.S., and Lew, F.H. (2011). Rapamycin suppresses mossy fiber sprouting but not seizure frequency in a mouse model of temporal lobe epilepsy. J. Neurosci. Off. J. Soc. Neurosci. *31*, 2337–2347.

Cai, D., Cohen, K.B., Luo, T., Lichtman, J.W., and Sanes, J.R. (2013). Improved tools for the Brainbow toolbox. Nat. Methods *10*, 540–547.

Chen, B., Chen, Z., Brinkmann, K., Pak, C.W., Liao, Y., Shi, S., Henry, L., Grishin, N.V., Bogdan, S., and Rosen, M.K. (2014). The WAVE Regulatory Complex Links Diverse Receptors to the Actin Cytoskeleton. Cell *156*, 195–207.

Chow, K.L., Masland, R.H., and Stewart, D.L. (1971). Receptive field characteristics of striate cortical neurons in the rabbit. Brain Res. *33*, 337–352.

Cooper, S.R., Emond, M.R., Duy, P.Q., Liebau, B.G., Wolman, M.A., and Jontes, J.D. (2015). Protocadherins control the modular assembly of neuronal columns in the zebrafish optic tectum. J. Cell Biol. *211*, 807–814.

Cooper, S.R., Jontes, J.D., and Sotomayor, M. (2016). Structural determinants of adhesion by Protocadherin-19 and implications for its role in epilepsy. eLife *5*.

Delva, E., Tucker, D.K., and Kowalczyk, A.P. (2009). The Desmosome. Cold Spring Harb. Perspect. Biol. *1*.

DeNardo, L.A., Berns, D.S., DeLoach, K., and Luo, L. (2015). Connectivity of mouse somatosensory and prefrontal cortex examined with trans-synaptic tracing. Nat. Neurosci. *18*, 1687–1697.

Depienne, C., and LeGuern, E. (2012). PCDH19-related infantile epileptic encephalopathy: an unusual X-linked inheritance disorder. Hum. Mutat. *33*, 627–634.

Depienne, C., Bouteiller, D., Keren, B., Cheuret, E., Poirier, K., Trouillard, O., Benyahia, B., Quelin, C., Carpentier, W., Julia, S., et al. (2009). Sporadic Infantile Epileptic Encephalopathy Caused by Mutations in PCDH19 Resembles Dravet Syndrome but Mainly Affects Females. PLoS Genet *5*, e1000381.

Depienne, C., Trouillard, O., Bouteiller, D., Gourfinkel-An, I., Poirier, K., Rivier, F., Berquin, P., Nabbout, R., Chaigne, D., Steschenko, D., et al. (2011). Mutations and Deletions in PCDH19 Account for Various Familial or Isolated Epilepsies in Females. Hum. Mutat. *32*, E1959–E1975.

Dibbens, L.M., Tarpey, P.S., Hynes, K., Bayly, M.A., Scheffer, I.E., Smith, R., Bomar, J., Sutton, E., Vandeleur, L., Shoubridge, C., et al. (2008). X-linked protocadherin 19 mutations cause female-limited epilepsy and cognitive impairment. Nat. Genet. *40*, 776–781.

Duszyc, K., Terczynska, I., and Hoffman-Zacharska, D. (2014). Epilepsy and mental retardation restricted to females: X-linked epileptic infantile encephalopathy of unusual inheritance. J. Appl. Genet.

Emond, M.R., Biswas, S., and Jontes, J.D. (2009). Protocadherin-19 is essential for early steps in brain morphogenesis. Dev. Biol. *334*, 72–83.

Emond, M.R., Biswas, S., Blevins, C.J., and Jontes, J.D. (2011). A complex of Protocadherin-19 and N-cadherin mediates a novel mechanism of cell adhesion. J. Cell Biol. *195*, 1115–1121.

European Chromosome 16 Tuberous Sclerosis Consortium (1993). Identification and characterization of the tuberous sclerosis gene on chromosome 16. Cell *75*, 1305–1315.

Fabisiak, K., and Erickson, R.P. (1990). A familial form of convulsive disorder with or without mental retardation limited to females: extension of a pedigree limits possible genetic mechanisms. Clin. Genet. *38*, 353–358.

Frank, M., and Kemler, R. (2002). Protocadherins. Curr. Opin. Cell Biol. *14*, 557–562.

Fryer, A.E., Connor, J.M., Povey, S., Yates, J.R.W., Chalmers, A., Fraser, I., Yates, A.D., and Osborne, J.P. (1987). EVIDENCE THAT THE GENE FOR TUBEROUS SCLEROSIS IS ON CHROMOSOME 9. The Lancet *329*, 659–661.

Gaitan, Y., and Bouchard, M. (2006). Expression of the δ-protocadherin gene Pcdh19 in the developing mouse embryo. Gene Expr. Patterns *6*, 893–899.

Garrett, A.M., Schreiner, D., Lobas, M.A., and Weiner, J.A. (2012). γ-protocadherins control cortical dendrite arborization by regulating the activity of a FAK/PKC/MARCKS signaling pathway. Neuron *74*, 269–276.

Goodman, K.M., Rubinstein, R., Thu, C.A., Bahna, F., Mannepalli, S., Ahlsén, G., Rittenhouse, C., Maniatis, T., Honig, B., and Shapiro, L. (2016). Structural Basis of Diverse Homophilic Recognition by Clustered α- and β-Protocadherins. Neuron *90*, 709–723.

Gumbiner, B.M. (1996). Cell Adhesion: The Molecular Basis of Tissue Architecture and Morphogenesis. Cell *84*, 345–357.

Gumbiner, B.M. (2005). Regulation of cadherin-mediated adhesion in morphogenesis. Nat. Rev. Mol. Cell Biol. *6*, 622–634.

Hatta, K., and Takeichi, M. (1986). Expression of N-cadherin adhesion molecules associated with early morphogenetic events in chick development. Nature *320*, 447–449.

Hatta, K., Nose, A., Nagafuchi, A., and Takeichi, M. (1988). Cloning and expression of cDNA encoding a neural calcium-dependent cell adhesion molecule: its identity in the cadherin gene family. J. Cell Biol. *106*, 873–881.

Hauser, W.A., and Kurland, L.T. (1975). The epidemiology of epilepsy in Rochester, Minnesota, 1935 through 1967. Epilepsia *16*, 1–66.

Hayashi, S., Inoue, Y., Kiyonari, H., Abe, T., Misaki, K., Moriguchi, H., Tanaka, Y., and Takeichi, M. (2014). Protocadherin-17 mediates collective axon extension by recruiting actin regulator complexes to interaxonal contacts. Dev. Cell *30*, 673–687.

Higurashi, N., Nakamura, M., Sugai, M., Ohfu, M., Sakauchi, M., Sugawara, Y., Nakamura, K., Kato, M., Usui, D., Mogami, Y., et al. (2013). PCDH19-related female-limited epilepsy: further details regarding early clinical features and therapeutic efficacy. Epilepsy Res. *106*, 191–199.

Hirano, S., and Takeichi, M. (2012). Cadherins in Brain Morphogenesis and Wiring. Physiol. Rev. *92*, 597–634.

Holmes, G.L. (1997). Epilepsy in the developing brain: lessons from the laboratory and clinic. Epilepsia *38*, 12–30.

Hoshina, N., Tanimura, A., Yamasaki, M., Inoue, T., Fukabori, R., Kuroda, T., Yokoyama, K., Tezuka, T., Sagara, H., Hirano, S., et al. (2013a). Protocadherin 17 regulates presynaptic assembly in topographic corticobasal Ganglia circuits. Neuron *78*, 839–854.

Hoshina, N., Tanimura, A., Yamasaki, M., Inoue, T., Fukabori, R., Kuroda, T., Yokoyama, K., Tezuka, T., Sagara, H., Hirano, S., et al. (2013b). Protocadherin 17 regulates presynaptic assembly in topographic corticobasal Ganglia circuits. Neuron *78*, 839–854.

Juberg, R.C., and Hellman, C.D. (1971). A new familial form of convulsive disorder and mental retardation limited to females. J. Pediatr. *79*, 726–732.

Junghans, D., Haas, I.G., and Kemler, R. (2005). Mammalian cadherins and protocadherins: about cell death, synapses and processing. Curr. Opin. Cell Biol. *17*, 446–452.

Kim, S.-Y., Chung, H.S., Sun, W., and Kim, H. (2007). Spatiotemporal expression pattern of non-clustered protocadherin family members in the developing rat brain. Neuroscience *147*, 996–1021.

Kim, S.Y., Mo, J.W., Han, S., Choi, S.Y., Han, S.B., Moon, B.H., Rhyu, I.J., Sun, W., and Kim, H. (2010). The expression of non-clustered protocadherins in adult rat hippocampal formation and the connecting brain regions. Neuroscience *170*, 189–199.

Kim, S.-Y., Yasuda, S., Tanaka, H., Yamagata, K., and Kim, H. (2011). Non-clustered protocadherin. Cell Adhes. Migr. *5*, 97–105.

Kobayashi, T., Minowa, O., Sugitani, Y., Takai, S., Mitani, H., Kobayashi, E., Noda, T., and Hino, O. (2001). A germ-line Tsc1 mutation causes tumor development and embryonic lethality that are similar, but not identical to, those caused by Tsc2 mutation in mice. Proc. Natl. Acad. Sci. U. S. A. *98*, 8762–8767.

Kostadinov, D., and Sanes, J.R. (2015). Protocadherin-dependent dendritic self-avoidance regulates neural connectivity and circuit function. eLife *4*, e08964.

Kou, Z., Wu, Q., Kou, X., Yin, C., Wang, H., Zuo, Z., Zhuo, Y., Chen, A., Gao, S., and Wang, X. (2015). CRISPR/Cas9-mediated genome engineering of the ferret. Cell Res. *25*, 1372–1375.

Krishna-K, K., Hertel, N., and Redies, C. (2011). Cadherin expression in the somatosensory cortex: evidence for a combinatorial molecular code at the single-cell level. Neuroscience *175*, 37–48.

Leckband, D., and Prakasam, A. (2006). Mechanism and Dynamics of Cadherin Adhesion. Annu. Rev. Biomed. Eng. *8*, 259–287.

Lefebvre, J.L., Kostadinov, D., Chen, W.V., Maniatis, T., and Sanes, J.R. (2012). Protocadherins mediate dendritic self-avoidance in the mammalian nervous system. Nature *488*, 517–521.

Leung, L.C., Urbančič, V., Baudet, M.-L., Dwivedy, A., Bayley, T.G., Lee, A.C., Harris, W.A., and Holt, C.E. (2013). Coupling of NF-protocadherin signaling to axon guidance by cue-induced translation. Nat. Neurosci. *16*, 166–173.

Marini, C., Mei, D., Parmeggiani, L., Norci, V., Calado, E., Ferrari, A., Moreira, A., Pisano, T., Specchio, N., Vigevano, F., et al. (2010). Protocadherin 19 mutations in girls with infantile-onset epilepsy. Neurology *75*, 646–653.

Markram, H., Toledo-Rodriguez, M., Wang, Y., Gupta, A., Silberberg, G., and Wu, C. (2004). Interneurons of the neocortical inhibitory system. Nat. Rev. Neurosci. *5*, 793–807.

Michetti, C., Castroflorio, E., Marchionni, I., Forte, N., Sterlini, B., Binda, F., Fruscione, F., Baldelli, P., Valtorta, F., Zara, F., et al. (2017). The PRRT2 knockout mouse recapitulates the neurological diseases associated with PRRT2 mutations. Neurobiol. Dis. *99*, 66–83.

Molumby, M.J., Keeler, A.B., and Weiner, J.A. (2016). Homophilic Protocadherin Cell-Cell Interactions Promote Dendrite Complexity. Cell Rep. *15*, 1037–1050.

Morishita, H., and Yagi, T. (2007). Protocadherin family: diversity, structure, and function. Curr. Opin. Cell Biol. *19*, 584–592.

Morishita, H., Umitsu, M., Murata, Y., Shibata, N., Udaka, K., Higuchi, Y., Akutsu, H., Yamaguchi, T., Yagi, T., and Ikegami, T. (2006). Structure of the cadherin-related neuronal receptor/protocadherin-alpha first extracellular cadherin domain reveals diversity across cadherin families. J. Biol. Chem. *281*, 33650–33663.

Muzumdar, M.D., Tasic, B., Miyamichi, K., Li, L., and Luo, L. (2007). A global double-fluorescent Cre reporter mouse. Genes. N. Y. N 2000 *45*, 593–605.

Nagar, B., Overduin, M., Ikura, M., and Rini, J.M. (1996). Structural basis of calcium-induced E-cadherin rigidification and dimerization. Nature *380*, 360–364.

Nicoludis, J.M., Lau, S.-Y., Schärfe, C.P.I., Marks, D.S., Weihofen, W.A., and Gaudet, R. (2015). Structure and Sequence Analyses of Clustered Protocadherins Reveal Antiparallel Interactions that Mediate Homophilic Specificity. Struct. Lond. Engl. 1993 *23*, 2087–2098.

Nicoludis, J.M., Vogt, B.E., Green, A.G., Schärfe, C.P., Marks, D.S., and Gaudet, R. (2016). Antiparallel protocadherin homodimers use distinct affinity- and specificity-mediating regions in cadherin repeats 1-4. eLife *5*.

Onda, H., Lueck, A., Marks, P.W., Warren, H.B., and Kwiatkowski, D.J. (1999). Tsc2+/– mice develop tumors in multiple sites that express gelsolin and are influenced by genetic background. J. Clin. Invest. *104*, 687–695.

Ozawa, M., and Kemler, R. (1998). Altered cell adhesion activity by pervanadate due to the dissociation of alpha-catenin from the E-cadherin.catenin complex. J. Biol. Chem. *273*, 6166–6170.

Patel, S.D., Chen, C.P., Bahna, F., Honig, B., and Shapiro, L. (2003). Cadherin-mediated cell-cell adhesion: sticking together as a family. Curr. Opin. Struct. Biol. *13*, 690–698.

Peñagarikano, O., Abrahams, B.S., Herman, E.I., Winden, K.D., Gdalyahu, A., Dong, H., Sonnenblick, L.I., Gruver, R., Almajano, J., Bragin, A., et al. (2011). Absence of CNTNAP2 Leads to Epilepsy, Neuronal Migration Abnormalities, and Core Autism-Related Deficits. Cell *147*, 235–246.

Pettitt, J. (2005). The cadherin superfamily. WormBook.

Piper, M., Dwivedy, A., Leung, L., Bradley, R.S., and Holt, C.E. (2008). NF-Protocadherin and TAF1 Regulate Retinal Axon Initiation and Elongation In Vivo. J. Neurosci. Off. J. Soc. Neurosci. *28*, 100–105.

Redies, C., Vanhalst, K., and Roy, F. van (2005). delta-Protocadherins: unique structures and functions. Cell. Mol. Life Sci. CMLS *62*, 2840–2852.

Ribich, S., Tasic, B., and Maniatis, T. (2006). Identification of long-range regulatory elements in the protocadherin-alpha gene cluster. Proc. Natl. Acad. Sci. U. S. A. *103*, 19719–19724.

Rise, M.L., Frankel, W.N., Coffin, J.M., and Seyfried, T.N. (1991). Genes for epilepsy mapped in the mouse. Science *253*, 669–673.

Rubinstein, R., Thu, C.A., Goodman, K.M., Wolcott, H.N., Bahna, F., Mannepalli, S., Ahlsen, G., Chevee, M., Halim, A., Clausen, H., et al. (2015). Molecular Logic of Neuronal Self-Recognition through Protocadherin Domain Interactions. Cell *163*, 629–642.

Ryan, S.G., Chance, P.F., Zou, C.H., Spinner, N.B., Golden, J.A., and Smietana, S. (1997). Epilepsy and mental retardation limited to females: an X-linked dominant disorder with male sparing. Nat. Genet. *17*, 92–95.

Scheffer, I.E., Turner, S.J., Dibbens, L.M., Bayly, M.A., Friend, K., Hodgson, B., Burrows, L., Shaw, M., Wei, C., Ullmann, R., et al. (2008). Epilepsy and mental retardation limited to females: an under-recognized disorder. Brain *131*, 918–927.

Schreiner, D., and Weiner, J.A. (2010). Combinatorial homophilic interaction between gamma-protocadherin multimers greatly expands the molecular diversity of cell adhesion. Proc. Natl. Acad. Sci. U. S. A. *107*, 14893–14898.

Shaw, C., Yinon, U., and Auerbach, E. (1975). Receptive fields and response properties of neurons in the rat visual cortex. Vision Res. *15*, 203–208.

Soba, P., Zhu, S., Emoto, K., Younger, S., Yang, S.-J., Yu, H.-H., Lee, T., Jan, L.Y., and Jan, Y.-N. (2007). Drosophila sensory neurons require Dscam for dendritic self-avoidance and proper dendritic field organization. Neuron *54*, 403–416.

Suo, L., Lu, H., Ying, G., Capecchi, M.R., and Wu, Q. (2012). Protocadherin clusters and cell adhesion kinase regulate dendrite complexity through Rho GTPase. J. Mol. Cell Biol. *4*, 362–376.

Suzuki, J., and Yurie, N. (1977). Seizure patterns and electroencephalograms of El mouse. Electroencephalogr. Clin. Neurophysiol. *43*, 299–311.

Tai, K., Kubota, M., Shiono, K., Tokutsu, H., and Suzuki, S.T. (2010). Adhesion properties and retinofugal expression of chicken protocadherin-19. Brain Res. *1344*, 13–24.

Takeichi, M. (1995). Morphogenetic roles of classic cadherins. Curr. Opin. Cell Biol. *7*, 619–627.

Takeichi, M., Atsumi, T., Yoshida, C., Uno, K., and Okada, T.S. (1981). Selective adhesion of embryonal carcinoma cells and differentiated cells by Ca2+-dependent sites. Dev. Biol. *87*, 340–350.

Tan, S.S., Faulkner-Jones, B., Breen, S.J., Walsh, M., Bertram, J.F., and Reese, B.E. (1995). Cell dispersion patterns in different cortical regions studied with an X-inactivated transgenic marker. Development *121*, 1029–1039.

Tasker, J.G., and Dudek, F.E. (1991). Electrophysiology of GABA-mediated synaptic transmission and possible roles in epilepsy. Neurochem. Res. *16*, 251–262.

Terracciano, A., Trivisano, M., Cusmai, R., De Palma, L., Fusco, L., Compagnucci, C., Bertini, E., Vigevano, F., and Specchio, N. (2016). PCDH19-related epilepsy in two mosaic male patients. Epilepsia.

Thomas, R.H., and Berkovic, S.F. (2014). The hidden genetics of epilepsy-a clinically important new paradigm. Nat. Rev. Neurol. *10*, 283–292.

Thu, C.A., Chen, W.V., Rubinstein, R., Chevee, M., Wolcott, H.N., Felsovalyi, K.O., Tapia, J.C., Shapiro, L., Honig, B., and Maniatis, T. (2014). Generation of single cell identity by homophilic interactions between combinations of α, β and γ protocadherins. Cell *158*, 1045–1059.

Tiao, Y.C., and Blakemore, C. (1976). Functional organization in the visual cortex of the golden hamster. J. Comp. Neurol. *168*, 459–481.

Uemura, M., Nakao, S., Suzuki, S.T., Takeichi, M., and Hirano, S. (2007). OL-protocadherin is essential for growth of striatal axons and thalamocortical projections. Nat. Neurosci. *10*, 1151–1159.

Wolverton, T., and Lalande, M. (2001). Identification and characterization of three members of a novel subclass of protocadherins. Genomics *76*, 66–72.

Wu, H., Luo, J., Yu, H., Rattner, A., Mo, A., Wang, Y., Smallwood, P.M., Erlanger, B., Wheelan, S.J., and Nathans, J. (2014). Cellular Resolution Maps of X Chromosome Inactivation: Implications for Neural Development, Function, and Disease. Neuron *81*, 103–119.

Yagi, T. (2012). Molecular codes for neuronal individuality and cell assembly in the brain. Front. Mol. Neurosci. *5*.

Yagi, T., and Takeichi, M. (2000). Cadherin superfamily genes: functions, genomic organization, and neurologic diversity. Genes Dev. *14*, 1169–1180.

Yamagata, K., Andreasson, K.I., Sugiura, H., Maru, E., Dominique, M., Irie, Y., Miki, N., Hayashi, Y., Yoshioka, M., Kaneko, K., et al. (1999). Arcadlin Is a Neural Activity-regulated Cadherin Involved in Long Term Potentiation. J. Biol. Chem. *274*, 19473–19479.

Yasuda, S., Tanaka, H., Sugiura, H., Okamura, K., Sakaguchi, T., Tran, U., Takemiya, T., Mizoguchi, A., Yagita, Y., Sakurai, T., et al. (2007). Activity-Induced Protocadherin

Arcadlin Regulates Dendritic Spine Number by Triggering N-Cadherin Endocytosis via TAO2β and p38 MAP Kinases. Neuron *56*, 456–471.

Yokota, S., Hirayama, T., Hirano, K., Kaneko, R., Toyoda, S., Kawamura, Y., Hirabayashi, M., Hirabayashi, T., and Yagi, T. (2011). Identification of the cluster control region for the protocadherin-beta genes located beyond the protocadherin-gamma cluster. J. Biol. Chem. *286*, 31885–31895.